Reconstruction of the Late Pleistocene and Holocene geomorphology of northwest Calvert Island, British Columbia

by

Jordan Blair Reglin Eamer

B.Sc. (honours with distinction), University of Victoria, 2010

M.Sc., University of Victoria, 2012

A dissertation submitted in partial fulfillment of the

requirements for the degree of

DOCTOR OF PHILOSOPHY

In the Department of Geography

Reconstruction of the Late Pleistocene and Holocene geomorphology of northwest Calvert Island, British Columbia

by

Jordan Blair Reglin Eamer

B.Sc. (honours with distinction), University of Victoria, 2010

M.Sc., University of Victoria, 2012

Supervisory committee:

Dr. I.J. Walker, Co-Supervisor

Department of Geography, University of Victoria

Dr. O.B. Lian, Co-Supervisor

Department of Geography, University of Victoria

Dr. J.J. Clague, Member

Department of Geography, University of Victoria

Dr. D.H. Shugar, Outside Member

School of Interdisciplinary Arts and Sciences, University of Washington Tacoma

Abstract

This dissertation presents results from a multi-year interdisciplinary study of the Late Quaternary geomorphic history of northwest Calvert Island, British Columbia, Canada. There is a considerable knowledge gap in the region pertaining to Cordilleran ice cover and extent as well as landscape response to a uniquely stable relative sea-level history. The objective of this study was to reconstruct this regional landscape response to deglaciation including post-LGM ice cover and extent, relative sea-level changes, coastal landform development, and climate and ecological variance. Methods used to inform this reconstruction included airborne lidar, aerial photography interpretation, sedimentary stratigraphy and detailed sedimentology of samples from shovel pits and lake cores, surficial geology and geomorphic mapping, palaeoecological examinations, and the development of a geochronology using radiocarbon and optical dating. To assist with landscape reconstruction, a new method was developed and used to differentiate littoral and aeolian sands in sediment samples that range in age from Mid to Late Holocene by using modern reference samples. The method utilized a standard optical microscope paired with freely available software (ImageJ) to characterize grain shape parameters. The method was tested on nearly 6,000 sand grains from samples of known and hypothesized depositional settings and was able to correctly identify the depositional setting for 76% of the samples. After testing, the method was used to differentiate littoral and aeolian sands in a number of shovel pit, exposure, and core sediment samples to give context to stratigraphic and geomorphic interpretations. A short-lived Late Pleistocene re-advance of Cordilleran ice occurred in the study area, with radiocarbon ages indicating ice advanced to, and then retreated from, the western edge of Calvert Island between 14.2 and 13.8 ka cal BP, respectively. Sedimentological and palaeoecological information that suggests a cold climate and advancing/retreating glacier as well as lidar remote sensing and field-based geomorphic mapping of moraines in the region provide evidence of the re-advance. After ice retreated from the area, a broad suite of geomorphic landforms developed, including flood plains,

aeolian dunes, beaches, spits, marshes, and tombolos. Coastal reworking was extensive, with progradation rates greater than 1 m a^{-1} occurring in some locations during the Late Holocene. These data provide the first evidence of a re-advance of the retreating ice sheet margin on the central coast of British Columbia, contribute an important methodology to advance Quaternary reconstructions, and give a unique account of the geomorphic development of a Pacific Northwest coastline that experienced little relative sea-level change over the Late Pleistocene and Holocene. Results help fill a spatial and temporal gap in the landscape history of British Columbia and have implications for climate and sea-level reconstructions, early human migration patterns, and the palaeoenvironment of an understudied area of the Pacific Northwest coast of North America.

Contents

Table of figures

Table of tables

Table of appendices

Acknowledgements

This research was supported financially and logistically by partners at the Hakai Institute and Tula Foundation, notably Eric Peterson and Christina Munck. Anyone reading this dissertation is encouraged to go to www.hakai.org to discover a wealth of science, discovery, and openly available data. Hakai staff scientists and facilities support staff provided invaluable assistance on the central coast. An NSERC Postgraduate Scholarship and a GSA Research Award also funded my contributions to this project, and the research was also supported by a Mitacs Elevate Postdoctoral Fellowship to Dan Shugar, NSERC Discovery grants to Ian Walker and Olav Lian, and a Canadian Foundation for Innovation Leaders Opportunity Fund grant to Ian Walker. Access to Hakai Luxvbalis Conservancy was provided through permit #105935. Valerie Behan-Pelletier of Agriculture and Agri-food Canada provided helpful identification of mites in the wetland sediments. Field work was supported by Jonathan Hughes, Christina Neudorf, Alex Lausanne, Libby Griffin, Jordan Bryce, Daniel Huesken, and Brie Mackovic, and lab work was supported by Alice Telka, Jennifer Eamer (née Lucas), Christina Neudorf, Libby Griffin, and Jordan Bryce. Notably, Olav Lian and his laboratory at the University of the Fraser Valley (Christina Neudorf, Brie Mackovic, Dan Huesken, Libby Griffin, and Jordan Bryce) spend considerable time and expended great effort in developing an appropriate methodology for optical dating on Calvert Island. My committee members were instrumental partners and support in the field, lab, and through the process of writing. In particular, my supervisor, Dr. Ian Walker, was instrumental to my academic development through nearly ten years of supervision, and I owe a debt of gratitude that words written here cannot begin to describe. My wife Jennifer and my two children Tyler and Fox continually inspired me, and my family as a whole was very supportive throughout the process: I owe everything to family. Thank you.

I recognize that this study took place on the traditional territory of the Heiltsuk First Nation and Wuikinuxv Nation, and am overwhelmingly grateful for the opportunity.

1. Introduction

1.1. Investigating the central coast of British Columbia, Canada: a unique opportunity to better understand the Late Quaternary landscape of the west coast of North America

At the Last Glacial Maximum, ca. 18,000 years ago, the Cordilleran Ice Sheet covered the majority of British Columbia, Northern Washington, Idaho, and Montana, and southern Yukon Territory (Clague and James 2002). Much is known about the extent of ice cover, ice character, and the legacy left in the sediments and on the landscape after the ice sheet's demise (see section 1.2.1, below). However, the spatial distribution of this understanding is fairly narrow, with the vast majority of studies focused on the Fraser and Puget lowlands in southwest British Columbia and northwest Washington State. A detailed chronology of ice sheet advance and non-uniform decay has been presented, debated, and updated over decades of research in those areas, and the effects of the ice sheet on relative sea-levels have been understood and continually refined over that time period (see section 1.2.2, below). Recently, a small body of research has presented a new, unique story of relative sea–level (RSL) for some locations along the ice sheet margin, one of minimal RSL change (McLaren et al. 2014; Shugar et al. 2014). This work occurred in a relatively understudied portion of the margin: the central coast of British Columbia. Research on sea-levels and ice cover in this region until this point had been sparse (e.g., Andrews and Retherford 1978), and research into Late Quaternary landscape development in an area with the stable relative sea-levels described in McLaren et al. (2014) equally so. This yielded an important gap in the knowledge of landscape dynamics following the retreat of the Cordilleran Ice Sheet. The establishment of the Hakai Institute in a strategic location on the central coast, providing access to a suite of sedimentary landforms in a region where they are rare and difficult to access, provided the opportunity for this research to help fill this gap.

The general purpose of this research is to better understand landscape development since the Late Pleistocene in this strategic location: northwestern Calvert Island, central coast of British Columbia, Canada. This includes knowledge of the extent of ice following Cordilleran Ice Sheet retreat, sea-level changes, climate and vegetation dynamics, and landform genesis, reworking, and erosion. This general purpose is explored through the following research objectives.

In section 2, to better understand the Late Pleistocene character of the Cordilleran Ice Sheet on northwestern Calvert Island, a Late Pleistocene re-advance of ice is documented using stratigraphy, sedimentology, geomorphology, and palaeoecology. In addition, five radiocarbon ages are used to constrain the re-advance as having occurred between 14.2 and 13.8 cal ka cal BP. Possible mechanisms for the initiation of ice re-advance likely included a cooling climate, however local topographic effects or a slippery deformable substrate may have also contributed.

In section 3, to define the depositional environment of stratigraphic units consisting mostly of sand and containing few diagnostic features (such as bedding structures), a method for determining the mechanism of transport for sand grains was developed. This method, based on the principle of aeolian sand sorting and utilizing an optical microscope and particle imaging software, enabled differentiation of aeolian and littoral sands in the study area, useful for landscape reconstruction of the sandy coastal landforms that developed through the Holocene. The method showed promising success, having identified the correct mechanism of transport 76% of the time.

In section 4, the summary manuscript for this dissertation, the objective was to determine the landscape response to deglaciation after the Last Glacial Maximum and associated RSL change on northwest Calvert Island, British Columbia. To investigate this objective, an airborne lidar dataset, sedimentological and stratigraphic data, palaeoecology, and a robust geochronology of 38 radiocarbon and 18 optical ages are used (Appendix 1). A landscape reconstruction from 15.1 ka cal BP to present involved localized proglacial sedimentation, extensive coastal reconfiguration, rapid shoreline

progradation (> 1 m a^{-1}), and isolated aeolian landform development. Together, these findings help fill the spatial and temporal gap in understanding of Late Quaternary landscape evolution on the Cordilleran Ice Sheet margin, inform studies of past climate and ecological conditions, and have implications for recent discoveries of Late Pleistocene human migration and habitation along the BC central coast.

1.2. Research context

1.2.1. The Cordilleran Ice Sheet in the Late Pleistocene – dynamics and legacy

The extent and retreat of the Cordilleran Ice Sheet (CIS) in British Columbia (BC) is summarized in several studies (e.g., Clague and James 2002; Menounos et al. 2009). Most of the evidence for CIS extent at the Last Glacial Maximum (LGM) comes from southern BC and Washington State (Booth et al. 2003), with evidence for sporadic or thin ice cover existing at the LGM at several spots along its western margin: refugia in Hecate Strait and on headlands, islands, and inter-fjord ridges on the west coast of Haida Gwaii (Clague et al. 1982a) as well as the west coast of Vancouver Island (Hebda et al. 1997) (Figure 1). The western terminus of the CIS in central BC is poorly constrained (e.g., Clague and James 2002; Margold et al. 2013; Taylor et al. 2014). Many areas providing data on CIS extent in this region comes from Hecate Strait and northeast Vancouver Island (Barrie et al. 2014), with evidence of ice cover between these two areas coming in the form of glacially-carved troughs in Queen Charlotte Sound (Luternauer et al. 1989) (Figure 1). Generally, coastal portions of western North America were mostly ice free by 19.6 to 19.0 ka cal BP and completely free of ice by 15.9 to 15.2 ka cal BP (Kelly 2003). The decay of the CIS was repeatedly interrupted by glacier still-stands and localized re-advances (e.g., Saunders et al. 1987; Clague et al. 1997; McCrumb and Swanson 1998; Friele and Clague 2002; Kovanen and Easterbrook 2002).

CIS behavior has been modeled using the Puget lobe, a lobe of the CIS that expanded into northwest Washington State, as it is particularly well-constrained, has good chronological control, clearly recognized boundaries, moderately definitive source area, and shows good expression of topographic effects and sedimentary deposits (Booth et al. 2003). Based on the equilibrium line altitude, ice thickness and surface slope calculated in Booth (1986), meltwater flow increases monotonically downglacier and less than 2% of the total ice flow is accounted for by internal deformation. Thus, basal sliding must account for nearly all of the predicted motion, calculated to be several hundred m per year (Booth et al. 2003). This velocity is comparable to measured velocities of modern ice streams (e.g., Alley et al. 1986; Bindschadler and Scambos 1991), thus, this system was one of rapid mass transport under a low driving stress across a bed of mainly unconsolidated sediment (Booth et al. 2003). The ice loading of sediments was low except near the lobe margins due to average pore-water pressures at the bed being near those of the ice overburden (Booth 1991), and, as such, shearing and streamlining were common processes acting on the landscape. This is supported by imagery showing many streamlined forms in the area (e.g., Kovanen and Slaymaker 2004a). The lack of evidence for a frozen substrate means the Puget lobe is a good approximation for most of southwest and coastal BC, as streamlined forms and evidence of subglacial streams suggests large areas of the subglacial bed in this region were unfrozen (Ryder et al. 1991). It is important to note that, although the Puget lobe has been suggested as an appropriate proxy for behavior of the entire CIS, it is likely that local conditions including climate, substrate, and topography all significantly contributed to CIS behavior in other regions. In addition, both Parkin and Hicock (1989) and Hicock and Dreimanis (1985) found evidence of brittle deformation in coastal lodgement tills interpreted to be from the last glaciation, suggesting the possibility that the CIS was polythermal or that the substrate was well-drained.

Sediments deposited as a result of the advance and retreat of the CIS can be organized into a number of well-defined formal stratigraphic units, differentiated based on lithostratigraphy,

allostratigraphy, sequence stratigraphy, and time stratigraphy. Quadra Sand (Clague 1976), ranging in age from about 30 to 20 ka cal BP (Clague et al. 2005), is a pro-glacial outwash stratigraphic unit deposited in front of the advancing CIS, with sequence stratigraphy typically being represented by a coarsening upwards sequence as the CIS became more proximal. It is one of the most conspicuous stratigraphic units in coastal BC and is often used for identifying evidence of the CIS and associated sediments. The lithostratigraphy consists mainly of horizontally and cross-stratified well-sorted sand, however minor silt and gravel exists (Armstrong and Clague 1977). Allostratigraphy of the Quadra Sand typically is represented by overlain till deposited from the advance of the CIS and underlain sediments of the Cowichan Head formation from OIS 3 (Armstrong and Clague 1977). Quadra Sands were deposited between the northern Georgia and southern Puget lowlands (SWC region, Figure 1) ahead of the advancing CIS as distal outwash aprons (Clague 1976). The sand likely accumulated on delta-top floodplains and ponds and in shallow subaqueous delta-front environments (Clague 1986).

Coquitlam Drift (Hicock et al. 1999), the unit representing the Coquitlam Stade that occurred around 21.5 ka cal BP (Ryder et al. 1991), can lie unconformably above the Quadra Sand unit. Again deposited prior to the LGM during a glacial period also referred to the Evans Creek Stade in the United States (Clague 1981), the lithostratigraphy is represented by till, glaciofluvial, ice-contact and glaciomarine sediments deposited as valley and piedmont glaciers pulsed into the Fraser Lowland from the Coast Mountains (Figure 1, section 2). It is differentiated from the later-deposited Vashon Drift by spatial extent, time stratigraphy, and allostratigraphy (it lies below the Vashon Drift), as sedimentology for drift units of the Fraser Glaciation are all very similar (Hicock and Armstrong 1981). Coquitlam Drift is typically overlain by a non-glacial organic-rich sediment package that also contains nonorganic silt, sand and gravel termed the Sisters Creek Formation (Hicock and Lian 1995). This unit represents the retreat of the glacial advance that was recorded in the Coquitlam Drift, and is overlain by Vashon Drift.

Quadra Sand (or Coquitlam Drift, if present) underlies sediments of glacial contact origin known as Vashon Drift, formally described in Hicock and Armstrong (1985). The lithostratigraphy of this unit is reprented by till and glaciofluvial and glaciolacustrine sediments, and the unit was deposited at the LGM in the Georgia basin (east coast of Vancouver Island, Figure 1, section 2), and as such was deposited between 17 and 14 ka cal BP in southwest BC and northern Washington State (Ryder et al. 1991; Hicock and Lian 1995). Flow indicators generally suggest that ice flow was in a southerly direction as ice proceeded down the Puget lowlands, however topographic controls changed flow direction to west down the Juan de Fuca Strait (west coast of Vancouver Island, Figure 1, section 2). The Vashon Drift, as a defined lithostratigraphic unit, is largely confined to southern BC and northern Washington State. However correlative glacial deposits based on time stratigraphy, allostratigraphy, and lithostratigraphy are found in Haida Gwaii (Clague et al. 1982b; Blaise et al. 1990; Mathewes et al. 2015), central BC (Lian and Hicock 2000), and to a lesser extent (as a younger, recessional till) in the Kitimat area (Clague 1984). The till found in Haida Gwaii is less prominent and suggests a lower ice depth and duration, and ice that deposited that unit likely originated from localized ice caps in the Insular Mountains of Haida Gwaii as discussed above (Clague 1981) (Figure 1, section 2). This is a clear example of how local conditions, such as climate or bed conditions, can make stratigraphic correlation across sediments deposited in the Late Quaternary difficult.

Vashon Drift is overlain by the recessional sedimentary unit regionally called the Capilano Sediments or the Fort Langley Formation, deposited between 13 and 11.3 ka cal BP (Clague 1981; Wassenaar et al. 1988). Lithostratigraphy is typically represented by a variety of sediments, including glaciomarine diamicton, marine silt and clay, subaqueous outwash, and deltaic sand and gravel. Sequence stratigraphy exhibits complex facies changes due to spatial and temporal variance in sediment supply as CIS ice decayed. It may contain tills deposited during short-lived re-advance, termed Sumas Drift, whose allo- and time stratigraphy is somewhat disputed but considered to have occurred between

14 and 11.2 ka cal BP (Clague et al. 1997; Kovanen and Easterbrook 2002). The Fort Langley Formation, Capilano Sediments, and Sumas Drift are typically found in southwest BC and Washington State, and are associated with decaying and/or re-advancing glaciers that have not been sufficiently mapped in the coastal regions of central BC to confirm their existence in these areas (Blaise et al. 1990; Barrie and Conway 1999).

1.2.2. Sea level changes following deglaciation in coastal British Columbia

RSL changes since the LGM are the result of many different factors acting on different scales at the earth surface. Factors are either oceanic in nature (eustasy and steric effects) or crustal (deformation, isostasy, and sedimentation), all of which interact to produce highly localized RSL changes at different points along the coast of BC (Shugar et al. 2014). Eustasic sea-level changes occur due to a change in the volume of ocean water (resulting from changes in the volume of ice on land) or changes in the size of the ocean basins (e.g., from sedimentation). There are a number of approaches for modeling eustatic sea-level changes, including growth rates of coral atolls (Fairbanks 1989), modeling of ice volume (Clark and Mix 2002), and tectonically stable coastal shelf deposits (Yokoyama et al. 2000). Steric effects result from the thermal expansion or contraction of ocean water. In the Late Pleistocene and Early Holocene, steric effects were minimal as compared to Late Holocene sea-level change (Smith et al. 2011), however as eustatic and isostatic effects diminished in the Mid to Late Holocene, steric effects became more pronounced. Crustal deformation along active subduction margins (e.g., the southwest BC coast) affect RSL through coseismic and interseismic subsidence and uplift of the land relative to the ocean (Shugar et al. 2014). Isostacy refers to the non-uniform depression of the earth's crust under the weight of ice sheets of varying thicknesses. Clague and James (2002) suggest that isostatic depression ranged from 300 m to 500 m in fjord heads at the base of the Coast Mountains in coastal BC to less than 150 m further west near the ice margin (Figure 1, section 2). Finally, sedimentation can cause RSL

increases (from compaction and loading) or decreases (from accumulation of nearshore sediments), and effects are most typically found at the outlets of large rivers (e.g., Milliman et al. 1989; Day et al. 1995; Mazzotti et al. 2009). Generally, the largest magnitude RSL changes since the LGM have come from a balance of isostatic adjustment of the crust and eustatic changes due to global ice volume.

RSL change in coastal BC is well documented in Shugar et al. (2014), and thus, will only be presented briefly here. In southern British Columbia, rapid deglaciation at the periphery of the CIS led to flooding of isostatically depressed lowlands, with depth of inundation increasing from west (+50 m on the west coast of Vancouver Island) to east (+200 m east of Vancouver, Clague 1981; Bobrowsky and Clague 1992) (Figure 1, section 2). Isostatic rebound was rapid and varied, and regions that were deglaciated first rebounded earlier than those deglaciated later. RSL fell rapidly in the Fraser lowland from 175 m to 60 m above present in less than a thousand years (James et al. 2002), continuing to 11 m below present by the early Holocene (Clague et al. 1982a), rising slowly to present for the rest of the Holocene. On the west coast of Vancouver Island, Late Pleistocene data is limited but suggests marine inundation to 50 m (Bobrowsky and Clague 1992) followed by a rapid fall to 46 m below modern sea-level (Dallimore et al. 2008) before rising to a few m above modern in the early Holocene. RSL has been falling in this area throughout the Holocene due to crustal uplift (Friele and Hutchinson 1993).

On the outer islands of Haida Gwaii (Figure 1, section 2), on the edge of the continental shelf, a markedly different sea-level response occurred (e.g., Clague et al. 1982a; Barrie et al. 1991; Hetherington et al. 2004; Wolfe et al. 2008). This area experienced a glacio-isostatic forebulge, or local uplift of the crust due to nearby ice loading, with RSL between 32 m and 150 m lower than present in the Late Pleistocene and early Holocene (Barrie and Conway 1999; Hetherington et al. 2004). As the forebulge collapsed, RSL rose rapidly to +15.5 m above modern sea-level by the Early to Mid Holocene and fell slowly to modern for the rest of the Holocene (Clague et al. 1982a; Wolfe et al. 2008).

On the central and inner north coast of BC, RSL experienced an east-west gradient controlled by isostatic depression and rebound of the crust due to ice loading. Retherford (1972) describes marine sediments at 230, 160, and 70 m above current RSL on the inner coast, interpreted as Late Pleistocene marine inundation following deglaciation. On the inner north coast, RSL fell from as high as + 50 m quickly to – 6.3 m between 14.5 to 13.5 ka cal BP with RSL rising to + 6 m by 9 ka cal BP followed by a gradual lowering to modern levels during the Holocene (Letham et al. 2016). Sea levels in Queen Charlotte Sound, west of the inner coast, have not been as well constrained, however evidence exists for parts of the Sound being subaerial prior to 9.7 ka cal BP, and thus, experiencing Late Pleistocene and Early Holocene sea-levels lower than present (Hetherington et al. 2004). A RSL change hinge-line between the isostatically depressed inner coast and forebulged outer coast has recently been proposed (McLaren et al. 2014; Shugar et al. 2014). The theory states that a balance between the dominant post-LGM forces on relative RSL in ice-marginal areas—isostatic adjustment and eustatic sea-level changes—must occur in a region that lies near the LGM ice margin. This gradient in RSL responses has been observed in the study area as occurring between the central BC mainland (isostatic depression) through Queen Charlotte Sound (forebulge) within an east to west distance of 75 km (Barrie et al. 2014S; Shugar et al. 2014). This region is one where land subsidence during glaciation and subsequent rebound following deglaciation is equally balanced with eustatic sea-level rise with the demise of the major ice sheets at the LGM.

1.2.3. Tectonic regime of coastal British Columbia

The tectonic regime of coastal BC is complex. On the north coast is a major strike-slip fault slip (Queen Charlotte-Fairweather), and on the south coast is a megathrust subduction fault (Cascadia). The former occurs between the major North American and Pacific Plates, whereas the latter occurs where the relatively young, buoyant crust of the Juan de Fuca Plate subducts under the North American Plate.

In addition, between the two faults, the Explorer Plate and Winona Block (Davis and Riddihough 1982) are independently subducting under the North American Plate (Mazzotti et al. 2003).

The major events associated with megathrust subduction faults are well documented, both including the potential for large earthquakes (e.g., Plafker 1972) and tsunamis (e.g., Kimura et al. 2012). Evidence for major earthquakes is mostly provided by sequence stratigraphy that indicates coseismic subsidence and interseismic uplift in areas on the overlying plate (e.g., Guilbault et al. 1996; Nelson et al. 1996; Shennan and Hamilton 2006). Coseismic subsidence occurs during a megathrust earthquake when the overlying plate drops in elevation following release of strain along the locked portion of the plate boundary, and the effects are typically found in coastal wetlands where soils are buried by marine or littoral sediments (Nelson et al. 1996). Along coastal BC, the last megathrust earthquake, occurring in January 1700 AD (Clague et al. 2000), caused 0.55 – 0.70 m of subsidence on the west coast of Vancouver Island (Guilbault et al. 1996). Evidence exists that large earthquakes (and tsunamis) associated with this subduction zone have occurred six or seven times in the past 3,000 years (Peterson et al. 2012), indicating that this has been a common (geologically speaking) event since the LGM.

Tsunamis generated by crustal movement along the fault boundary during the same event have been shown to inundate coastal areas up to 15-20 m above sea-level at the heads of some inlets (Clague et al. 2000). Coastal effects from tsunamis have included the formation of new inlets and the breaching of barrier islands, erosion in river mouths and tidal channels, the generation of large return channels, or area reduction in reef islands (Ruiz et al. 2013). In coastal BC, geologic evidence most commonly exists as sheets of sand and gravel preserved in stratigraphic sequences that are otherwise dominated by peat and mud (i.e., those found in wetlands) which fine landward and may contain marine fossils (Clague et al. 2000).

Although not considered as dramatic as megathrust fault events, the Queen Charlotte-Fairweather strike-slip fault generates large earthquakes, including an M_w 7.8 occurring as recently as

2012 (Lay et al. 2013). While mainly considered a transform fault, some areas of the fault have a minor thrust component (James et al. 2013, 2015; Lay et al. 2013). During the 2012 earthquake, coseismic displacement of up to a metre occurred on Haida Gwaii (James et al. 2013) as a result of this thrusting plate boundary motion.

1.3. Dissertation structure and conventions

This dissertation is structured around three manuscripts (sections 2, 3, and 4) that were developed from research on Calvert Island that was conducted between May 2012 and July 2015. Section 2 is to be published in the May 2017 issue of Quaternary Research, and section 3 was published in the Journal of Sedimentary Research in January 2017. Section 4 is to be submitted to Boreas. These sections are bookended with an introductory section (1) that sets broader research context and a summary section (5) that reviews key findings of the research.

Horizontal locations are reported in UTM coordinates (zone 9) using the NAD83 datum. Reported elevations in this dissertation are relative to 2012 mean sea-level (msl), based on the geodetic datum CGVD28 and hybrid geoid model HTv2.0. For all data locations, elevation was determined by field GPS collection of horizontal coordinates which were corroborated with a project DEM. This DEM was generated using airborne lidar data that were collected in August 2012 from a fixed wing aircraft at a flight height above the ground surface of 1150 m. The average below-canopy ('ground') point density throughout the study region was approximately 1 pt m^{-2}. This was interpolated into a 2m resolution DEM using the nearest neighbour method (using the average elevation per pixel) and vertical accuracies of $\pm$ 0.15 m can be assumed based on calibration of the raw lidar data.

Reported ages in this dissertation are in calendar years BP (before present, AD 1950). Calibration of radiocarbon ages was carried out using the Calib 7.0 program (Stuiver et al. 2013), using the INTCAL13 dataset for terrestrial samples and MARINE13 dataset for marine samples, with a lab error multiplier of

1. For marine samples, a reservoir correction (331 a) was applied based on the weighted mean of the 10 nearest known-age samples (see http://calib.qub.ac.uk/marine/). For optical dating, an experimental procedure was developed specifically for the sands found on Calvert Island, and a summary is provided in Appendix 3. Full details are published in Neudorf et al. (2015b).

2. A glacial re-advance during retreat of the Cordilleran Ice Sheet, British Columbia central coast

2.1. Abstract

Descriptions of the Cordilleran Ice Sheet retreat after the Last Glacial Maximum (LGM) have included short-lived re-advances occurring during, or as a result of, the Older and Younger Dryas stadial periods and into the Holocene, but identification of these events has been largely limited to southwest and central British Columbia and northwest Washington State. We present evidence of a Late Pleistocene re-advance of Cordilleran ice occurring on the central coast of British Columbia on Calvert Island, between northern Vancouver Island and Haida Gwaii. Evidence is provided by sedimentological and palaeoecological information contained in a sedimentary sequence combined with geomorphic mapping of glacial features in the region. Results indicate that a cold climate existed between 15.1 and 14.3 ka cal BP and that ice advanced to, and then retreated from, the western edge of the island between 14.2 and 13.8 ka cal BP. These data provide the first evidence of a major fluctuation in the retreating ice sheet margin in this region, and suggest that a cold climate was a major factor in ice re-advance. These data contribute to the understanding of past temperature, ice-loading and crustal response, the nature of ice margin retreat, and the palaeoenvironment of an understudied area of the Pacific Northwest.

Keywords: Cordilleran Ice Sheet, Late Pleistocene, glacial re-advance, geomorphic mapping, stratigraphy, palaeoecology, macrofossils, Dryas

2.2. Introduction

Although the timing and extent of advance and retreat of the Cordilleran Ice Sheet (CIS) in the Pacific Northwest is well documented along its southern and northern margins (e.g., Clague et al. 1980; Hicock et al. 1982; Barrie and Conway, 1991; Jackson et al. 1991; Easterbrook 1992; Clark et al. 1993; Clague et al. 1997; Hebda et al. 1997; Clague and James 2002; Kovanen and Slaymaker 2004a, b; Lakeman et al. 2008; Taylor et al. 2014), little is known about the pattern of retreat along the central coast of British Columbia (BC) (e.g., Clague 1985; Luternauer et al. 1989; Barrie et al. 1991). This gap in knowledge is likely due to landform preservation and exposure in the region, with the majority of the landforms associated with the western termini of the CIS on the central coast currently submerged at the edge of the continental shelf, in Queen Charlotte Sound (cf. Clague and James 2002). In addition, the BC central coast is well-forested, in places has high relief, and is sparsely populated, leading to difficulties with access and landform identification from conventional remotely sensed data sources (e.g., aerial photography and satellite imagery). Accessibility to this coastline has recently been improved, with the founding of the Hakai Institute on Calvert Island (Figure 1), which supports several collaborative geographical, geological, biological and archaeological research projects along the central coast.

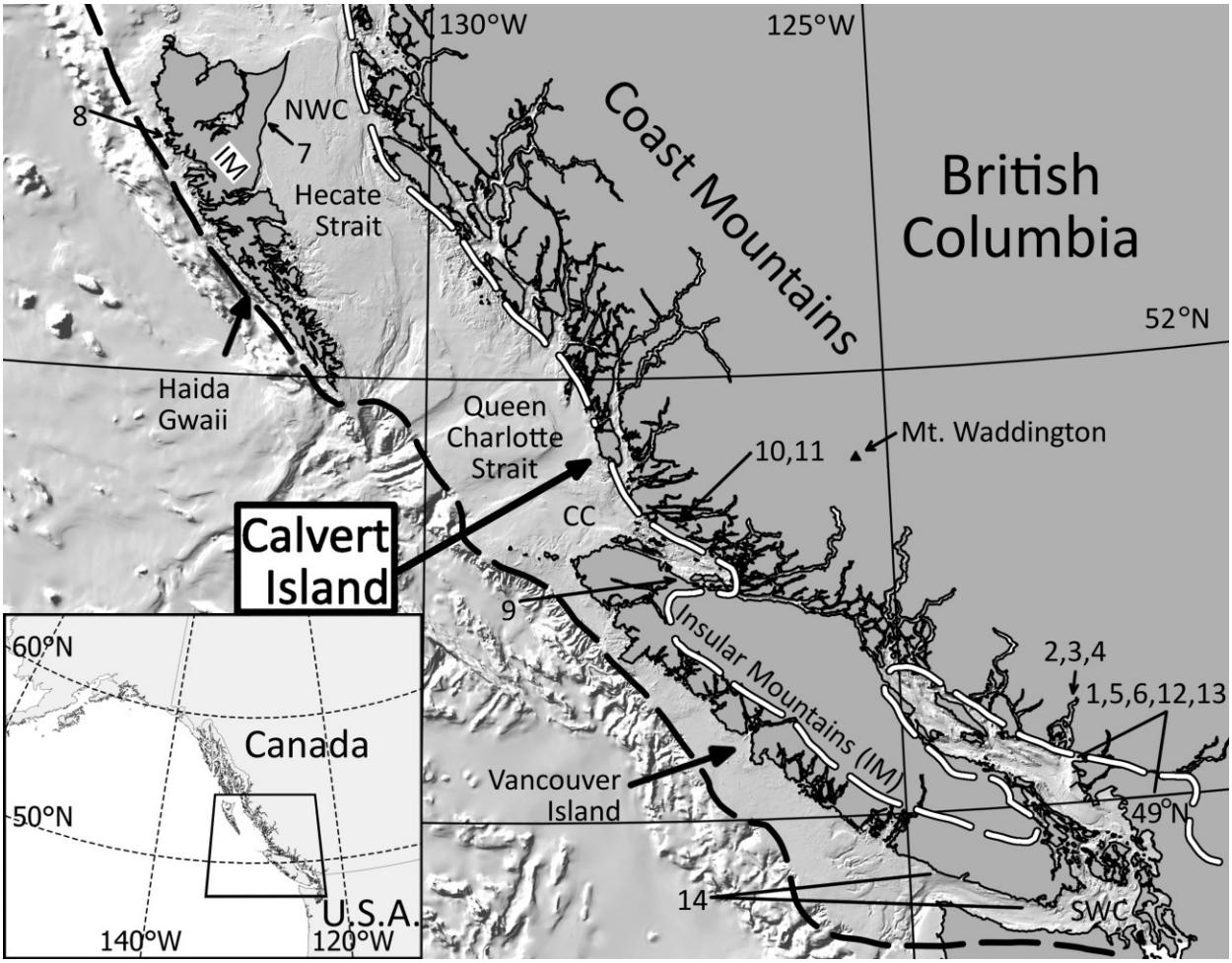

Figure 1. Study area (Calvert Island) on the central coast of British Columbia. Inset map shows the location of Figure 1 (black square). Source areas for Cordilleran Ice include the Coast Mountain range and the Insular Mountains on Haida Gwaii and Vancouver Island. Dashed lines show ice extent at the Local Last Glacial Maximum (18 ka, black) and the early stage of deglaciation (14 ka, white) from Taylor et al. (2014). Regions of palaeoclimate reconstructions using lake cores (referred to in the discussion) are provided: NWC = the north west coast, CC = central coast and northern Vancouver Island, and SWC = south west coast (including the Fraser and Puget lowlands). Sites presented in Figure 6 are numbered as follows: 1. Locations of Sumas phase II,III,IV (Kovanen and Easterbrook 2002), 2. Squamish moraine (Friele and Clague 2002), 3. Squamish valley kame (Friele et al. 1999), 4. Howe Sound moraine (McCrumb and Swanson, 1998), 5. Chilliwack Sandur (Saunders et al. 1987), 6. Bradner Pit (Clague et al. 1997), 7. Cape Ball (Warner 1984), 8. Hippa Island (Lacourse et al. 2012), 9. Misty Lake (Lacourse, 2005), 10. Woods Lake (Stolze et al. 2007), 11. Tiny Lake (Galloway et al. 2008), 12. Marion Lake (Mathewes and Heusser 1981), 13. Mike Lake (Pellatt et al. 2002), 14. East Sooke Fen, Pixie Lake, and Whyac Lake (Brown and Hebda 2002).

The chronology of growth and decay of the CIS for all of BC is summarized by Clague and James (2002), and more recently by Menounos et al. (2009), with most of the evidence for ice extent coming from southern BC and Washington State (Booth et al. 2003). Evidence for sporadic or thin ice cover at the last glacial maximum (LGM) exists in several places along the western CIS margin. In northwest BC,

biological refugia were postulated in Hecate Strait, on nunataks in the Insular Mountains, and on headlands, islands, and in inter-fjord ridges on the west coast (Clague et al. 1982a; Mathewes et al. 2015). The western terminus of the CIS (e.g., Margold et al. 2013; Taylor et al. 2014; Figure 1), with a postulated refugium on Brooks Peninsula (Hebda et al. 1997), suggests that ice did not quite reach the edge of the continental shelf along the entire west coast of Vancouver Island. Along the central coast of BC, ice advanced down fjords and valleys of coastal mountains and extended out on to, and in places to the edge of the continental shelf (Josenhans et al. 1995). The extent of ice cover on the continental shelf between Haida Gwaii and northern Vancouver Island is still poorly constrained, with most of the data for the region coming from Hecate Strait and northeast Vancouver Island (Barrie et al. 2014). Geomorphic evidence exists for ice streaming onto the shelf edge in several large glacially-carved troughs (Luternauer et al. 1989; Mathews 1991), but till was either not deposited in them, or was eroded during periods of subsequent sea-level change that may have exposed the troughs to wave and tidal erosion (Barrie et al. 1991). Ice from the northern Coast Mountains that had previously coalesced with glaciers from Haida Gwaii started to retreat between 18.3 and 17.0 ka cal BP (Blaise et al. 1990) and between 16.0 and 14.2 ka cal BP the ice sheet had retreated from Hecate Strait with mainland ice confined to fjords (Clague 1985). In general, coastal portions of western North America once covered by the CIS were completely free of ice by 15.9 to 15.2 ka cal BP (Kelly 2003).

The decay of the CIS was repeatedly interrupted by glacier still-stands and localized re-advances (e.g., Saunders et al. 1987; Clague et al. 1997; McCrumb and Swanson 1998; Friele and Clague 2002; Kovanen and Easterbrook 2002). Climate may have been a mechanism for ice re-advance, as there are several well-documented post LGM cold-climate periods, for example the Older Dryas (14.1 ka cal BP), Inter-Allerod (13.2 ka cal BP), and Younger Dryas (12.3 ka cal BP) (Lowe et al. 2001), or the Heinrich event 1 period (17.5-14.7 ka cal BP) marked by warm-cold oscillations (Kiefer and Kienast 2005), that have affected the Pacific Northwest (Kienast and McKay 2001; Menounos et al. 2009). For instance, the

Younger Dryas, which may have been a global phenomenon, has been linked to several advances along the CIS margin (e.g., Mathewes et al. 1993; Gosse et al. 1995; Lowell et al. 1995; Benson et al. 1997; Hendy et al. 2002). Lakeman et al. (2008) provides a review of CIS ice advances that occurred during the Younger Dryas interval, and more recently Mood and Smith (2015) document a Younger Dryas aged glacial advance on Mt. Waddington, 200 km east of our study area on Calvert Island. Some disagreement exists on the timing and extent of what is termed the "Sumas Stade" (see Clague et al. 1997; Clague et al. 1998; Easterbrook and Kovanen 1998), a period of Late Pleistocene local ice advance along the southern CIS margin. Kovanen and Easterbrook (2002) argue for three or four advances in the Fraser and Puget lowlands that are coincident with the Inter-Allerød cold period and Younger Dryas data. In contrast, Clague et al. (1997) and Hicock et al. (1999) present differently-timed, non-climatological mechanisms for ice re-advance (discussed below). Friele and Clague (2002) found evidence that glaciers advanced twice in Howe Sound, a fjord in the Coast Mountains immediately northwest of the Fraser Lowland, and that the advance may correspond with the Sumas event and Younger Dryas cold climate period. Pre-Younger Dryas glacial advances have also been identified in the southern Canadian and northern American Rocky Mountains (Osborn and Gerloff 1997) and are reviewed by Menounos et al. (2009).

The above glacial re-advances may have been triggered by changes in climate, but others may have been the result of other mechanisms, associated RSL changes (which include eustatic and isostatic effects), grounding line flux, and changing subglacial conditions (e.g., Hicock et al. 1999, Kovanen and Slaymaker 2003, Menounos et al. 2009). For example, Clague et al. (1997) provide evidence for two "Sumas" advances older than the Younger Dryas cold climate period. Hicock et al. (1999) suggest that deformable bed conditions (soft, wet, muddy substrate) present in the now-subaerial Fraser Lowland may have been another factor contributing to localized ice advance. Menounos et al. (2009) discuss how topographic effects, such as elevation-driven resurgent alpine glaciers that came in to contact with

stagnant ice of the CIS, or small aspect-driven cirque glaciers forming in basins that were previously ice free, may also have contributed to localized ice re-advance already initiated by some other driving force.

Calvert Island contains several distinct landforms and a sedimentary sequence that provides data on the nature and timing of an advance and retreat of glaciers in the region during the overall retreat of the CIS. In this section we: 1) describe and interpret the sedimentary sequence, 2) present information on the age of the glacial advance that deposited the sediments, 3) describe the palaeoecology inferred from organic material found in sediments deposited just prior to the advance, and 4) discuss the implications of these data as they pertain to regional geomorphology, climate, ecosystems, and deglaciation in coastal BC and other regions of the CIS.

2.3. Study area

Calvert Island is located on the central coast of BC in Queen Charlotte Sound, about 70 km northwest of Vancouver Island and about 200 km southeast of Haida Gwaii (Figure 1). Bedrock is composed mainly of early Cretaceous tonalite, quartz diorite, granite, granodiorite and diorite of the Calvert Island Pluton with diorite-dominated rocks of unknown age cropping out mostly in the central, eastern, and southeastern parts of island (Roddick 1996). Relief in the area ranges from mountains as high as 1017 m (Mount Buxton) to relatively flat alluvial plains formed in glacial sediments near present sea-level. The western coastline is predominantly bedrock, with accretionary shoreline characterized by cobbly to sandy embayments (with localized coastal dunes), tombolos, and spits. Exposed glacial sediments on Calvert Island are largely confined to the central-west portion of the island, with the landscape otherwise notably absent of much surficial cover, particularly in the northwest. Moraines are small (generally less than five m high and 25-35 m wide) and most are isolated, except along the west central coast where a series of what are likely recessional moraines exist. Small areas of glaciofluvial outwash exist in the northwest part of the island adjacent to the moraines. Raised (relict) shorelines and

extensive relict beach plains also exist, however sea-level has fluctuated less than a few m since near the end of the Late Pleistocene (McLaren et al. 2014). This is a postglacial RSL response markedly different from those in nearby areas on the coast where fluctuations of more than 100 m were common (Shugar et al. 2014).

2.4. Methods and data

2.4.1. Geomorphology and geography of surficial deposits

Information on surficial landforms and related deposits was collected using airborne lidar data collected in August 2012 from a fixed wing aircraft at an altitude above ground level of 1150 m (requests for these data can be made at http://data.hakai.org/). The average below-canopy ('ground') point density throughout the study region was approximately 1 pt m^{-2}, however, in some areas the point density was closer to 2 pts m^{-2}. These data were used to create a 2 m resolution bare earth digital elevation model (DEM), using the nearest neighbor interpolation method and the inter-cell average elevation (Figure 2). Coincident 0.15 m-resolution digital orthophotos were also collected and used to aid in analysis. These data were largely used to identify and delineate glacigenic features on the landscape, including a semi-continuous moraine that extends across the northwest of Calvert Island (Figure 2).

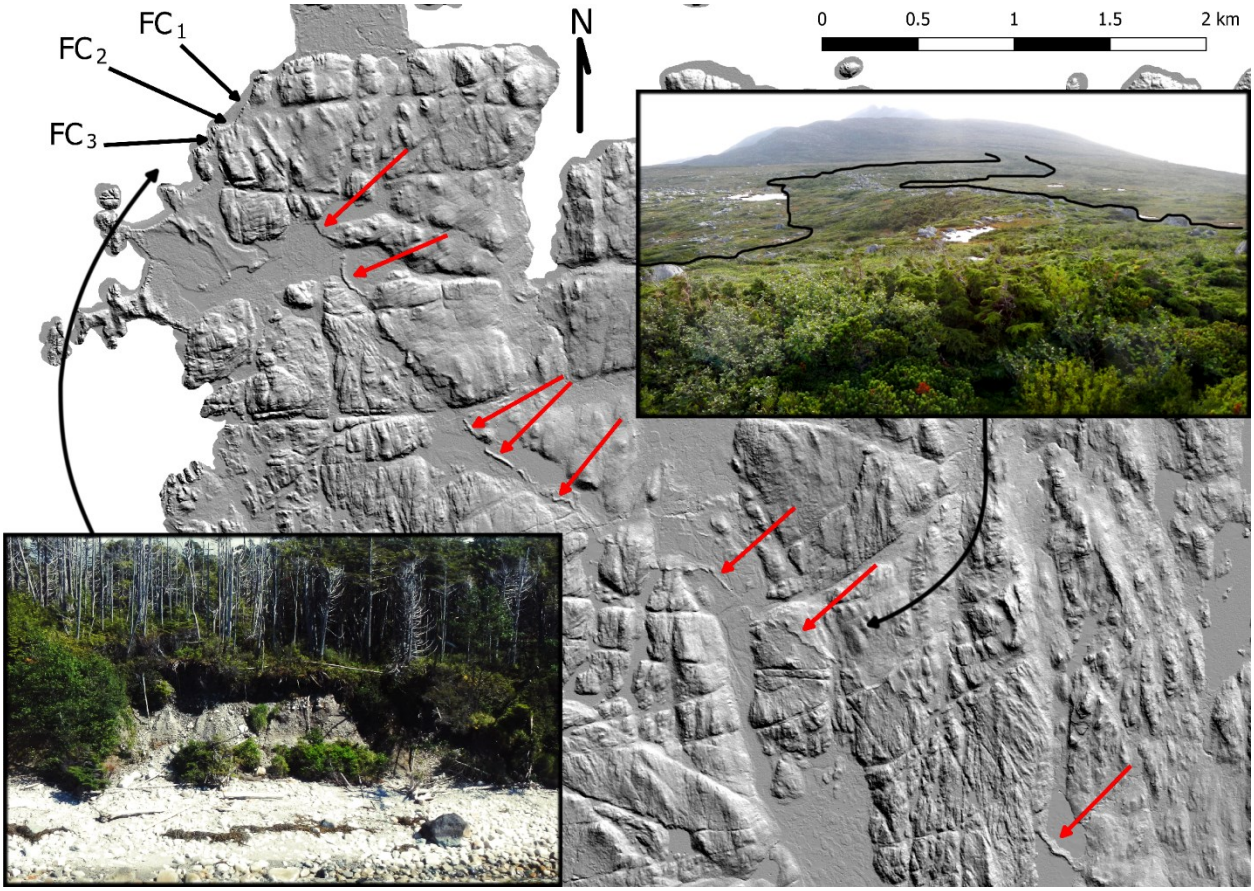

Figure 2. Bare-earth lidar hillshade of the northwest corner of Calvert Island. The location of the three stratigraphic sections (FC_1, FC_2, FC_3) are shown. Red arrows highlight the semi-continuous moraine that extends south-east from these exposures. This moraine is shown (and outlined) in the upper inset photo. The lower inset photo is an oblique airphoto showing the coastal north-northwest facing bluff that contains section FC_1; the orientation of the photo is looking south-southeast.

2.4.2. Stratigraphy and geochronology

The stratigraphy exposed at Foggy Cove, a wave-cut bluff on northwest Calvert Island, was analyzed in three sections (FC_1, FC_2, and FC_3, Figures 2, 3, 4) between 2012 and 2014. Lithostratigraphic units were identified based on colour, texture, sedimentary structures, clast lithology and shape, and the nature of contacts between units. The strike and dip of planar structures and the trend and plunge of stone long (*a*) axes (clast fabrics) in diamictons were measured using a Brunton structural compass or a Suunto compass with a dip needle. Only clasts with *a*:*b* ratios $\geq$ 1.5:1 were measured, and an attempt was made to keep a single fabric measurement (consisting of >50 individual clasts) within a zone of 2 m^2.

Fabric data were analyzed using Stereonet 9 (Allmendinger et al. 2012, Cardozo and Allmendinger 2013) and the orientation tensor (eigenvalue) method (Mark 1973). The results were plotted as contoured lower hemisphere equal-area projections. The size, shape and lithology were recorded for clasts in diamicton used in fabric analysis that were >0.01 m in diameter (*b*-axis), while matrix samples (or a bulk sample, if clasts were <0.01 m diameter) were collected from all sedimentary units for grain size analyses. Grain size analysis was performed by mechanical sieving using W.S. Tyler Canadian Standard Sieve Series at quarter-ϕ intervals for grain sizes between -1 and 4 ϕ (2 and 0.062 mm), and a Malvern Mastersizer laser granulometer for grain sizes between 3.5 and 10 ϕ (0.075 and 0.001 mm). Overlap was used to determine the offset, if any, of the two methods for grain size determination (Shugar and Clague 2011). The method of Folk and Ward (1957) was used for analyzing grain size distributions and for derivation of grain size classes and physical descriptions. Appendix 1 provides the metadata and ages of samples collected for accelerator mass spectrometry (AMS) radiocarbon dating, with a description of sample location and type given in the results section below.

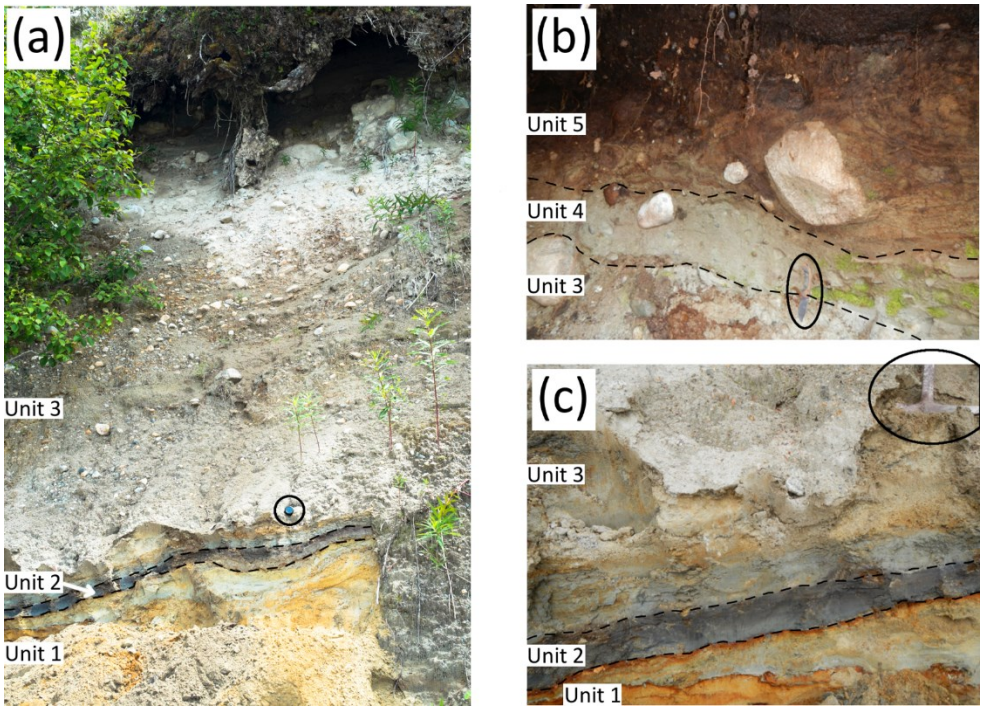

Figure 3. The lithostratigraphic units described in this study: (a) Section FC_1, with camera lens cap for scale, (b) section FC_3, with pocket knife for scale, and (c) close up view of the base of section FC_1, with rock hammer for scale.

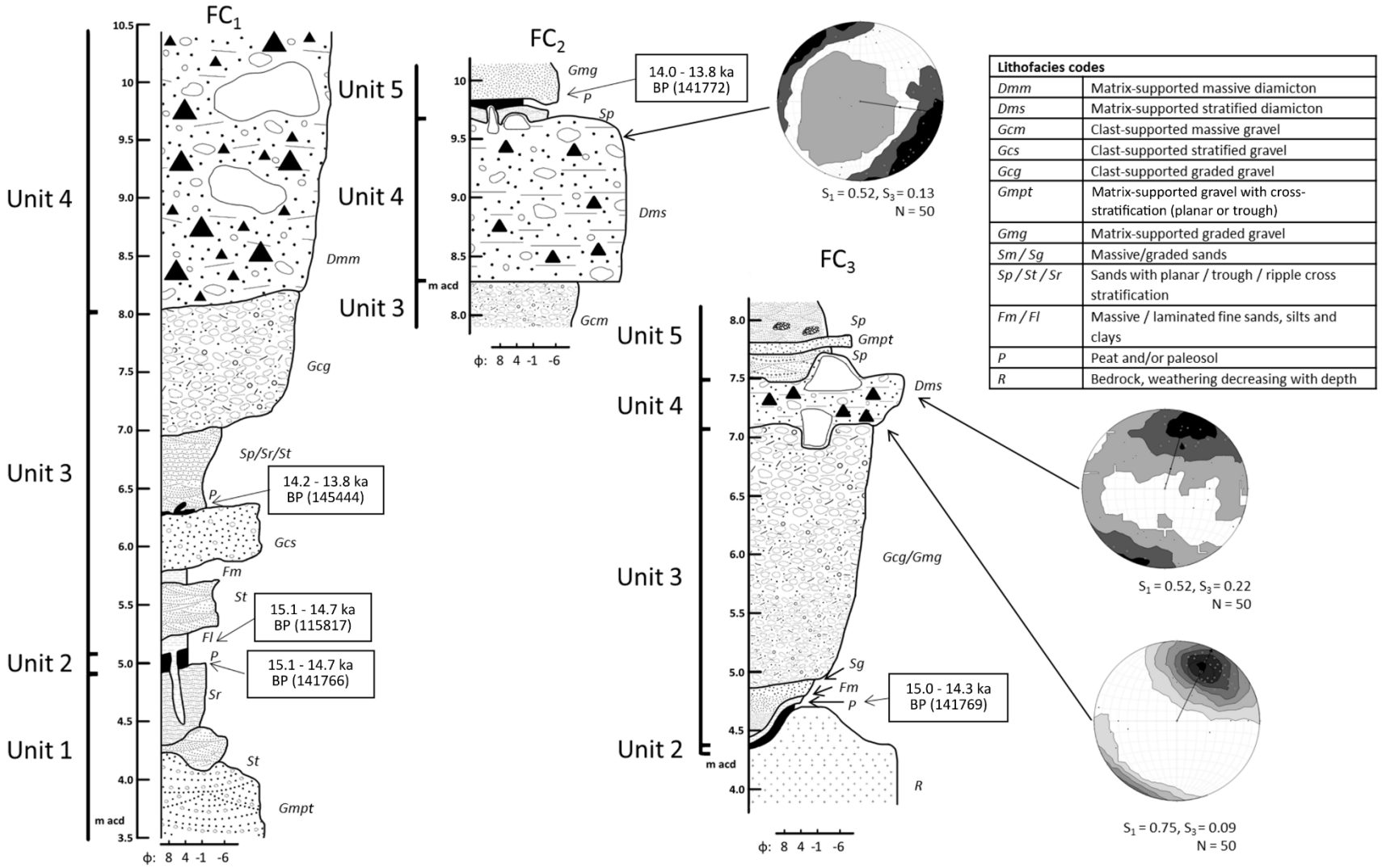

Lithofacies codes	
Dmm	Matrix-supported massive diamicton
Dms	Matrix-supported stratified diamicton
Gcm	Clast-supported massive gravel
Gcs	Clast-supported stratified gravel
Gcg	Clast-supported graded gravel
Gmpt	Matrix-supported gravel with cross-stratification (planar or trough)
Gmg	Matrix-supported graded gravel
Sm / Sg	Massive/graded sands
Sp / St / Sr	Sands with planar / trough / ripple cross stratification
Fm / Fl	Massive / laminated fine sands, silts and clays
P	Peat and/or paleosol
R	Bedrock, weathering decreasing with depth

Figure 4. Stratigraphic logs of three key sections exposed at Foggy Cove (FC_1, FC_2, and FC_3). Stone a-axis fabric diagrams shown with number of clasts measured (N) and eigenvalues S_1 and S_3. Radiocarbon ages are shown calibrated, with the laboratory number in brackets (Appendix 1).

2.4.3. Macrofossils

A cube of fibrous, organic-rich material, 0.05 m per side, was collected from silt and fine sand at the base of section FC_1 (Figure 3, unit 2) and was analyzed for plant and insect macrofossils. The procedure for isolating macrofossils for analysis involved the standard technique of wet sieving with warm tap water (Warner 1990; Birks 2001) with slight modifications: the sample was soaked in warm water and the organic material floating on the surface was gently decanted into a 100 mesh Canadian Standard Tyler series sieve (mesh opening 0.15 mm). The remaining sample was sieved through nested 20 and 40 Canadian Standard Tyler series sieves (mesh opening 0.85 mm and 0.425 mm, respectively) using a swirl technique to separate the organic fraction from the fine sand mineral component. The float fraction (>0.15 mm) and all material greater than 0.425 mm were examined using a binocular microscope, and plant and insect fossil remains were isolated for identification and for potential AMS ^{14}C dating.

2.5. Results

2.5.1. Lithostratigrahic units – descriptions and chronology

Sedimentary exposures on Calvert Island are uncommon; areas of exposed bedrock with little to no surficial sediments being common. Wave eroded dunes are, in places, found landward of sandy beaches in the northwest of the island, while mass wasting on the central-east mountainous areas has exposed thin sediment covers consisting of silt, sand, and gravel. The thickest exposures of sediments found to date (> 40 m), interpreted to be glacigenic, are exposed in the sea cliffs behind 3 Mile Beach on the west coast near the centre of the island. These exposures are difficult to access, but are a target for future work.

The sediments in Foggy Cove sections FC_1, FC_2, and FC_3, can be divided into five lithostratigraphic units (Figures 3, 4) and these are described and interpreted below, with unit numbers increasing from the base. Andrews and Retherford (1978) described and interpreted similar stratigraphy in the northwest part of Calvert Island close to the site used for this study, however they did not provide precise coordinates for their sections. Our field observations do not closely match theirs, which included ~3 m of till at elevations where the sediments are determined to be outwash in this study (3.5 – 6.5 m above msl) and a radiocarbon age from bulk organic material collected at the top of their section (6780 ± 360 BP; GaK-5302) that Andrews and Retherford (1978) suggest was likely a minimum age due to contamination from groundwater exchange (refer to Figure 4 from this study and Figure 2A from Andrews and Retherford (1978) for differences in stratigraphic and sedimentologic observations at Foggy Cove). These differences may be due to more than three decades of bluff erosion.

Unit 1 is 1–3 m thick and is exposed for several tens of m along the bluff. The variable apparent thickness is due to an overall strike and dip of the beds of 350°/25°, which results in a thinner exposure to the east as the unit dips into the modern beach. It is absent at section FC_3, as unit 2 at FC_3 section lies directly on bedrock. Unit 1 was not observed at section FC_2, but it may underlie slumped sediment at the base of the section. Unit 1 consists of three beds: The lowest bed, 0.75 m thick, is mostly matrix-supported and consists of sub-rounded pebbles of mixed lithology that grade into very poorly sorted (polymodal), clast-supported, sub-angular gravel. Trough and planar cross-bedding were observed in this bed. A lower contact was not observed as the unit becomes obscured at the base by modern beach and colluvial deposits. The spaces between the pebbles are filled with a pinkish grey (5YR 6/2) coarse sand matrix, and in rare places the matrix is absent of clasts and shows horizontal laminae that are black (10YR 2/1). The middle bed, 0.40 m thick, consists of trough and planar cross-bedded, moderately sorted, coarse sand with a few lenses of gravel. The sand is red (2.5YR 4/8) and, in places, thin cemented zones are found between bedding planes. Channel bed erosion and subsequent infill is observable at

several locations in this bed. The lower contact is sharp and undulatory. The upper bed of unit 1, 0.65 m thick, has a sharp highly undulatory lower contact. It consists of inversely graded light red (2.5YR 6/6) and light reddish grey (2.5YR 7/1) sand, with the grey tones dominant in the finer fraction of sediment (fine sand and silt). The sediment has a trimodal size distribution, and is poorly sorted, containing some silt and gravel.

Unit 2 is composed of one bed that is 0.10 m thick. It is laterally uniform in thickness and composition, and was observed at sections FC_1 and FC_3. The only difference between the two sites occurs below unit 2, where at FC_3 the contact is more undulatory and unit 1 is absent. Unit 2 is organic-rich (80% organic matter by volume), and contains very dark grey (10YR 4/1) poorly sorted very fine sand. Organic material is spread evenly throughout the unit and consists mainly of compacted, matted vegetation containing macrofossils. Minor gravel exists as outsized lonestones; there is a high proportion of silt (36%), and there are no observable sedimentary structures. Three samples of this unit were collected for radiocarbon dating (Appendix 1): Two samples were extracted from bulk sediment collected vertically across the unit at FC_1 and FC_3 (sample CIRC15b was collected near the base of the unit and sample CIRC18c was collected near the top, both representing a time-of-death for marsh vegetation) and a wood fragment (sample CIRC14) was collected from the middle of the unit at FC_1. This bed has the best chronological control, with three radiocarbon ages (Appendix 1, Figure 4) that collectively constrain its deposition to between 15.1 and 14.3 ka cal BP.

Unit 3 is between 2 and 3 m thick and consists of more than five beds with particle sizes ranging from medium silt to cobbles, with each individual bed ranging from 0.10 m to 1.5 m thick. The lower contact of unit 3 is gradational and no more than 1 cm thick. The sediment type in the lowest bed (which is 0.10 m thick) is light grey (10YR 7/1), poorly sorted medium silt with minor (0.2%) gravel and sand. Little to no organic material is observed in the lower bed of this unit. At one location, sediments at its base have been injected downward ~1 m, through unit 2 and into unit 1. Above the lowest bed, a series

of beds that coarsen upward (Figures 3, 4) occur. Vertical organization of the beds varies laterally across the exposure, but generally beds above the lowest one are composed of moderately well sorted light brown (7.5YR 6/3) medium sand that has trough (major) and planar (minor) cross-bedding. Above the cross-bedded sands, beds are grey (5Y 5/1) and consist of clast-supported, cobble diamicton with minor boulder sized clasts (>0.5m diameter) in a poorly sorted, very coarse, sand matrix. In places, along the exposure, alternating beds of clast-supported gravel and well-sorted sands are observed, and in others, reverse grading is observed. The sediments within the alternating beds typically have the strongest expression of cross bedding and their thicknesses vary across the exposure from ~0.1 to ~3 m, although generally the beds containing larger clast sizes are thicker. Cobbles are sub-rounded and dominated by the local granodiorite lithology with minor amounts (10%) of allogenic basalt and greenstone clasts. Striae or stoss-lee features indicative of subglacial transport or deposition on clasts are absent. In the middle of unit 3 (1.4 m above the lower contact) is an undulatory bed of organic-rich, dark reddish brown (5YR 2/2) fine sand that has well-preserved sharp lower and upper contacts. At the upper and lower contacts of the organic-rich sediments are beds of light grey (10R 7/1) fine sand with planar cross bedding. Continuity of the bed and preservation of the contacts suggest in-situ deposition. Radiocarbon dating of a wood fragment indicates that the organic-rich layer contains plant material that had died between 14.2 and 13.8 ka cal BP (sample CIRC25, Appendix 1, Figure 4).

Unit 4 consists of a single bed, up to 1.5 m thick, of clast-poor, highly compacted, massive, matrix-supported diamicton. The lower contact is undulatory and sharp. Clasts are subangular, a large proportion (65%) are sub-spherical, and few had stoss-lee (bullet) forms, and no striations could be seen on their surfaces. Clasts ranged in size from pebbles to boulders > 2 m in diameter. Clasts are largely of local provenance (80% granodiorite) but some are volcanic and metamorphic in composition. The matrix is poorly sorted, dominated by grey (5YR 6/1) fine sand and medium silt, and is notably finer than the matrix in unit 3. Pebble *a*-axis fabric was measured near the top of unit 4 at sections FC_2 and FC_3 and at

the base of the unit of section FC_2. The fabrics taken from the top of the unit have spread unimodal distributions with trend/plunge values of 22°/16° and 126°/9°, respectively (S_1 values of 0.52), however, the fabric taken from section FC_2 is a stronger (S_1 value of 0.75) unimodal distribution, with the principal eigenvector (V_1) plunging 24° to the northeast (33°).

Unit 5 is 0.6 m thick, and has an upper contact that disappears under the overhanging root mat at both sections FC_2 and FC_3; the unit is not observed at section FC_1. Unit 5 consists of multiple beds of planar and trough cross-bedded fine, medium and coarse sands with minor gravel, as well as gravel beds that are matrix supported and are either graded or showing minor cross-bedding. The coarse sand is reddish brown (5YR 4/4) and the medium and fine sands are grey (5YR 6/1). A few cobbles and boulders are present, and these are sub-rounded to rounded. The lower contact is undulatory and sharp, and in places, drapes over boulders in unit 4. Coarse sand is localized in lenses to the west of the boulders. At section FC_2, an organic-rich bed containing fossil roots and wood fragments is found near the base of this unit (Figures 3, 4); one of the wood fragments yielded a radiocarbon age between 14.0 and 13.8 ka cal BP (sample CIRC20a, Appendix 1, Figure 4).

2.5.2. Macrofossils - unit 2

The distinctive carpels of *Triglochin maritima* (seaside arrowgrass) (Figure 5a), an aquatic or semi-aquatic grass of wet habitats of tidal marshes, mudflats, ponds and wet meadows are fairly abundant in unit 2. Equally abundant are seaside arrowgrass stalk fragments (Figure 5b) of which one was radiocarbon dated from this unit (Appendix 1, 15.1 to 14.7 ka cal BP, sample CIRC15b). Next abundant are *Carex* lenticular type (sedges) a grass-like perennial herb found primarily in wetlands such as marshes, calcareous fens, bogs, peatlands, ponds, stream banks, riparian zones, and alpine tundra (Jermy et al. 2007). Minor occurrences of other plants and shrubs include *Fragaria chiloensis* (coastal or beach strawberry), and *Empetrum nigrum* (crowberry). Beach strawberry is common in present-day

coastal BC, being found on dry to mesic sand dunes and rocky coastal bluffs just above high tide. The decumbent evergreen crowberry shrub can be found growing in the lowland to alpine zones in wet to moist bogs, meadows, open forests, alpine fellfields, and cliffs in BC. Mosses are not abundant with only stem fragments of a few species being recovered, none of which were *Sphagnum* sp. (sphagnum moss). Noteworthy is the absence of any macrofossil remains of treed species.

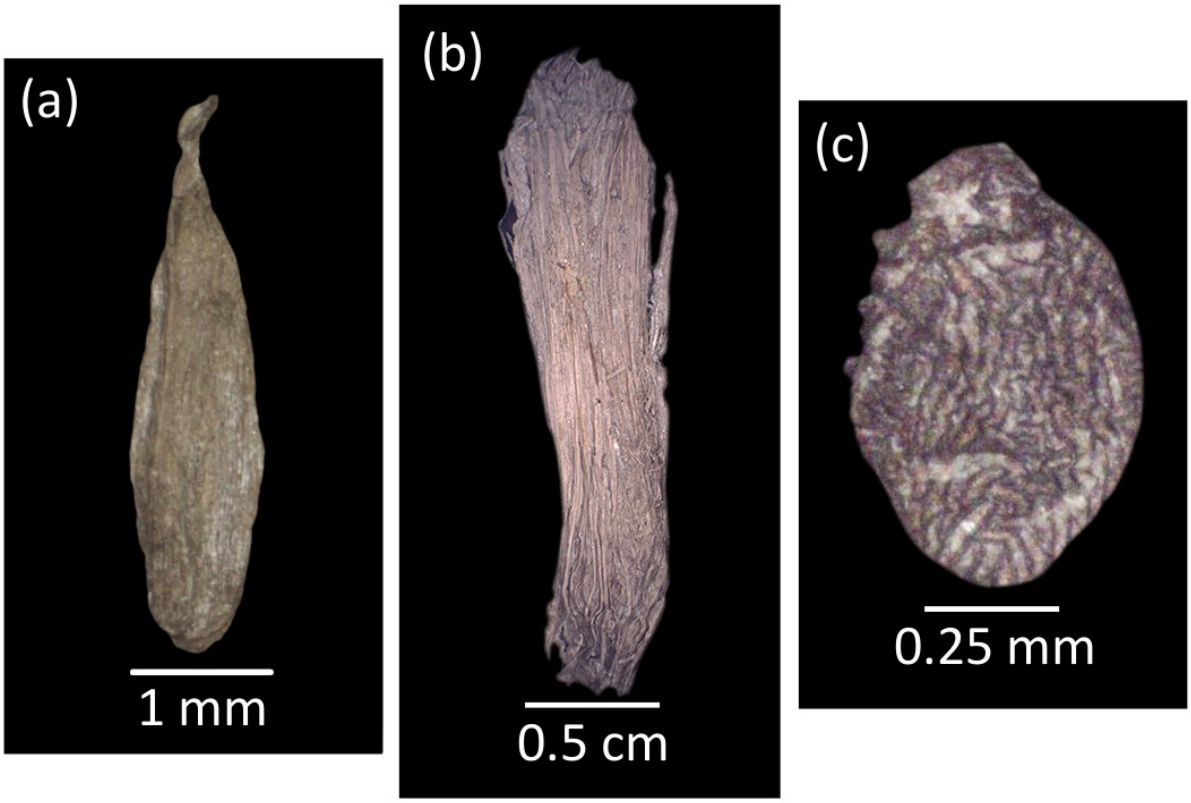

Figure 5. Examples of key macrofossils collected from unit 2. (a) Carpel of *Triglochin maritima* (seaside arrowgrass). (b) Stalk fragment of *Triglochin maritima*. (c) Fossil *Ameronothrus lineatus* (oribatid mite).

Fossil insects include *Saldidae* (shore bugs), *Cicadellidae* (leafhoppers) and *Hydraenidae* — *Octhebius* sp. (minute moss beetle). Shore bugs inhabit beaches and shore lines of lakes, streams and ocean as well as springs, bogs, and salt marshes. They are able to survive in or on the water surface or when they are submerged on beaches at high tide (Usinger 1968). Members of the minute moss beetles are found at the water's edge in both lacustrine and fluvial habitats as well as intertidal areas (littoral

zone substrata). Many *Diptera* (fly) pupae of one type occur in unit 2. Although the pupae could not be identified, they most likely belong to flies that live and forage along the wrack zone just above the mean high tide line where debris is deposited on the sand. Arachnids included *Erigone* sp. (dwarf spider) and, of particular interest, the oribatid mite *Ameronothrus lineatus*. Species of *Erigone* are small spiders that live near water where they place their 5 cm square webs between grasses (Bristowe 1958). Some species are found on the seashore (e.g., *Erigone arctica*) where they spin webs in cavities of vegetation and amongst pebbles where the sea covers them at high tide. They survive under water with air stored in their book lungs and trachea (Bristowe 1958). Abundant *A. lineatus* fossils were identified (Figure 5c) – a species that is common along seashores in the littoral zone (Hammer 1952), and can be found between the high water mark (rarely inundated) to the upper sub-tidal zone areas that are permanently submerged. *A. lineatus* has an Arctic and subarctic distribution and occurs today in coastal areas in the Yukon Territory, Northwest Territories and Nunavut, but not in present day BC; they can tolerate extreme cold weather (Coulson and Birkemoe 2000).

2.6. Discussion

2.6.1. Unit interpretation

Sediments exposed at the base of the coastal bluff at Foggy Cove (unit 1) were deposited in a fluvial or deltaic environment, or possibly a transition between the two as grain size decreases upward in the unit. Trough cross-bedded sand and gravel that generally fine upwards and contain erosional and undulatory contacts between the beds indicate a migrating channel system, consistent with a braided stream network. The silt and fine sand near the upper portion of the unit represents a more quiescent, or distal, zone of deposition, however, poorly sorted sands, gravels, and silts suggest a varying energy regime consistent with migrating channels. This sequence indicates either a minor transgression of sea-

level (cf. McLaren et al. 2014) or a change in the basin configuration (such as the development of a marsh), with fluvial sediments being deposited in a gradually deepening water column.

Unit 2 was deposited in a tidal marsh, as evidenced by the fine-grained sediments and fossil assemblage. The modal grain size is a very fine sand, suggesting that the sediments in this unit were deposited in a low energy setting. The rare clasts of gravel may have a glacigenic origin (ice-rafted debris), a low energy fluvial origin (flood events depositing rare clasts) or a coastal origin, such as a marsh, where storm events transport rare clasts much further inland. The floral and faunal assemblages from unit 2 portray a coastal, tidally submerged, grass — sedge wetland marsh within a protected embayment. Water within the embayment was shallow with frequent fluctuations of water levels. Freshwater input was probably limited to runoff and precipitation. The wetland was subjected to periodic rise and fall of tidal waters so that the chemistry of the water was saline or brackish. Seaside arrowgrass and some species of sedges are capable of tolerating halophytic conditions. Many of the plants in unit 2 have distributions that are circumpolar, living in the north at or above tree line including the Arctic and subarctic. Seaside arrowgrass distribution is circumpolar growing north to, or slightly beyond the limit of trees. *Empetrum nigrum* (crowberry) is circumpolar occurring as far north as the Arctic islands and Greenland. *Fragaria chiloensis* (coastal strawberry) is limited to Pacific coastal areas as far north as Alaska, including into the Aleutian Islands. Of significance is the oribatid mite, *Ameronothrus lineatus*, which is presently found only in the coastal regions of the Arctic and subarctic. This indicates climate was much colder at Foggy Cove than present when unit 2 was deposited. Thus, based on the geochronology and palaeoecology, unit 2 was deposited when climate was similar to that of the modern Arctic and in ice-free conditions, indicating that sediments that overlie this unit at Foggy Cove would have been deposited after this time (as early as 15.1 ka cal BP).

The moderate sorting and upward coarsening nature of the sediments, together with the presence of trough and planar cross-bedding, is consistent with unit 3 being deposited by meltwater

flowing from an advancing glacier. The very fine grained sediment at the base of the unit suggests deposition in standing water when glaciers were distal from the site. The interbedding of coarser and finer beds suggest a fluctuating energy regime likely associated with a migrating channels in a braided stream or on an outwash plain. The injection feature at the base of FC_1 indicates that the lower bed of this unit had a significant pore water content and that it experienced loading, which is consistent with overriding ice. The organic-rich layer deposited on cross-bedded fine sand likely formed when vegetation grew in an abandoned channel or on a point bar that was subsequently buried as the channel migrated. Based on the interpretation of this unit and the age determined from radiocarbon sample CIRC25 (Appendix 1, Figure 4), these sediments were deposited between 14.2 and 13.8 ka cal BP.

The presence of a fine (massive) matrix supporting large clasts, a strong unimodal clast a-axis fabric near the lower contact, and a sharp (erosional) lower contact, suggest that unit 4 is a subglacial till. This till would have been formed from ice that overrode and reworked the underlying glaciofluvial sediments, as well as from sediment derived from relatively local bedrock sources. The lack of abundant abrasion features on stones, and two weak pebble a-axis fabrics near the top of the unit, may cast some doubt on this interpretation. However, a paucity of glacigenic features on stones in diamictons dominated by coarse grained lithologies (e.g., granites), and weak fabrics in stone-rich diamictons where clast collisions don't allow for the development of strong fabrics, have been noted in other studies (e.g., Hicock and Lian 1999; Neudorf et al. 2015a).

Trough cross bedding, a sharp (erosional) lower contact, a multi-modal grain size distribution, and sub-rounded to rounded clasts suggest that the sediments in unit 5 were fluvially deposited. The organic-rich layer with fossil roots and wood fragments represents a palaeosol that formed, or re-worked organic material that was deposited, near the middle of this unit (Figure 4). Observed in-situ fossil roots and root casts suggest that the former is more likely, and thus, this organic-rich layer suggests a hiatus in deposition following ice retreat between 14.0 and 13.8 ka cal BP, where the

landscape at this site stabilized (Appendix 1, Figure 4) and soil was able to form. The soil was eventually buried by fluvial sediments (unit 5).

2.6.2. Section interpretation and evidence for glacial advance and retreat

The lithostratigraphic, palaeoecological, and chronological information presented above suggest that the following sequence of palaeoenvironments was present at Foggy Cove: i) Before 15.1 ka cal BP (radiocarbon samples CIRC14, 15b, 18c, Appendix 1), a fluvial environment existed that was transitioning into a deltaic environment (unit 1), ii) Between 15.1 and 14.3 ka cal BP (samples CIRC14, 15b, 18c, Appendix 1), a tidal marsh was present in a cold Arctic to subarctic climate, indicated by abundant seaside arrowgrass and orbatid mites (unit 2), iii) Between 14.2 and 13.8 ka cal BP (sample CIRC25, Appendix 1), glaciers were advancing toward foggy cove, and glaciofluvial sediments were being deposited in front of the ice margin (unit 3), iv) Between 14.2 and 13.8 ka cal BP, based on bounding radiocarbon ages (sample CIRC25 below unit 4, and sample CIRC20a above unit 4, Appendix 1, Figure 4), ice was present for a short period of time (at most 400 years), depositing subglacial till (unit 4), and v) Between 14.0 and 13.8 ka cal BP (sample CIRC20a, Appendix 1), ice retreated from the area, depositing thin beds of sand, gravel, and boulders as the ice melted (unit 5). Because there is no evidence of overturned beds, folding, major bio- or cryo-turbation, or pressure induced injection of sediment in units 3-5, there is no reason to question that, according to superposition, unit 4 was emplaced after unit 3 and before unit 5. This means that sometime between 14.2 and 13.8 ka cal BP, unit 4 was emplaced, and ice was present.

The sedimentological and palaeoecological data presented here suggest that the Foggy Cove stratigraphic sequence represents glacial advance over a tidal marsh environment and subsequent retreat. An alternative hypothesis, however, could be that the sequence instead represents paraglacial sedimentation, and the organic units found in the middle of units 3 and 5 represent reworked organic

material that were stable surfaces on a higher plateau (cf. Lian and Hickin 1996). In this scenario, the diamicton found in units 3 and 4 could have been deposited as debris flows in an aggrading fluvial environment. This alternate hypothesis is not likely for several reasons. The debris flows discussed in Lian and Hickin (1996) required destabilized steep slopes, which are not present in the region surrounding Foggy Cove. No beds in units 3 and 4 were observed having distinct, inter-bed inverse grading, typical of debris flows. The regional geomorphology surrounding Foggy Cove suggests that ice was present at least as far as Foggy Cove, which is supported by the presence of a semi-linear and semi-continuous moraine with large bouldery sediments that is aligned with the Foggy Cove exposure (Figure 2). The morphology of the moraine (<5 m thick and topographically controlled) suggests that it was not associated with glacial advance during the LGM, but with a later advance. The diamicton comprising unit 4 has a distinct fabric that trends NE-SW, perpendicular to the moraine in the study area, and debris flows rarely exhibit sustained unidirectional strain sufficient for the development of well-defined unimodal clast fabrics (cf. Hicock et al. 1996).

2.6.3. Palaeoclimatic interpretation in a regional context

The Late Pleistocene palaeoclimate inferred by this study is consistent with other regional studies in coastal BC (Figure 1, Figure 6). About 90 km south of the study area, Seymour Inlet and northern Vancouver Island had a climate characterized as cold and dry prior to 13.9--13.8 ka cal BP (Lacourse 2005; Stolze et al. 2007; Galloway et al. 2009), when a shift to a warmer climate is observed. These observations were based on palynological records recovered from lake cores. This chronology is very similar to that inferred by the sediments deposited at Foggy Cove, with a cold climate occurring between 15.1 and 14.3 ka cal BP and a retreat of ice occurring prior to 14.0 – 13.8 ka cal BP. Further north, at Haida Gwaii, and along the northwest coast of BC, the transition from a cool climate to a warmer, wetter climate occurred slightly later, from 13.7 to 13.3 ka cal BP (Warner 1984; Lacourse et al.

2012). On the southwest BC coast, including southern Vancouver Island and the Fraser Lowland, the transition from cool to warm occurs around 14.0 to 13.7 ka cal BP (Mathewes and Heusser 1981; Pellatt et al. 2002), with Brown and Hebda (2002) suggesting that average summer temperatures began to increase as early as 14.9 ka cal BP. It should be noted that sea-surface temperature estimations off the west coast of Vancouver Island from Kienast and McKay (2001) suggest cooling into the Oldest Dryas occurring ~15 ka cal BP and warming from the Bølling oscillation occurring by ~14 ka cal BP, which aligns well with the geochronology presented in this study.

2.6.4. Relation to other post-LGM advances in BC and possible mechanisms for ice advance

The timing of the Late Pleistocene glacial re-advance reported here, between 14.2 and 13.8 ka cal BP (Figure 4, Appendix 1), may be an anomaly in BC as it appears to be out of phase (Figure 6) with the pre-Younger Dryas advances documented in the Fraser Valley of southwest BC and Puget Lowland of Washington State (e.g., Saunders et al. 1987; Clague et al. 1997; McCrumb and Swanson 1998; Friele et al. 1999; Friele and Clague 2002; Kovanen and Easterbrook 2002). Kovanen and Slaymaker (2003) provide a minimum age for ice re-advance in northwest Washington State that indicates ice re-advanced prior to 13.1 – 12.8 ka cal BP[1] (11.1 ka ^{14}C BP, AA-27066) and more recently, Menounos et al. (2009) refer to the Sumas advance occurring sometime after 14.5 ka cal BP, both overlapping with the findings of this study. The advance documented at Foggy Cove occurred shortly after the Oldest Dryas cold-climate period, defined as occurring before 14.7 ka cal BP (Lowe et al. 2001, Figure 6), which aligns well with regional palaeoclimate reconstructions (discussed above, Figure 1, Figure 6) that indicate climate warming did not occur until after the end of the Older Dryas in the central and northern latitudes of BC.

[1] Note that the original radiocarbon age was recalibrated using Calib 7.0 for consistency with other reported ages in this manuscript and is therefore slightly different than the original calibrated age reported in Kovanen and Easterbrook (2002).

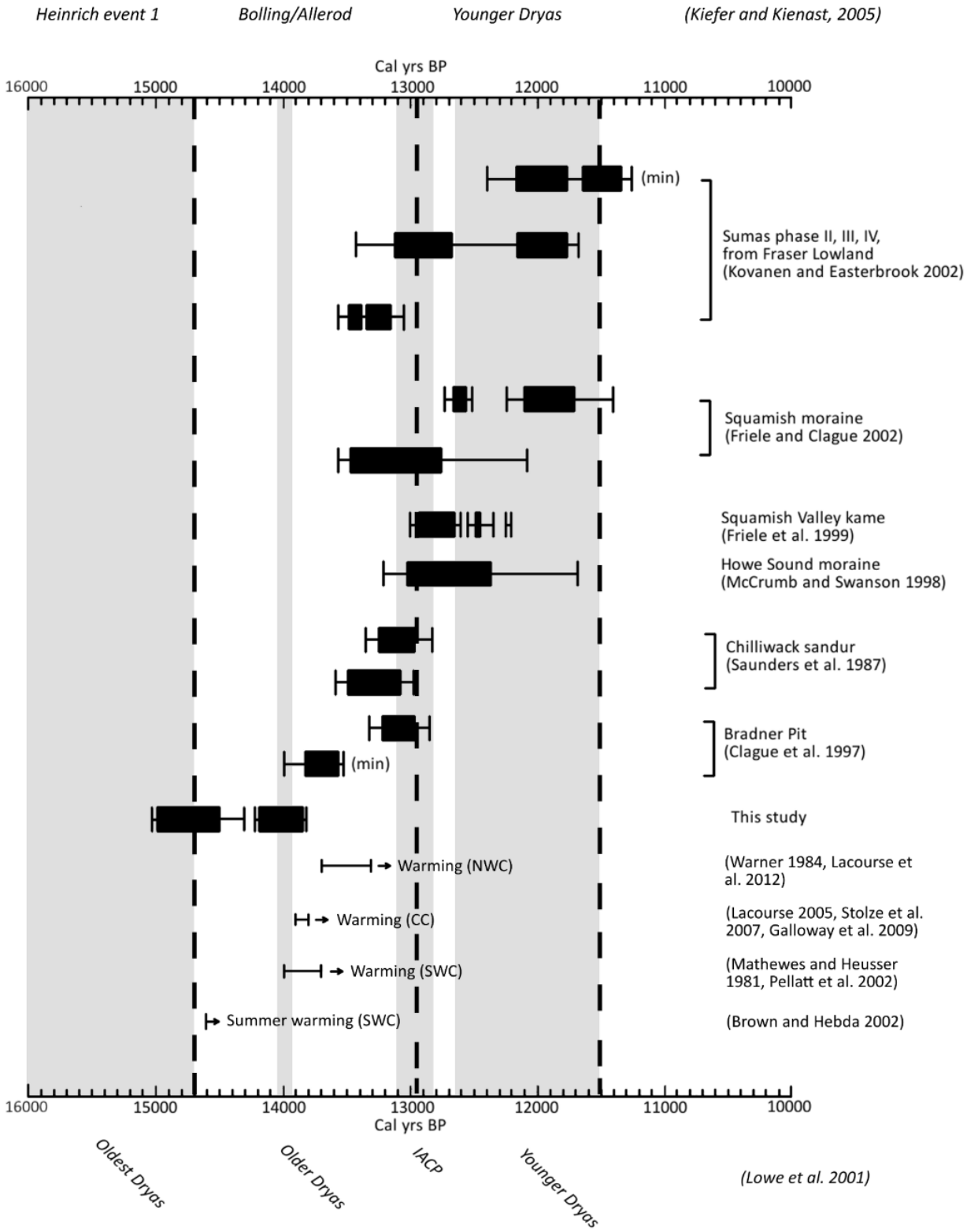
Heinrich event 1
Bolling/Allerod
Younger Dryas
(Kiefer and Kienast, 2005)
Cal yrs BP
16000
15000
14000
13000
12000
11000
10000
(min)
Sumas phase II, III, IV,
from Fraser Lowland
(Kovanen and Easterbrook 2002)
Squamish moraine
(Friele and Clague 2002)
Squamish Valley kame
(Friele et al. 1999)
Howe Sound moraine
(McCrumb and Swanson 1998)
Chilliwack sandur
(Saunders et al. 1987)
Bradner Pit
(Clague et al. 1997)
(min)
This study
Warming (NWC)
(Warner 1984, Lacourse et al. 2012)
Warming (CC)
(Lacourse 2005, Stolze et al. 2007, Galloway et al. 2009)
Warming (SWC)
(Mathewes and Heusser 1981, Pellatt et al. 2002)
Summer warming (SWC)
(Brown and Hebda 2002)
Oldest Dryas
Older Dryas
IACP
Younger Dryas
(Lowe et al. 2001)

Figure 6 (previous page). Timing of late glacial advances and retreats in coastal areas of British Columbia and Washington State. Solid bars and brackets indicate 1σ and 2σ of the calibrated calendar age from original radiocarbon ages, respectively. Cold climate periods from Lowe et al. (2001) (IACP = Inter Allerød Cold Period) are shaded and labelled at the bottom of the figure, while climate periods identified for the northeast Pacific in Kiefer and Kienast (2005) are bracketed by dashed lines and labelled at the top of the figure. All advances shown here follow initial retreat of the Cordilleran Ice Sheet from the study area. Where there are multiple age ranges per advance (for example, the range for this study), the older age indicates the limiting age of glacial re-advance, and the younger age indicates the limiting age for final retreat. Climate data (the bottom four bars) show the range over which the climate began warming toward Holocene temperatures for each region: NWC = the north west coast, CC = central coast and northern Vancouver Island, and SWC = south west coast (including the Fraser and Puget lowlands). Note also that each region and the area for each study is located on Figure 1.

Alternatively, Kiefer and Kienast (2005) establish the Heinrich event 1 climate period (17.4-14.7 ka cal BP) as characterized by oscillating warm and cold intervals, and this may have allowed for a short advance near the end of this time period (Figure 6). Noteworthy is that the Calvert Island re-advance is the northern-most of the lowland re-advances shown in Figure 6, and the latitude-dependent lag in climatic warming observed in palaeoclimatic reconstructions (e.g., climate remains colder longer at higher latitudes, as discussed in the previous section, shown in Figure 6, and shown in Kiefer and Kienast (2005)) may mean that there is a relation between the Foggy Cove re-advance and others. However, perhaps the most conspicuous aspect of the data shown in Figure 6 is the lack of a clear link between late glacial advances in BC and Washington State and established cold-climate periods, especially given that there is clear evidence for these cold-climate periods occurring in the region (e.g., Mathewes et al. 1993, Gosse et al. 1995, Benson et al. 1997, Kiefer and Kienast 2005).

The orbatid mites found in unit 2 at the base of the Foggy Cove stratigraphic sequence were deposited between 15.1 and 14.3 ka cal BP, just prior to ice re-advance. This evidence suggests a colder climate similar to that of the present day Arctic. These conditions were present at the study site after the local LGM and it is reasonable to assume that the climate was warming prior to 15.1 ka cal BP, which initiated CIS retreat (e.g., Clague and James 2002). A warming climate may have been supplemented by a rising RSL causing increased marine glacier calving (cf. Clague et al. 1997), however regional RSL reconstructions extending to 15 ka cal BP suggest a sea-level in the Calvert Island region that was stable and near present-day levels (McLaren et al. 2014; Shugar et al. 2014). A regional reversal of this warming trend may have occurred at Calvert Island. If a cooling climate was a major contributive factor to the re-

advance, then the re-advance may have been augmented by glaciers reforming in the prominent cirques on Mount Buxton in the centre-east of the island, and interacting with stagnant ice (remnants of the CIS) in the lowlands, similar to the topographic effects described by Menounos et al. (2009). It is also possible that the re-advance on Calvert Island was not associated solely with climate cooling, but perhaps also as a result of an emerging sea floor that provided a deformable (slippery) substrate (e.g., Hicock and Fuller 1995; Hicock et al. 1999; Lian and Hicock 2000). Muddy sediments found at the base of sections FC_1 and FC_3 provide support for this, however the RSL curve for the region indicates that sea-level was higher at the time of re-advance (as much as 6 m; McLaren et al. 2014), and there is no sedimentological or geomorphic evidence for a rapid drop in sea-level following the deposition of unit 2.

2.7. Conclusions

Records of Late Pleistocene glacial re-advances following the Cordilleran LGM are rare. This study presents a suite of lithostratigraphic and palaeoecological information that together strongly suggest a late glacial re-advance on Calvert Island, BC, between 14.2 and 13.8 ka cal BP. The presence of orbatid mites in sediments near the base of the Foggy Cove stratigraphy, which are only associated with today's Arctic environments, suggest that the cause was a cold climate. A cold climate existing during this time interval agrees with other regional palaeoclimatic reconstructions in coastal BC based on palynology from lake cores. However, the evidence for a re-advance presented here occurs earlier than other documented re-advances in the region. This lack of synchronicity indicates that local factors, such as the emergence of a deformable, slippery substrate that reduced shear stress at the base of a retreating glacier, may, in some cases, dominate the regional-scale climate drivers of CIS change during retreat. More research on the largely unexplored BC central coast is needed to refine the timing and ascertain the regional extent of this event.

3. Distinguishing depositional setting for sandy deposits in coastal landscapes using grain shape

3.1. Abstract

Several methods exist that use sediment properties to characterize depositional setting and related mechanism of transport, including analysis of grain-size distributions, sediment petrology, micromorphology, and grain structure. Techniques that rely on electron or optical microscopy produce results with varying degrees of success and applicability. Here, a new method is presented and used to differentiate between littoral and aeolian sands that were extracted from recently formed landforms, as well as landforms that are from Mid to Late Holocene in age. The method utilizes a standard optical microscope with a mounted digital camera, paired with freely available software (ImageJ) to characterize grain shape parameters. The method was tested on nearly 6,000 sand grains from samples with varied transport histories, and it was found that grain solidity was the most distinguishable characteristic between aeolian and littoral samples, differentiating them 86% of the time for calibration samples. The method was used to correctly identify the mechanism of transport for 76% of the samples. Patterns in the results indicated that this method could be extended to link potential sediment sources to various depositional basins, and future work includes testing the method in areas with a different mineralogy and/or landscape history.

3.2. Introduction

Differentiation of beach and coastal dune environments in the Quaternary record is important for environmental reconstructions and interpreting changes in relative sea-level. For example, estimating the elevation difference between a coastal foredune and the intertidal beach helps refine the indicative meaning, or relationship of a sample to tidal range, of those landforms (Shennan et al. 2006). Efforts to characterize depositional setting based on sediment characteristics have included scrutiny of traditional grain-size distributions (GSD) (e.g., Mason and Folk 1958; Friedman 1961; Folk 1966; Visher 1969; Rogerson and Hudson 1983; Sun et al. 2002; Shugar and Clague 2011; Purkait and Majumdar 2014), analyses of sediment petrology (e.g., Potter 1986; Kasper-Zubillaga and Dickinson 2001), examination of grain micromorphology as seen in thin section (e.g., Lewis et al. 2010; van der Meer and Menzies 2011; Bendle et al. 2015; Neudorf et al. 2015a), and analyses of grain structure parameters derived from electron microscopy (e.g., Krinsley and Donahue 1968; Clague 1976; Culver et al. 1983; Mazzullo et al. 1986; Vos et al. 2014) or simple optical microscopy (e.g., Fournier 1964; Soutendam 1967; Warnke and Gram 1969; Moss and Green 1975).

The contrast in sand transport processes is significant between coastal dunes (dominated by aeolian processes) and intertidal beaches (controlled by littoral processes). This is largely due to the transport medium, with water providing more buoyancy force which reduces the downward gravitational force and grain momentum when compared to wind. This results in less impact force when water-entrained grains impact the bed, and also a higher impact threshold for maintaining grain entrainment. This leads to detectable differences in both the size distribution and shape of sand grains contained in these respective deposits. Generally, GSDs of littoral sands are negatively skewed or symmetric, while those of aeolian sands are more positively skewed (Mason and Folk 1958; Friedman 1961). Although this general tendency does not hold true everywhere (e.g., Friedman 1961; Rogerson and Hudson 1983; Purkait and Majumdar 2014), the application of more advanced statistics has resulted

in greater success in discerning the mechanism of transport (e.g., Vincent 1986; Purkait 2010). In addition, surface microstructures on sand grains, to the extent where grain roundness is affected, can be used to indicate longshore transport (e.g., Kasper-Zubillaga et al. 2005) or, importantly for this study, aeolian transport processes. This can be attributed to a number of processes, including preferential chemical weathering of aeolian sediments (Kasper-Zubillaga et al. 2005) or because wind preferentially entrains spherical and rounded sand grains. On the latter, particle shape has implications for the internal angle of friction in coastal sediments (Stark et al. 2014), and can affect grain packing, the point of initiation and the rate of aeolian sediment transport (Anderson et al. 1991). Thus, aeolian sediment transport on a beach results in shape sorting, where a deflation lag with high proportions of irregular and angular grains remains, and an increasing concentration of spherical and rounded sand grains occurs several metres downwind of the beach surface (Mazzullo et al. 1986).

In this study, two-dimensional shape parameters of individual grains were investigated to test the hypothesis that sand grains associated with aeolian transport could be differentiated from those associated with littoral transport using this method alone. The main objective of this study was to develop a method that required minimal equipment, freely available software, and a user-friendly methodology. The resulting method involved a standard binocular optical microscope with digital camera and the freely distributed image-analysis software, ImageJ (Rasband 2010). The method is described and evaluated using samples from modern and relict (Holocene age) beach and dune systems found on Calvert Island on the central coast of British Columbia, Canada.

3.3. Study area

Calvert Island is located on the central coast of British Columbia in Queen Charlotte Sound, about 70 km northwest of Vancouver Island and about 200 km southeast of Haida Gwaii (Figure 7). The bedrock is composed mainly of Early Cretaceous tonalite, quartz diorite, granite, granodiorite, and

diorite of the Calvert Island Pluton with diorite-dominated rocks of unknown age cropping out mostly in the central, eastern, and southeastern parts of island (Roddick 1996). Exposed glacial sediments on Calvert Island are largely confined to its western half, with inland areas otherwise absent of much surficial cover, particularly in the northwest. Small areas of glaciofluvial outwash have been mapped in the northwest part of the island. Raised (relict) shorelines also exist, and it is believed that RSL has fluctuated less than a few m since the Late Pleistocene (McLaren et al. 2014), which is markedly different from other neighboring regions on the Pacific coast of North America (Shugar et al. 2014). The west-facing coastline is predominantly bedrock except in the northwest, where cobbly and sandy embayed beaches with localized dunes, tombolos, and spits (Figure 7) occur. The northwestern portion of Calvert Island contains a high proportion of the Mid to Late Holocene accretionary sediments. Their geochronology suggests a complex landscape history that is difficult to interpret based on landform associations alone (Neudorf et al. 2015b).

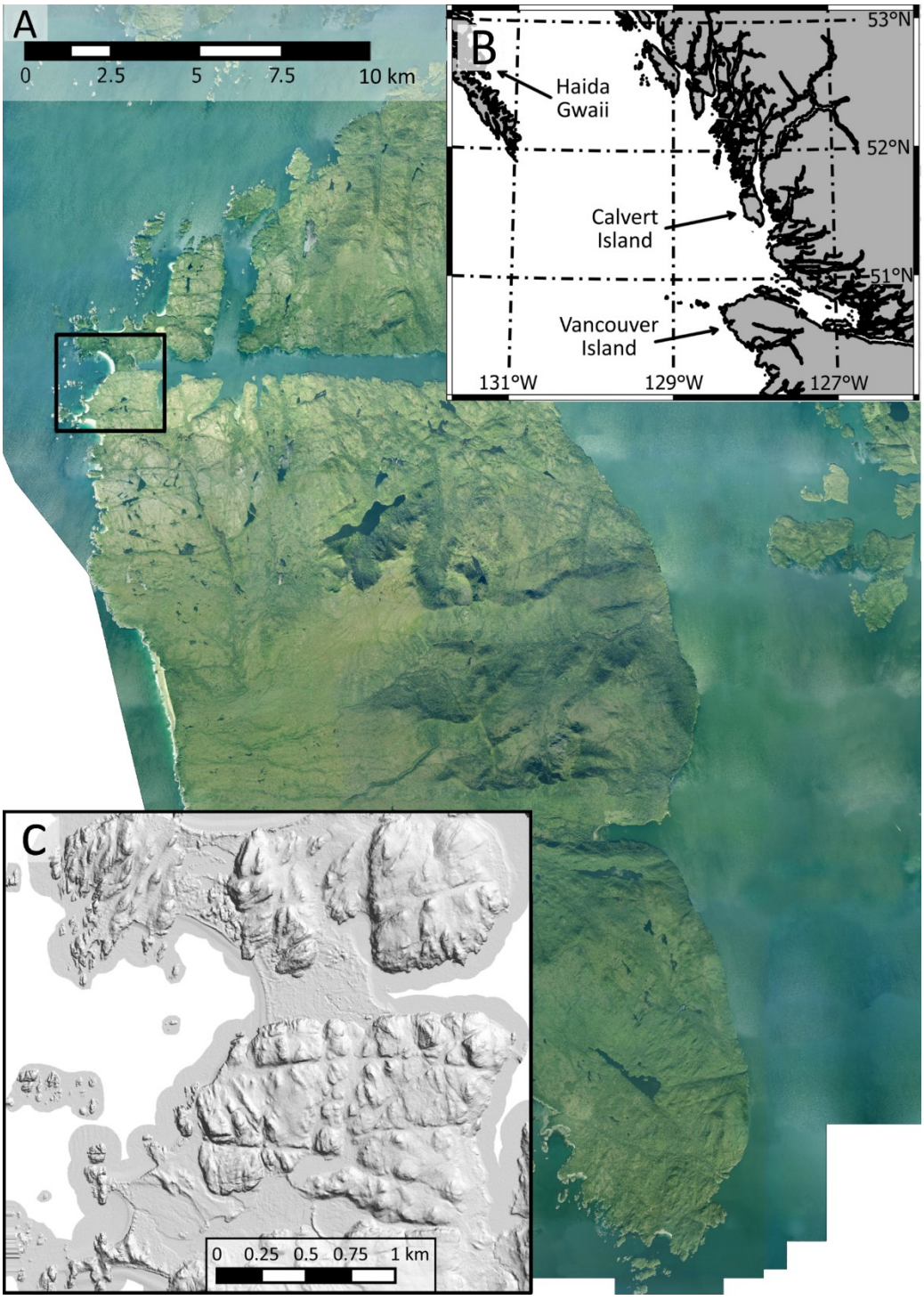

Figure 7. A: Digital orthophoto of Calvert Island, on the central coast of British Columbia. Box shows the location of the study area, shown in C. B: Inset map in upper right shows the location of the study area on the Pacific coast of British Columbia. C: Inset map showing the 2 m hillshaded lidar DEM for the study area. The lidar data were obtained and processed by Rob Vogt of the UNBC lidar Research Group, Derek Heathfield of the Hakai Institute Coastal Sandy Ecosystem Program, and Dan Shugar and Jordan Eamer of the Coastal Erosion and Dune Dynamics laboratory.

3.4. Methodology

The method developed for this study involved the following five stages: (1) samples were collected from a variety of modern, active beach and dune settings to form a calibration dataset; (2) calibration samples collected in the first step were mechanically sieved into ¼ ϕ Wentworth size classes and subsampled in each size class with a sufficient sample size; (3) subsamples of several hundred grains from each size class were imaged and shape parameters were calculated using the ImageJ software; (4) the size class and shape parameters that show the largest statistical difference between littoral and aeolian sands were selected by difference of mean statistical tests; and (5) using the ideal size class and shape parameters, the calibration samples were compared to additional samples to determine the mechanism of transport (MoT). Each step is described in detail below.

3.4.1. Sample collection

Samples used in this study included a range of modern and Mid to Late Holocene shovel test and core samples (Figure 8) collected from diagnostically distinct landforms. Modern sand samples were collected to approximately 10 cm depth from the surface, and relict sand samples were collected below modern soils, from the parent material (C horizon) wherever possible.

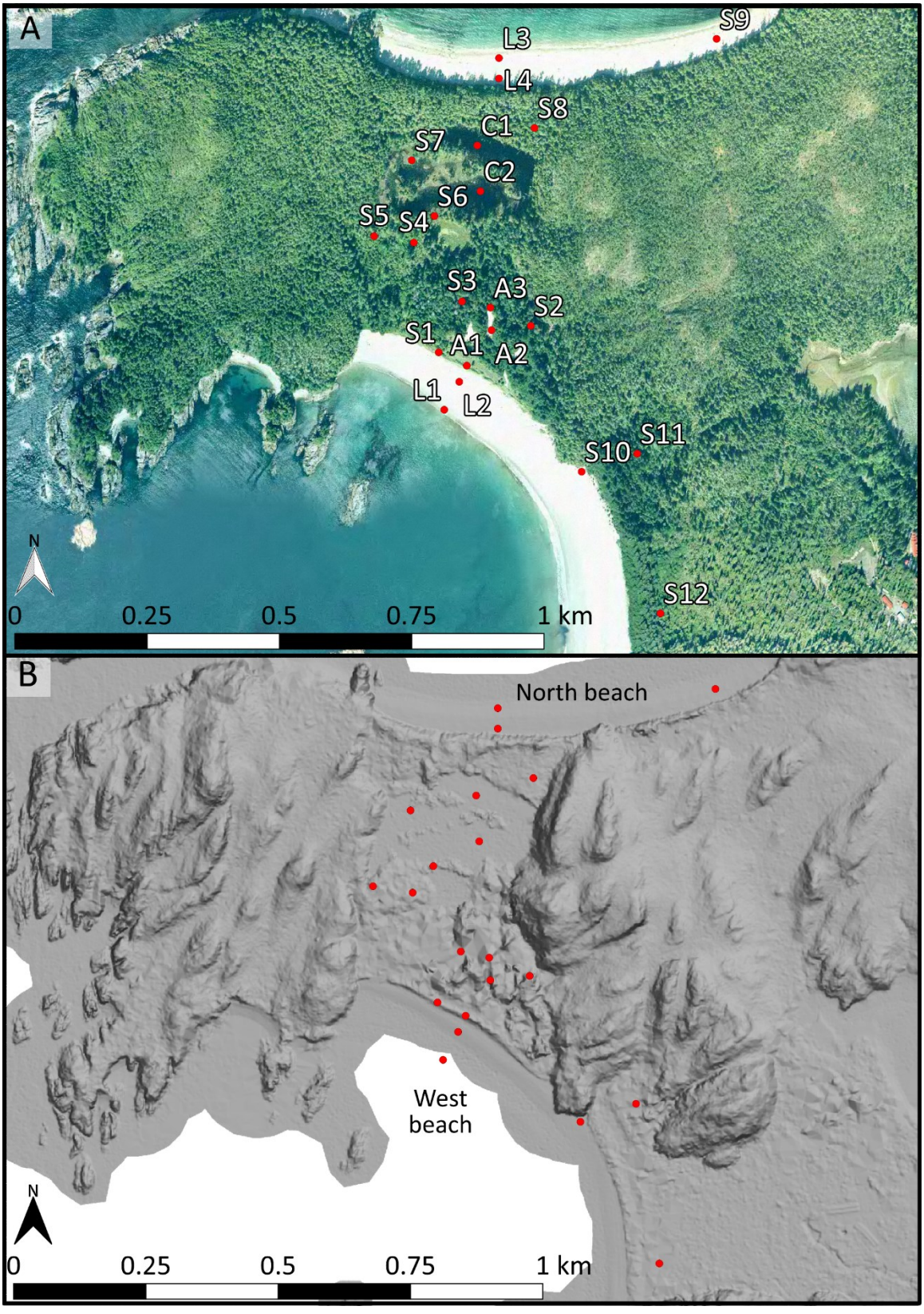

Figure 8. Locations of the samples used in this section. A: Digital orthophoto with sample labels. B: The hillshade lidar DEM from Figure 7 with beaches labeled.

For method development, lower- and upper-littoral-zone samples were collected from both West and North beaches (samples L1, L2, L3, and L4, Figure 8) to provide calibration samples and to represent potential source sediments for aeolian transport into the region between the beaches. The lower beach (intertidal) samples were taken just above low tide and represent sediments deposited on the foreshore by littoral processes. The upper beach (backshore) samples were collected approximately one meter seaward from incipient dunes, so as to best represent a beach sediment still dominated by littoral processes, yet influenced partly by aeolian transport. It is recognized that the processes of sediment transport at the beach-dune interface are complex and, thus, sediment properties in this zone are expected to be highly variable spatially and temporally (Houser 2009). However, the sampling methodology, where a depth-integrated sample was taken in areas with clear aeolian influence (edge of incipient dunes), should allow some confidence that upper-beach samples include some aeolian and some littoral sand. Modern dune samples collected for calibration were collected from the established foredune crest (sample A1), an unvegetated deflation basin in a blowout dune (sample A2), and a vegetated depositional lobe of a blowout (sample A3), with landform morphology indicating potential landward aeolian sediment transport from the positions of sample A1 to A2, and A2 to A3. It is important to note that this portion of the landscape was much more active and connected, with respect to aeolian activity, as recently as the late 1990s. For the calibration dataset, this progression on West beach (L1 to A3) represents a cross-shore profile to show decoupling of shape-sorted grains from swash to dune and farther landward.

Samples from other geologic studies performed in the area, specifically a Late Pleistocene landscape reconstruction, were used to develop and validate the method described here. Ancillary data, including soil properties, fossils, stratigraphy, landform geomorphology, and geochronology have allowed interpretation of the MoT. Samples include modern dune and beach samples (S1 and S10,

respectively), relict dune complex samples (S2, S3, S4, S5, S8), relict foredune samples (S6, S7, S11, S12), and one relict beach sample (S9) (Figure 8). These samples were collected in conjunction with sampling for optical dating in a related study (Neudorf et al. 2015b). Between 200 and 400 g were collected for these samples at depths ranging from 20 to 60 cm below the ground surface, depending on the amount of soil development and the depth of the C horizon. All samples have associated ages determined from optical dating and are Mid Holocene (4.20 ± 0.33 ka) to modern (0.032 ± 0.005 a) in age (Neudorf et al. 2015b), thus, providing a good temporal range of samples from which to develop and test the method.

Five samples were also collected from two percussion cores (C1 and C3) obtained in a lake basin between West and North beaches that is partially divided by a ridge of vegetated unconsolidated sand (interpreted as a foredune) and bedrock (Figure 8). The samples were collected from distinct sand beds at depths of 49, 62, and 95 cm (samples C1-49, C1-62, and C1-95) in core 1, and 20 and 40 cm (samples C3-20 and C3-40) in core 3. The sand beds are separated by organic material, and some of this was used for accelerator mass spectroscopy radiocarbon dating, and have ages that date to the Late Holocene, with basal ages of 1700 – 1820 cal yr BP. One sample of well-sorted aeolian sand that yielded an optical age of 645 ± 64 cal yr BP (Neudorf et al. 2015b) was collected from a vibracore sample from the foredune ridge in the lake.

3.4.2. GSD and subsampling

For all samples, except those collected from cores (due to insufficient mass), GSDs were obtained by mechanical sieving using WS Tyler test sieves stacked at 1/4 ϕ intervals. For each sample, 200 g of sediment was dried in a laboratory oven for 24 hr at 105°C and subsequently mechanically split. Samples were sieved in a Ro-Tap sieve shaker for 15 minutes and each sieve fraction was weighed with an electronic balance. Textural parameters (mean, sorting, skewness, and kurtosis) were calculated graphically using the Folk and Ward (1957) method and GRADISTAT Version 8 (Blott and Pye 2001). In

addition, one-way analysis of variance (ANOVA) statistical tests were performed on each textural parameter separated into aeolian and littoral sample groups. For example, one of the four hypothesis tests was as follows: H_0: The two sample groups (eolian or littoral) of mean grain-size are drawn from the same population; H_1: The two sample groups of mean grain-size are drawn from different populations. The ANOVA statistical tests were used to determine if a statistical difference between aeolian and littoral samples could be detected based on traditional GSD metrics.

As grain microstructures can be related to grain-size (Vos et al. 2014), the sieving stage of the method involved sampling to determine the size class that best shows differences in grain shape as a function of MoT, described below. Also, a small range of grain-sizes resulted in easier filtering of imagery, also described below. Vos et al. (2014) suggest that a size class range from 3.25 ϕ to -1 ϕ is preferred for microtexture evaluation. The GSD of sediments from this study show that the 3 ϕ to 1.5 ϕ grain-size classes had sufficient grains for a representative statistical distribution (several hundred). Subsamples of several hundred grains were selected randomly using a spatula from each 1/4 ϕ sieve for each sample (including the cores) for use in the following analyses.

3.4.3. Subsampling and structural characterization

Subsamples were analyzed on a petri dish with an optical stereo microscope with 2-90X magnification and an attached digital camera with a resolution of 5 MP (Figure 9A). Samples were magnified 20X; however, as long as a minimum pixel count of 200 per object is obtained (Kröner and Carbó 2013), other combinations of camera resolution and magnification are possible. The magnification had no bearing on results otherwise, as grain-size in the image is irrelevant in the analysis (only shape).

Images from each 1/4 ϕ size class were imported into the ImageJ shape-analysis software (Rasband 2010) (Figure 9A). One method for deriving grain structure is provided in a downloadable macro plug-in for ImageJ (see Lewis et al. 2010). However, for this study, a simplified workflow was

developed due to the bulk nature of the sediments, in contrast to Lewis et al. (2010), who examined thin sections prepared from cores. To convert the grain images to shapes required first thresholding images to black and white binary images (Figure 9B). For the samples in this study, it was found that the Triangle thresholding method (Zack et al. 1977) utilizing the YUV color space (Y representing the luminance (brightness) component and UV representing the two chrominance (color) components) provided ideal thresholding for quartz grains. Next, thresholded binary images were measured for particle structure using the built-in ImageJ functionality (shape descriptor outputs described below). At this stage, particle size limits were specified as digital raster area limits per particle, and holes and edge effects (e.g., dark spots in the middle of grains causing a "hole" when the threshold was applied, and grains cut off at the edge of images) were eliminated.

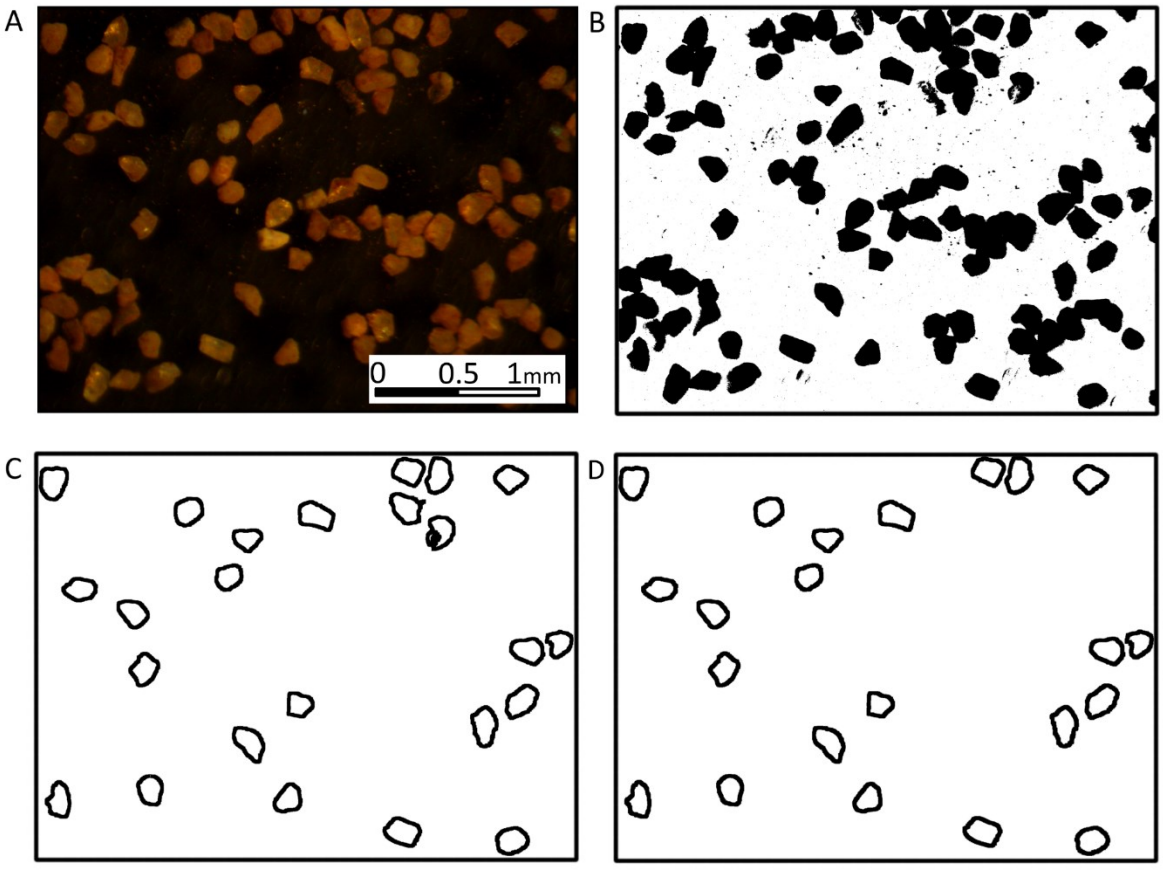

Figure 9. A: True color microphotograph of several dozen sand grains from a sample in the study area. B: Binary thresholded image of the same sample. C: Outline diagram of the same sample, with each particle that was not removed using the size threshold remaining. D: Manually edited image from which shape descriptors can be calculated.

As the particles were of a uniform size class, setting a narrow particle size limit reduced the amount of touching grains assigned to one particle (too large) as well as particulate matter that was difficult to threshold out (too small). This produced an image of particle outlines (Figure 9C), each assigned unique numerical labels that were used for manual removal of anomalous or poorly digitized grains (Figure 9D). The shape descriptors produced by the previous step in ImageJ include circularity, aspect ratio, roundness, and solidity. While these terms are familiar to sedimentologists, when applied to two-dimensional images they differ slightly from three-dimensional interpretations. Circularity is defined as

$$4\pi\left(\frac{Area}{[Perimeter]^2}\right)$$

and can range from zero to one, with one being a circle. This approximates sedimentological sphericity as described by Wadell (1932) and Krumbein (1941), but in two dimensions. Aspect ratio is simply

$$\frac{Major\ Axis}{Minor\ Axis}$$

and is a measure of elongation of the ellipse fitted to the particle as seen in two dimensions. Roundness is defined as

$$4\left(\frac{Area}{\pi[Major\ Axis]^2}\right)$$

which is similar to circularity in that a value of one would represent a circle. Roundness, however, measures area relative to a fitted ellipse, so it ignores irregular borders, and thus, is different from the sedimentological definition of grain roundness as defined by Wadell (1932). The final measure is solidity, defined as

$$\frac{Area}{Convex\ area}$$

which measures the irregularity of the border, analogous to the sedimentological definition of roundness. Convex area, as calculated in this measure, can be described as the area of a polygon created

around your shape with no interior angles greater than 180^{o}, having the effect of all vertices of the polygon pointing away from the interior of the shape. These descriptors are illustrated in Figure 10.

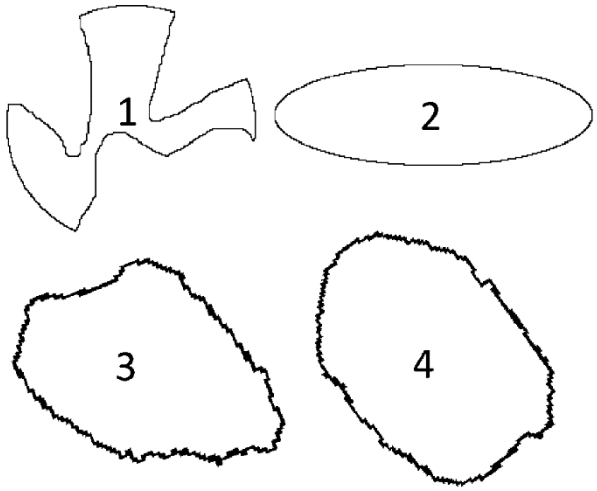

Figure 10. Exaggerated artificial "grains" (1 and 2), developed to illustrate the four shape descriptors calculated in ImageJ, and example grains from L1 (3) and A1 (4). Note that particle 1 is a circular grain with an irregular outer surface, and particle 2 is an elongate grain with a smooth outer surface. Shape descriptors for grains 1, 2, 3, and 4, respectively, are: circularity = (0.21, 0.58, 0.65, 0.73), aspect ratio = (1.50, 3.18, 1.52, 1.44), roundness = (0.67, 0.32, 0.66, 0.69), solidity = (0.53, 0.98, 0.92, 0.96).

3.4.4. Hypothesis testing – determination of ideal grain-size and shape

The process described in above was repeated a minimum of five times for each 1/4 ϕ grain-size class of two calibration samples considered to be ideal representations of littoral and aeolian environments (L1 (littoral) and A1 (eolian)) (Figure 8). This was done to get a better distribution of shape descriptors, with a minimum of 100 grains sampled (Table 1). Generally, as grain-size decreased, number of grains sampled increased, as would be expected at a constant magnification. The results were aggregated for each size class, and the distributions were compared between the littoral and aeolian sand using hypothesis testing (Table 1), where the null hypothesis is that the distribution of aeolian and littoral sands are not statistically different, with the alternate hypothesis is that the distribution of aeolian and littoral sands are statistically different .

Table 1. Results of hypothesis testing for samples A1 and L1 for various grain diameters (D), with number of grains analyzed (n), decision (Y = statistically different, N = not statistically different) and t-test statistic in brackets. The mean solidity value for A1 and L1 are shown in the right-hand column.

D (ϕ)	n	Circularity	Aspect Ratio	Roundness	Solidity	
					Different?	μ (A,L)
1.5	184	Y (6.17)	N (0.48)	N (1.45)	Y (2.86)	0.898,0.860
1.75	259	Y (4.89)	N (1.31)	Y (2.03)	Y (3.28)	0.898,0.863
2	706	Y (2.58)	N (1.79)	Y (2.29)	N (1.29)	0.881,0.872
2.25	531	Y (2.82)	N (0.54)	N (1.32)	N (1.76)	0.882,0.895
2.5	604	Y (5.78)	Y (3.34)	Y (3.31)	Y (5.15)	0.925,0.913
2.75	747	Y (5.18)	Y (2.53)	N (1.46)	Y (4.67)	0.920,0.901
3	818	Y (8.46)	N (0.61)	N (0.31)	Y (6.03)	0.921,0.901

First, an *F*-test of the equality of two variances was performed to compare the distributions (required for a valid *t*-test), with a *t*-test (*p*-value of 0.05) following to determine if the distributions of shape descriptors are statistically different from each other, used to test the hypothesis. An ideal grain-size for this method can be defined as the grain-size class that shows, between a littoral and aeolian sand, statistically different distributions of all shape descriptors, or as the grain-size that shows the strongest statistical difference in one (or more) shape descriptors. For this study, the former definition of ideal grain-size was used, and this was determined to be the 2.5 ϕ grain-size class (Table 1). Shape descriptors were then analyzed using the rest of the calibration samples (Table 2).

Table 2. Results of shape-parameter analysis for all calibration samples. n is the number of grains analyzed, μ is the mean, σ2 is the variance. Note the consistently different mean and variance for the solidity variable between littoral and aeolian samples.

	***D* = 2.5ϕ**					
	n	**Circularity**	**Aspect Ratio**	**Roundness**	**Solidity**	
		μ	μ	μ	μ	σ^2
A1	433	0.695	1.487	0.766	0.925	0.003
A2	267	0.686	1.363	0.755	0.929	0.009
A3	255	0.677	1.394	0.738	0.924	0.009
L1	351	0.665	1.476	0.708	0.913	0.012
L2	198	0.672	1.410	0.735	0.922	0.022
L3	203	0.677	1.373	0.748	0.912	0.013
L4	277	0.674	1.409	0.732	0.920	0.011

The samples listed in Table 2 expanded the calibration dataset and resulted in a greater range of littoral and aeolian samples for comparison. In a broader-scale environmental reconstruction, this is akin to developing a full calibration dataset to compare to samples of unknown transport history. These data were also used to determine which shape parameters provide the best statistical separation of littoral and aeolian sand. In this study, circularity and solidity are consistently different between littoral and aeolian sands, and when hypothesis testing using difference of means is performed, solidity performed consistently better as a variable to differentiate littoral and aeolian sediments with an 86% success rate of prediction. This is compared to 43% for circularity and 48% for aspect ratio and roundness (Table 3). The mean value for solidity was higher for aeolian sands than for littoral sands (Table 2); however, it is conceded that the differences in mean values are within the reported variances. This was considered acceptable because the goal of this step of the method was to identify the ideal grain-size for differentiation. Of note, the higher average solidity values and lower variance in solidity values for aeolian sediments is consistent with the concept of shape sorting via aeolian processes preferentially entraining rounder grains (Mazzullo et al. 1986), as there is sufficient variance in solidity in the initial (littoral) grain population.

Table 3. Results of hypothesis testing for the four shape descriptors calculated for the calibration samples, with decision (Y = statistically different, N = not statistically different) and *t*-test statistic in brackets. Note that the hypothetical case where all aeolian sands are classified as statistically different from littoral sands would result in only Y within the outlined box and N outside of the box.

Circularity	A1	A2	A3	L1	L2	L3	L4
A1							
A2	N (1.76)						
A3	N (1.29)	N (0.79)					
L1	Y (5.78)	Y (5.98)	Y (6.10)				
L2	N (0.64)	N (1.12)	N (0.47)	Y (3.41)			
L3	N (1.28)	N (0.68)	N (0.47)	Y (5.94)	N (0.52)		
L4	N (1.11)	N (1.06)	N (0.26)	Y (2.11)	N (0.27)	N (0.323)	
Aspect ratio	A1	A2	A3	L1	L2	L3	L4
A1							
A2	Y (2.63)						
A3	Y (3.57)	N (1.20)					
L1	Y (3.34)	Y (5.34)	Y (5.27)				
L2	Y (2.32)	N (1.43)	N (0.60)	Y (2.47)			
L3	Y (4.37)	N (0.38)	N (0.60)	Y (5.79)	N (1.34)		
L4	Y (3.02)	N (1.77)	N (0.65)	Y (4.92)	N (0.06)	N (1.57)	
Roundness	A1	A2	A3	L1	L2	L3	L4
A1							
A2	Y (2.51)						
A3	Y (2.94)	N (1.33)					
L1	Y (3.31)	Y (5.75)	Y (5.49)				
L2	N (1.31)	Y (2.43)	N (0.25)	Y (1.98)			
L3	Y (3.75)	N (0.52)	N (0.25)	Y (6.07)	N (1.07)		
L4	Y (2.46)	N (1.75)	N (0.53)	Y (3.14)	N (0.22)	N (1.44)	
Solidity	A1	A2	A3	L1	L2	L3	L4
A1							
A2	N (1.04)						
A3	N (1.04)	N (1.15)					
L1	Y (5.15)	Y (6.25)	Y (6.41)				
L2	N (1.61)	Y (1.98)	Y (2.85)	N (0.60)			
L3	Y (1.98)	Y (2.82)	N (1.84)	Y (5.67)	N (0.02)		
L4	Y (3.21)	Y (2.17)	Y (2.02)	N (1.52)	N (0.86)	N (0.99)	

3.4.5. Hypothesis testing – remaining samples

Following the determination of the ideal grain-size (2.5 ϕ) and shape descriptor (solidity), the distributions of solidity values from the ideal grain-size class from the calibration dataset were compared to samples of inferred MoT (S1 to S12, C1, and C3) to test the method. This involved obtaining subsamples of grains in the 2.5 ϕ size class of each sample, calculating the shape parameters from that subsample, and hypothesis testing to compare the distributions of solidity values from each sample against those of the calibration samples. Hypothesis testing was first conducted using the two calibration samples considered to be ideal representations of aeolian and littoral environments (A1 and L1). If the sample was found to be statistically consistent with one of these calibration samples, the sample was assigned an MoT: aeolian or littoral. If the sample was found to be statistically different from both calibration samples, then more tests were conducted using the remaining calibration samples (A2, A3, L2, L3, and L4).

3.5. Results

3.5.1. Grain-size distributions

A graphic of the four GSD summary statistics are shown in Figure 11. The summary statistics of the GSD as well as the results of the one-way ANOVA tests are shown in Table 4. Figure 11 shows that basic grain-size summary statistics are not sufficient to elucidate transport mechanism. This is perhaps due to a fairly wide spread in the mean grain-size and sorting of the aeolian sediments, which can be largely attributed to two dune sediment samples from the western portion of the study area. One sample (S5) was poorly sorted when compared to other samples, and another (S4) was finer than other samples. Even if those are treated as outliers, however, MoT differentiation is difficult. In addition, skewness, which can be diagnostic in aeolian or beach environments (Mason and Folk 1958), did not

clearly distinguish between these environments here (Figure 11). Generally, the only observable difference in Figure 11 is the generally higher kurtosis values for littoral samples, but it is hardly diagnostic. This is reflected in the one-way ANOVA tests, where the only test that yielded a *p*-value at all close to the cutoff α of 0.05 was between the distribution of aeolian and littoral kurtosis values (Table 4); however they were still found to be drawn from the same statistical distribution (i.e., kurtosis could not be used with these samples to statistically differentiate aeolian and littoral sediments).

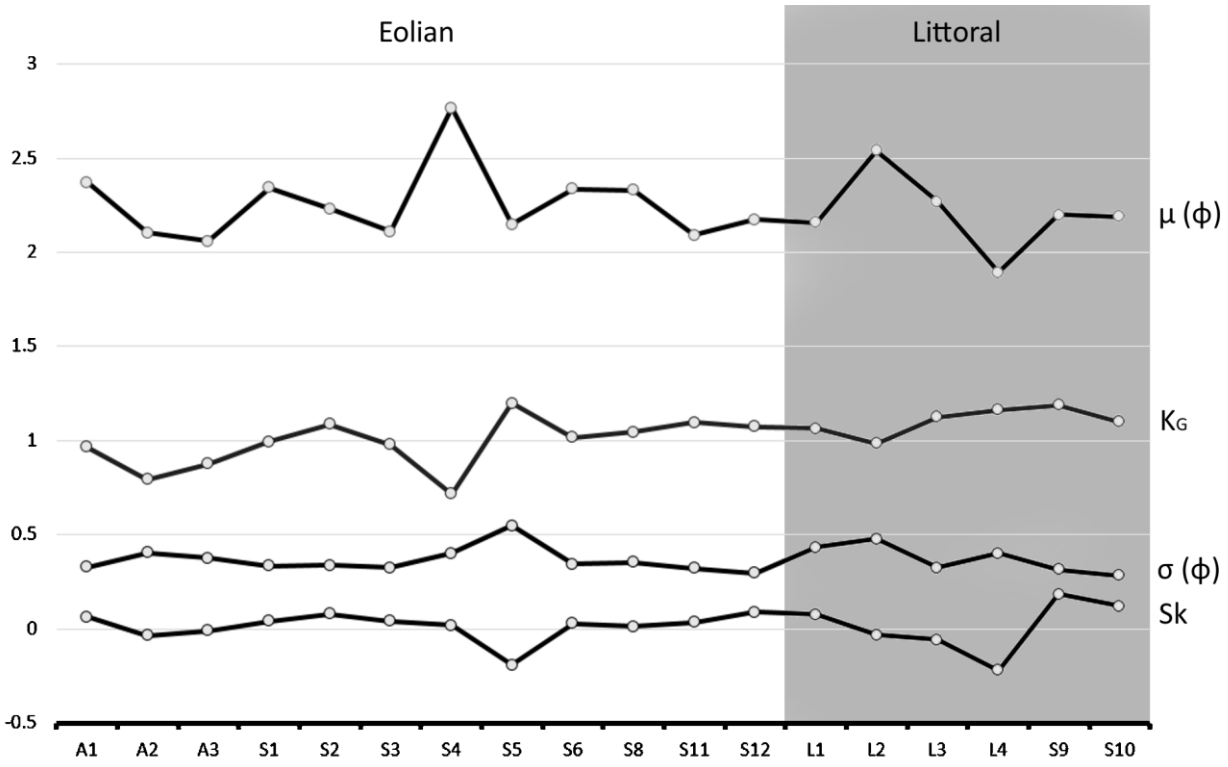

Figure 11. Plot of GSD summary statistics: mean (μ) and standard deviation (σ) in phi, kurtosis (Kg) and skewness (Sk). Littoral samples are plotted in the shaded area for clarity.

Table 4. Grain-size summary statistics for samples analyzed in this section and results of one-way ANOVA statistical test. The hypothesis test is as follows: H_0: The two sample groups (eolian or littoral) are drawn from the same population; H_1: The two sample groups are drawn from different populations.

MoT	Sample	D (ϕ)	Sorting (σ ϕ)	Skewness	Kurtosis
eolian	**A1**	2.372	0.327	0.063	Mesokurtic (0.965)
	A2	2.104	0.405	-0.035	Platykurtic (0.795)
	A3	2.059	0.376	-0.011	Platykurtic (0.877)
	S1	2.344	0.336	0.042	Mesokurtic (0.993)
	S2	2.230	0.337	0.081	Mesokurtic (1.086)
	S3	2.110	0.324	0.042	Mesokurtic (0.977)
	S4	2.767	0.401	0.019	Platykurtic (0.718)
	S5	2.149	0.549	-0.193	Leptokurtic (1.198)
	S6	2.338	0.344	0.027	Mesokurtic (1.017)
	S8	2.331	0.353	0.014	Mesokurtic (1.045)
	S11	2.091	0.323	0.034	Mesokurtic (1.095)
	S12	2.174	0.295	0.089	Mesokurtic (1.074)
littoral	**L1**	2.159	0.433	0.076	Mesokurtic (1.066)
	L2	2.541	0.477	-0.033	Mesokurtic (0.985)
	L3	2.269	0.325	-0.058	Leptokurtic (1.126)
	L4	1.894	0.403	-0.219	Leptokurtic (1.163)
	S9	2.200	0.317	0.184	Leptokurtic (1.189)
	S10	2.191	0.284	0.122	Mesokurtic (1.099)
Reject H_0?(p-value)		No (0.65)	No (0.80)	No (0.96)	No (0.06)

3.5.2. Using the ideal grain-size and solidity shape descriptor to predict MoT

When the solidity shape descriptor was calculated for the other samples (S2 to S9, S11, S12, C1, and C3), it could be used to predict the MoT as inferred from ancillary data or the modern landform (S1, S10) 76% of the time (Table 5). The method performed well on littoral sediments, correctly identifying all of them. The aeolian sand samples that were not statistically differentiated from beach sands (S2, S4, S12, and C03-20) all could be identified as aeolian samples if the statistical threshold was lowered. The most similar calibration sample (corresponding to the lowest t-test statistic) for each sample was A1, the modern foredune sample. Lowering the statistical threshold, however, would increase the likelihood of Type 1 error. A plot of the mean solidity values and the variance in the distribution of the values shows that solidity is higher in aeolian samples and, generally, variance in aeolian solidity values is lower (Figure 12). This plot contrasts with Figure 11, where there was no clear difference in the GSD summary

statistics between aeolian and littoral samples, and could reflect a difference in the variables involved in the physical processes of sediment transport (mineralogy, roundness, fluid flow competency, and beach fetch) that are discussed below.

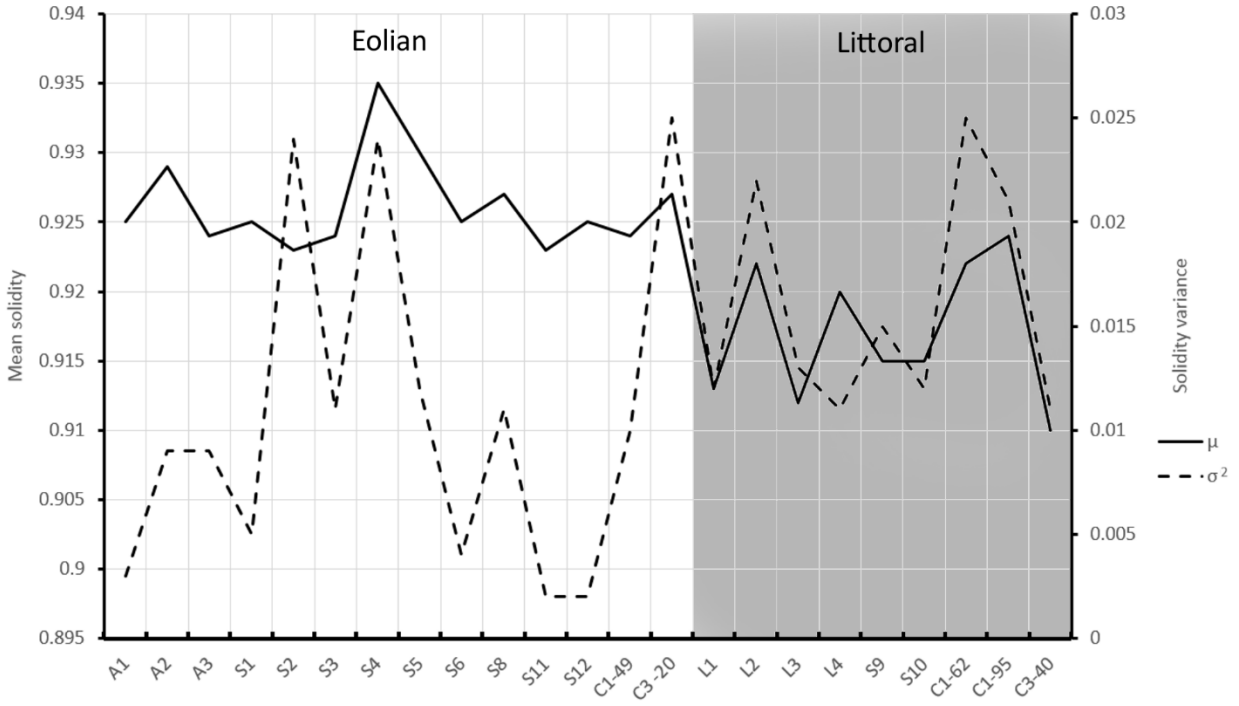

Figure 12. Plot of mean solidity values (μ) and the variance in the distribution of solidity values (σ^2) for each sample. Littoral samples are plotted in the shaded area for clarity. Note the lower mean solidity values and generally higher variance found in littoral samples.

Table 5. Results of hypothesis testing for samples with the number of sand grains (n), MoT as interpreted from ancillary data (section 3.4.1), and decision (Y = statistically different, N = not statistically different) with the *t*-test statistic in brackets. If the "not statistically different" decision (N) at the 95% confidence level corresponded with the MoT as inferred from ancillary data (Eolian or littoral), then the method was labeled correct (Yes). This table is a subset of Appendix 2.

	n	MoT	A1	A2	A3	L1	L2	L3	L4	Correct?
S1	247	Eolian	N (0.65)			Y (4.03)				Yes
S2	154	Eolian	Y (2.76)	Y (2.90)	Y (2.09)	Y (5.47)	Y (3.01)	Y (4.98)	Y (3.62)	No
S3	237	Eolian	Y (3.33)	Y (2.04)	N (0.91)	Y (4.48)				Yes
S4	298	Eolian	Y (3.63)	Y (3.45)	Y (4.36)	Y (5.11)	Y (3.84)	Y (4.91)	Y (4.69)	No
S5	191	Eolian	Y (2.91)	N (1.49)	Y (2.19)	Y (4.30)				Yes
S6	223	Eolian	N (0.54)			Y (2.74)				Yes
S7	310	Eolian	N (1.88)			Y (2.22)				Yes
S8	288	Eolian	Y (2.13)	N (1.61)	Y (3.67)	Y (5.83)				Yes
S11	250	Eolian	N (1.29)			Y (3.81)				Yes
S12	188	Eolian	N (0.44)	Y (2.54)	Y (3.34)	N (1.45)	N (1.57)	N (0.95)	Y (2.34)	No
C01 - 49	224	Eolian	N (0.80)			Y (5.59)				Yes
C03 - 20	207	Eolian	Y (2.32)	Y (2.79)	Y (3.19)	Y (4.99)	Y (3.90)	Y (4.74)	Y (3.82)	No
S9	204	Littoral	Y (4.59)			N (1.10)				Yes
S10	321	Littoral	Y (3.35)			N (1.73)				Yes
C01 - 62	213	Littoral	Y (4.47)			Y (2.59)	N (0.89)	Y (2.95)	Y (2.00)	Yes
C01 - 95	189	Littoral	Y (5.43)			Y (2.46)	N (1.44)	N (1.83)	Y (2.10)	Yes
C03 - 40	145	Littoral	Y (4.19)			Y (2.02)	Y (2.55)	N (1.06)	Y (2.46)	Yes

3.6. Discussion

3.6.1. Effectiveness of the method

This section documents a new, efficient method for differentiating sediments transported via aeolian or littoral processes that requires only inexpensive equipment and free software. It requires a relatively small sample size to produce a statistically robust distribution of sand-grain shape parameters. In practice, this method could, with additional pre-processing to remove cementation, be applied to consolidated sands or sediments that have undergone partial or complete diagenesis. When GSD analyses fail to yield any diagnostic traits from which distinct mechanisms of transport can be discerned (e.g., Table 4, Figures 5, 6), or when they need additional evidence to support findings, this method can be used to provide additional diagnostic results to aid in interpretations of mechanisms of transport (MoT) and help with broader landscape interpretation and/or reconstruction. The method is non destructive, and the grain population used can be recombined with the original sample. The small sample size allows researchers to apply the method to sediments obtained using a range of sample collection methods, such as cores, grab samples, or augers. While it was found that solidity was the shape parameter most useful for differentiating littoral and aeolian sediment in this study, the variety of shape parameters calculated by ImageJ may assist in extending the method to different MoT or regional settings where other parameters may be more significant in detecting differences.

Decoupling of distinct grain solidity classes occurred over relatively short distances in this study, but decoupling of distinct grain-size classes did not (cf. Bauer 1991). This may be attributable to the different physical processes acting on the grain that initiate transport. Decoupling of sediments into different grain-size classes depends largely on the specific shear stress acting on the bed overcoming the gravitational force provided by grains of different mass; larger, heavier grains provide a greater resistance than smaller, lighter grains. Shape sorting, however, results from a change in the internal

angle of friction and the amount of packing, where well rounded grains will have fewer contact points (lower internal friction) and are less likely to pack tightly, thereby reducing the magnitude of shear stress required to initiate transport. There may be certain combinations of mineralogy, roundness, fluid flow competency, and beach fetch that yield conditions right for shape sorting and others for size sorting, although this was not discernible in this study.

When the calibrated method was applied to samples for which there were ancillary data to support an MoT, or to samples collected from a modern landform, it provided corroborating evidence of the MoT for 76% of the samples. Of the remaining samples, statistically ambiguous results (i.e., results that did not identify an MoT with 95% confidence) still yielded information leading toward the likely MoT through the lowest test statistic and, thus, the calibration sample most similar to the test sample. The aeolian samples whose MoT was successfully identified in Table 5 show that the results might be used for discriminating the type of aeolian or littoral depositional setting. For example, S6, S7, S11, and C01-49 were all identified as being most similar to calibration sample A1, which was collected from the modern foredune. The interpretation that these samples represent sediments deposited in a foredune agrees with ancillary data, which suggest that these sands are part of a foredune complex. Two samples (S5 and S8) were identified as having sediments derived from an MoT most similar to the calibration sample from the deflation basin of a blowout dune (A2). The bare-earth DEM (Figure 8) shows that both samples were collected in low-relief, topographically flat regions and, thus, are unlikely to be part of a foredune ridge (A1) or a depositional lobe (A3). Finally, sample S3 was determined to be most similar to calibration sample A3, and it appears in the lee of a large, ~15m-tall, blowout depositional lobe. Thus, the most likely MoT for sample S3 is by wind in the area of flow separation and grain fallout behind a dune in an environment similar to a depositional lobe.

3.6.2. Limitations of the methodology and future work

The method presented can be modified in future studies to broaden its application or to further investigate sediment transport processes and related depositional settings. In landscapes with a more complex geomorphic history (e.g., an embayed beach with appreciable fluvial inputs), a calibration dataset that includes more, or different, MoTs might be used to differentiate a broader suite of landforms or strata (e.g., fluvial, glaciofluvial, lacustrine, or marine). Also, mineralogical separation to isolate quartz or different opacities of quartz could be useful for improving the method or expanding it to different MoTs (cf. Gomez et al. 1988). In this study, grains were separated for mineralogy through the digital thresholding process (Figure 9B); darker grains such as micas and opaque feldspars were removed by the triangle thresholding method based on the YUV color space. A basic assumption of this approach is that, by thresholding out darker grains, the remaining mineralogy of the sample is largely homogeneous (in this case, composed mostly of quartz). Thresholding techniques might be further facilitated by using sediment that consists of minerals with distinct colors or opacities. For example, the thresholding technique could be used to remove light-colored (quartz) grains to isolate and examine only feldspars or heavy (e.g., magnetite) grains. Future work could also investigate regional sediment transport histories that influence particle shape. It is possible that the transport histories of the samples presented here are more complex than littoral transport to the backshore followed by aeolian transport over the beach and into dune deposits.

In addition, the geological setting and resulting sedimentological properties of the study area may partly control shape sorting or grain rounding. For instance, the northwestern portion of Calvert Island consists mainly of coarse-grained granodiorite (Roddick 1996) that erodes readily under current climatic conditions. Weather stations installed on the island give annual temperature averages of between 9 and 10 degrees Celsius and mean annual precipitation of 3,000 to 3,500 mm, conditions that are conducive to extensive bedrock weathering. This weathering produces regolith and sand-size

"young" sediments with subangular grains that can be modified over relatively short distances by wind or water. The recently stabilized landforms on Calvert Island's northwestern coast preserve these young sediments (Neudorf et al. 2015b), which still contain appreciable amounts of feldspar that has yet to disintegrate into clays.

These sedimentological properties are in contrast to those in other coastal regions that contain more mature sediments, or sediments that are much less resistant to weathering. For example, minor glaciation in Australia (both spatially and temporally) through the Pleistocene (Barrows et al. 2001) resulted in the development of very mature sands consisting of well rounded, mostly quartz grains. It is possible that in that environment the method presented here could be unsuccessful, as subtle differences in well-rounded quartz grains would be difficult to resolve in two-dimensional imagery. In Hawaii, coastal sediments are typically dominated by calcareous sands eroded from fringing reefs, with minor fractions of mafic volcanic minerals (Fletcher et al. 2011). These sands, which are highly susceptible to weathering and dissolution, are much softer than quartz and feldspar, and thus, the window for shape sorting that generates appreciable differences in grain rounding may be too small to detect using our method.

3.7. Conclusions

The aim of this study was to develop a method that requires inexpensive and easily obtainable equipment and software that differentiates littoral and aeolian sediments to aid in landscape interpretation and environmental reconstruction using sands stored in relict landforms. The method is based on the principle of shape sorting due to aeolian transport (Mazzullo et al. 1986). It was found that solidity, akin to sedimentological roundness, most commonly (86% of the time) showed a statistical difference between littoral and aeolian sands. The method performed well, predicting the MoT of sands of relict landforms 76% of the time. Avenues for further investigation of this method include testing in

different geomorphic, mineralogic, and climatic environments, extension to different MoTs, and performing basic mineralogical separation beforehand. Opportunities for integration of these data with other diagnostic sand-grain data (such as petrology, electron microscopy, or GSD) exist. Some evidence suggests that our method may also predict subenvironments (such as upper beach, lower beach, foredune crest, or depositional lobe) from calibration samples.

4. Late Quaternary landscape evolution in a region of stable postglacial relative sea-levels, British Columbia central coast

4.1. Abstract

After retreat of the Cordilleran Ice Sheet, and as glacioisostatic adjustments on the central coast of British Columbia proceeded, a complex coastline emerged and RSL rapidly reached equilibrium, maintaining stability over the Late Pleistocene and Holocene. This study provides a Late Quaternary reconstruction of the landscape evolution of a geographically distinct location on the central British Columbia coast, northwest Calvert Island, which is located on the eastern edge of Queen Charlotte Sound between northern Vancouver Island and southern Haida Gwaii. Elsewhere in coastal BC, on the northern coast of British Columbia, RSL was as much as -150 m below modern levels, and on the southern coast of British Columbia near Vancouver, RSL was as much as +200 m higher. Geomorphological observations from lidar imagery, sedimentological and palaeoecological evidence, and a robust luminescence and ^{14}C-based chronology spanning the last 15,000 years are used to reconstruct the landscape of northwest Calvert Island following CIS retreat. These include a Late Pleistocene, post-LGM re-advance of glacial ice and minimal subsequent RSL change. Localized proglacial sedimentation, extensive coastal reconfiguration (e.g., rapid shoreline progradation of >1 m a^{-1}), and isolated aeolian landform development and stabilization have all shaped the island's northwest coast through postglacial time. These findings have implications for the understanding of the drivers of sedimentary processes and recent discoveries of Late Pleistocene human habitation in the region.

4.2. Introduction

British Columbia's (BC's) Pacific coastline has been subjected to significant changes in glacial cover, climate, and RSL during the Late Quaternary. Following the Last Glacial Maximum (LGM), which for the Cordilleran Ice Sheet (CIS) occurred sometime between 18 and 16 ka cal BP (Clague et al. 1980; Hicock et al. 1982; Clague and James 2002), glacial retreat was staggered and involved several re-advances of ice (e.g., Saunders et al. 1987; Clague et al. 1997; Friele and Clague 2002; Kovanen and Easterbrook 2002; Menounos et al. 2009). This was influenced by climate through the Late Pleistocene, where a number of established cold-climate periods occurred as an anomaly to the general warming trend, such as the Older Dryas (~14 ka cal BP), the Inter-Allerød Cold Climate period (~13.1 – 12.8 ka cal BP), and the Younger Dryas (~12.6 – 11.5 ka cal BP) (Lowe et al. 2001, Figure 6). Fluctuating ice cover resulted in high-magnitude changes in RSL along the coast, mainly due to variable isostatic adjustment and changes to the global volume of water in the ocean basins (eustatic sea-level). Spatial variations in RSL change at the regional scale in the northeast Pacific are very apparent (Shugar et al. 2014), including a RSL hinge zone where relatively little change took place (e.g., McLaren et al. 2014).

Recent investigations into the character and extent of ice cover on the BC coast have yielded many syntheses of the knowledge of the CIS, including the timing of LGM advance and retreat (Clague and James 2002), extent (Clague 2009), impact on the continental shelf (Barrie et al. 2014), and post-LGM re-advances of ice (Menounos et al. 2009). Specific knowledge pertaining to the CIS on the central coast of BC, however, is lacking, with inferences on extent and character based mainly on data from large glacial troughs on the continental shelf (e.g., Luternauer et al. 1989; Barrie et al. 1991; Josenhans et al. 1995; Barrie et al. 2014). The troughs are generally believed to have resulted from erosion by coalescing ice streaming southwest from Hecate Strait (Figure 13). Little knowledge of terrestrial CIS ice on the central coast exists, aside from a recent study that has identified a locally significant re-advance of the CIS at 14.2 ka cal BP that retreated from the study area at 13.8 ka cal BP (section 2). Most work

has focused on the Coast Mountains to the east (Figure 13; Menounos et al. 2009; Margold et al. 2013; Taylor et al. 2014; Mood and Smith 2015).

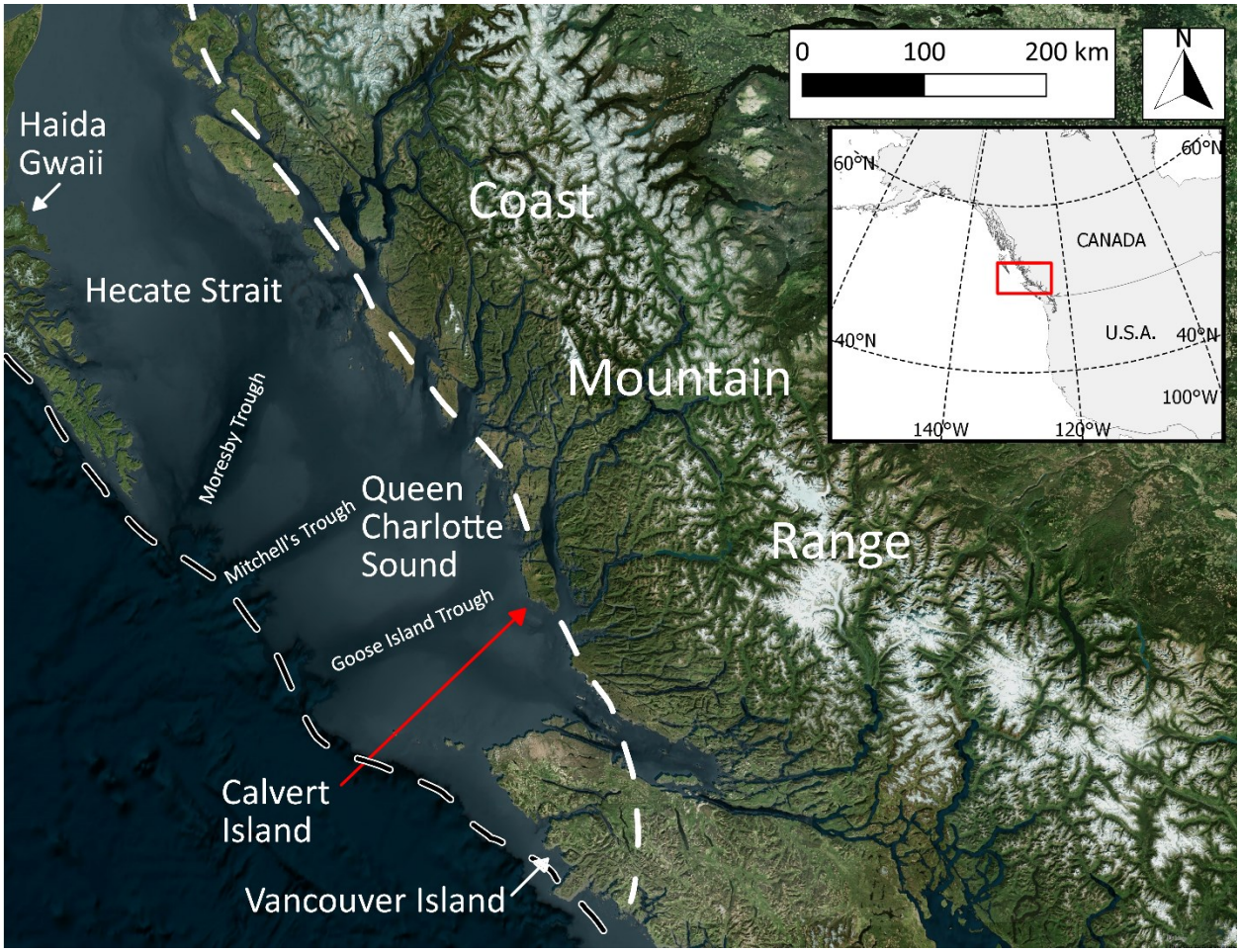

Figure 13. Map of the central British Columbia coast. Black dashed line shows the estimated extent of the CIS ice at the LGM (Taylor et al. 2014) and the white dashed line shows the hinge line, a zone of little RSL change following deglaciation (Shugar et al. 2014), with dash over Calvert Island removed for clarity. Moresby, Mitchell's, and Goose Island Troughs are collectively discussed above and below.

A RSL hinge-line between the isostatically depressed inner coast and forebulged outer coast has recently been proposed in several studies: McLaren et al. (2011; 2014) have provided evidence of RSL stability over much of the Holocene from two regions on the central BC coast, while Shugar et al. (2014) extended this sea-level hinge to the entire northeast Pacific (the southern portion shown in Figure 13). The central coast region is one where land subsidence during glaciation and subsequent rebound following deglaciation is equally balanced with eustatic sea-level rise associated with the demise of the

major ice sheets following the LGM. The hinge-line zone represents an area that may be rich in archaeological finds, with areas of continuous occupation of more than 10,000 years possible (McLaren et al. 2015).

This section documents the Late Quaternary evolution of a coastal region that lies along the RSL hinge line in coastal British Columbia (Figure 13). An interdisciplinary approach utilizing remotely sensed data, stratigraphy and sedimentology, geochronology, and palaeoecology is used to make inferences about the extent of ice following the LGM, the nature of proglacial sedimentation, coastal evolution, and palaeoenvironments from 15.1 ka cal BP to present.

4.3. Research Area

Calvert Island is ~300 km^2 and is located at the eastern edge of Queen Charlotte (QC) Sound between Haida Gwaii to the north, Vancouver Island to the south, and the Coast Mountains to the east; it is exposed to the Pacific Ocean on its west coast (Figure 13). The island lies within the Coastal Western Hemlock biogeoclimatic zone, characterized by the prominence of *Tsuga heterophylla* (Western hemlock), *Thuja plicata* (Pacific red cedar), and *Picea sitchensis* (Sitka spruce). Understory includes abundant mosses in poorly drained areas and sedges (e.g., *Elymus mollis* (Dune wild rye)) in well drained areas. Climate is classified as temperate oceanic (Cfb) in the Köppen-Geiger climate classification system (Peel et al. 2007), and local weather stations installed on the island show mean annual temperatures between 9 and 10 ^oC and precipitation ranging from 3,000 to 3,500 mm. Wind exposure is high, typically from the southeast, with gusts of over 25 m s^{-1} common in winter months.

The island is largely early Cretaceous granitoid rocks of the Calvert Island Pluton (CIP) that range from granite to diorite (Roddick 1996), and are similar in composition to plutonic rocks of the Coast Mountains. The western portion of the island is characterized by a combination of rocks of the CIP, Late Quaternary glacial deposits, and numerous gravel and sand beaches (Figure 14). Active aeolian sand

dunes are limited to beaches at the northwestern corner of the island and are typically backed by extensive stabilized dunes and beach ridges. The tectonic setting of the central coast is characterized by the confluence of the Cascadia subduction zone to the south and the QC-Fairweather strike-slip fault to the north (Clague 1989). Recent work shows that the latter also has a minor thrust component (James et al. 2013; Lay et al. 2013; Szeliga 2013; James et al. 2015).

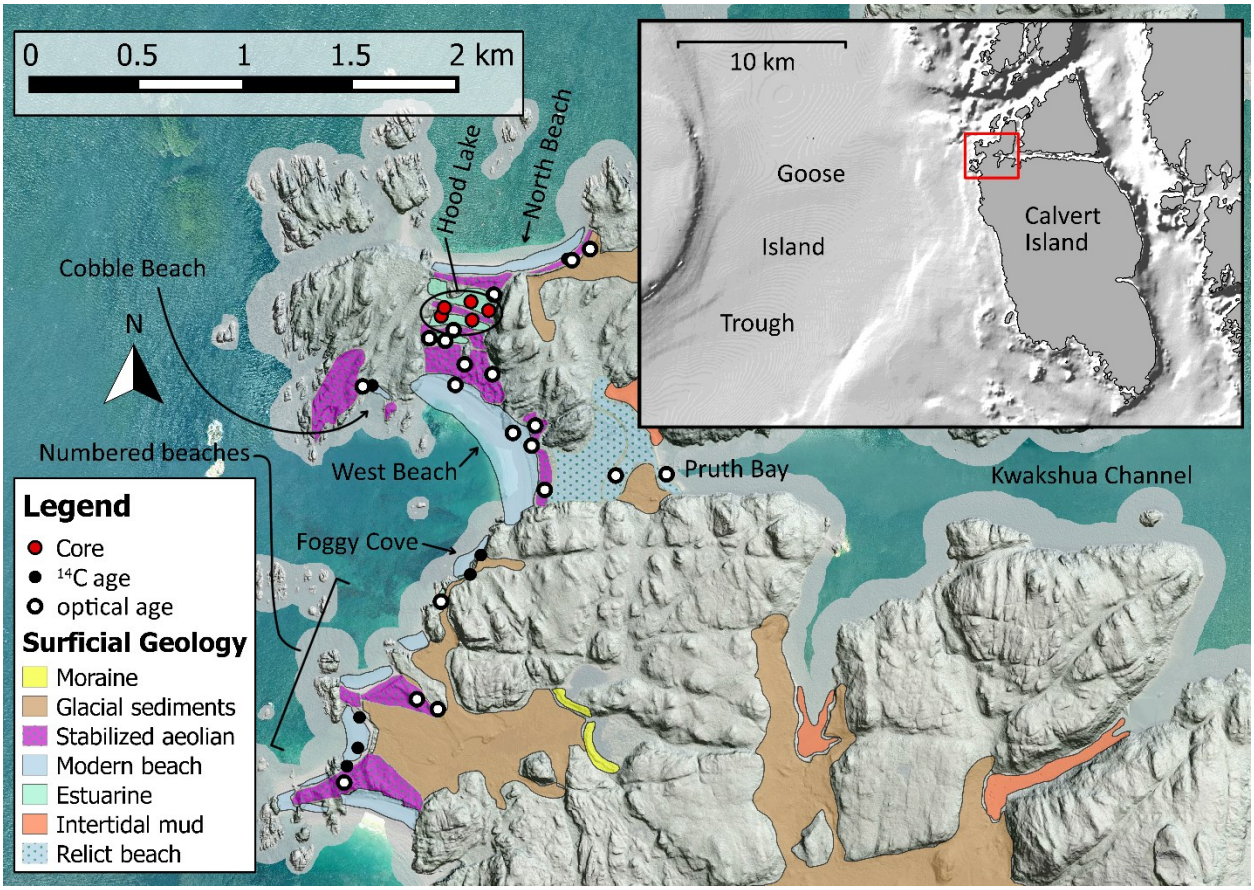

Figure 14. Study area on northwestern Calvert Island with surficial geology, geochronology sample and core locations, and regions discussed in the results and discussion are labeled. Inset map shows the location of the study area (red box) on Calvert Island. Note that several geochronological samples also came from cores (Appendix 1). Base map is a 2 m lidar bare earth digital elevation model prepared by the authors.

Queen Charlotte Sound comprises an expansive portion of the continental shelf and consists of three banks separated by glacial troughs (Barrie et al. 2014; Figure 1). The troughs are 10-40 km wide, up to 500 m deep, trend SE – NW, and are capped primarily by mud (Barrie et al. 2014) and till units that may indicate multiple glaciations (Barrie et al. 1991). Ice that initially eroded these troughs was likely

sourced from Haida Gwaii and the Coast Mountains, merging in Hecate Strait during the LGM (Barrie and Bornhold 1989). Ice flowed south, coalesced with ice from troughs in QC Sound, and extended to the shelf edge (Josenhans et al. 1995). Some areas of the shelf in QC Sound were sub-aerial as RSL remained low through the Late Pleistocene and Early Holocene. Ice rapidly retreated between 14.1 and 12.9 ka cal BP, and the region was largely ice free by 13.5 - 13 ka cal BP (Hetherington et al. 2004).

4.4. Methods

4.4.1. Mapping

Landforms and surficial geology were initially mapped using an airborne lidar dataset collected in August 2012 from a fixed wing aircraft at a nominal flight height of 1150 m above ground level. The average below-canopy ('ground') sampling point density along each flightline was approximately 1 pt m^{-2}. Coincident 0.15 m resolution digital orthophotos were also used to aid in analysis and interpretation. A digital elevation model (DEM) was generated by applying automated canopy filters and manual ground classification procedures to the raw lidar point cloud, and the resulting ground surface point cloud was interpolated using nearest neighbor with a 2 m cell resolution.

4.4.2. Geochronology

A geochronology for this study was developed using a combination of 38 new AMS ^{14}C ages from organic materials and 18 new optical age samples of sands from stabilized sedimentary landforms (Appendix 1). Two additional AMS ^{14}C ages from McLaren et al. (2014) were also used. Samples for AMS ^{14}C dating consisted of macrofossils which were collected from a combination of outcropping organic mats, organic-rich sediments, or from pond cores. Samples were processed at the W.M. Keck Carbon Cycle Accelerator Mass Spectrometry Laboratory in Irvine, California (UCIAMS), and the five samples in section 2 (labeled Foggy Cove in Appendix 1) were pre-processed (cleaned and identified) by Alice Telka

(Paleotec Services Ottawa). AMS ^{14}C ages are presented as 2-sigma calibrated age ranges and are reported as kilo-calendar years (ka) BP (before AD 1950). Calibration was carried out using the Calib 7.1 program (Stuiver et al. 2013) using the INTCAL13 radiocarbon database for terrestrial samples and MARINE13 for marine samples, with a lab error multiplier of 1. Plant macrofossils were preferentially selected to avoid the marine reservoir effect, however several shell samples were submitted and were corrected using a marine reservoir correction based on a weighted mean, ΔR, of the nearest 10 known-age samples (Appendix 1). The development and testing of laboratory procedures used for optical dating in the study area is summarized in Appendix 3, can is thoroughly covered in Neudorf et al. (2015b).

4.4.3. Lithostratigraphy

Exposures of Late Quaternary stratigraphic sequences are rare on northwestern Calvert Island, as the landscape consists largely of low-relief surficial veneer or bedrock outcrops. Two exposures of sediments in coastal bluffs on the west coast of the island were examined: one at Foggy Cove and the other at Cobble Beach (Figure 14). Sediments exposed at Foggy Cove have provided the majority of information on the geomorphology and ecology of the Late Pleistocene and Early Holocene landscape, and findings are reported in section 2.

The stratigraphy exposure at Cobble Beach (Figure 14) is more limited than that at Foggy Cove, with the former consisting of an organic-rich unit at the base directly overlain by 6.2 m of sand. At this site, lithostratigraphy was recorded and sand samples were collected for grain-size and shape analyses to help inform depositional environment (see section 3). Chronology was provided by ^{14}C and optical dating (Appendix 1). Surficial materials in locations without sedimentary exposures were examined in 25 shovel pits, four lake percussion cores, and one vibracore from a ridge bisecting the two main basins of Hood Lake (Figure 14). For each shovel pit, the sedimentological characteristics similar to those described at stratigraphic exposures were documented (e.g., grain size, colour, structures, contacts, and

grading). Where organic materials was present, samples were collected for AMS ^{14}C dating (e.g. samples CIRC8, 12, 16a,b; Appendix 1), and at the majority of pits an optical dating sample was also collected. Care was taken to extract samples for optical dating from the C horizon (typically > 0.40 m depth) of the soil profile to reduce the impact of bioturbation and the movement of dissolved minerals through the profile (Lian and Roberts 2006). Percussion cores were obtained from Hood Lake using a lightweight percussion core sampling system (Reasoner 1986). Core sediments were logged and sampled for grain size and palaeoecological analysis. In addition to the percussion cores, one 1.5 m subaerial vibracore was taken (Figure 14). This core was sampled for grain size and shape analysis (see below) and for ^{14}C and optical dating.

4.4.4. Sediment sampling

Sediment samples were collected alongside geochronological samples and were analyzed for grain size and shape; grain shape parameters were analyzed to help determine environment of deposition (e.g., littoral versus aeolian, methodology described in section 3 (Appendix 2)). Samples for grain size analysis and shape parameters were collected in the C horizon (> 0.40 m depth) in cases where there was appreciable soil development to avoid grain alteration.

4.4.5. Palaeoecology

Two key sites were sampled for detailed palaeoecological investigation: Foggy Cove and Hood Lake (Figure 14). Section 2 describes the palaeoecological methods employed at Foggy Cove, and the diatom and macrofossil assemblage from cores collected in Hood Lake record the palaeoecology of an accretionary complex between North and West beaches. Cores C01 and C03 from Hood Lake (Figure 14) were sampled for palaeoecological analysis. ^{14}C dating of seven macrofossil samples (Appendix 1) from C01 and five from C03 provided the geochronology. Samples were processed using standard techniques

and microfossils were mounted in Naphrax diatom medium. Identification was conducted under 400x magnification, aided by freely available diatom databases (e.g., Campeau et al. 1998). Macrofossils were extracted and identified using available fossil keys (van Barneveld et al. 1980). The macrofossil assemblage and preservation were also investigated in organic mats found on North and 4th beaches.

4.5. Results

4.5.1. Landform geomorphology, sedimentology, and stratigraphy

i) Numbered beaches - In this region (Figures 14, 15) there are two relict moraines, composed of large boulders (some more than several m in diameter), that impound lakes to the east. The southernmost moraine-dam has a breach at its northern end. The northern-most moraine-dammed lake was cored in 2012 (McLaren et al. 2014) and core stratigraphy indicated the presence of blue clay below 0.2 m of brown silty clay with charcoal, needle fragments, sclerotia, and conifer seeds that dated to 14.6 – 14.2 ka cal BP (HW6-b, Appendix 1). Above this, a gyttja layer containing a *Pinus contorta* seed, a *Picea spp.* seed, and needle fragments was dated to 13.4 – 13.3 ka cal BP (Hw6-a, Appendix 1).

A large plain of unconsolidated sediments is arranged into terraces downstream (west) of the dammed lakes, with evidence of modern and relict channel erosion (Figure 15). The upper terrace is comprised of mixed pebble-gravel-sands and the lower terrace is coarse to fine sands. Further west, backing the modern beaches, are high (>10 m) relict dune ridges consisting of well-sorted medium to fine sands with an aeolian grain shape (CIDS 10, Appendix 2) that dated to 8.55 ± 1.37 cal ka cal BP (CIDS 10, Appendix 2). A dune-capped tombolo (nearly 40 m above msl) between 4th and 7th beaches dated to 3.75 ± 0.34 cal ka cal BP (sample CIDS8, Appendix 1). Relict dunes back all but 2nd beach, which is composed of a cobble and boulder upper beach and sandy intertidal zone. Third beach is sandy and cuspate, with a boulder lag along the western edge. Fourth beach has a boulder lag near the northern edge and cobble/gravel lags in the lower intertidal zone along the span of the beach.

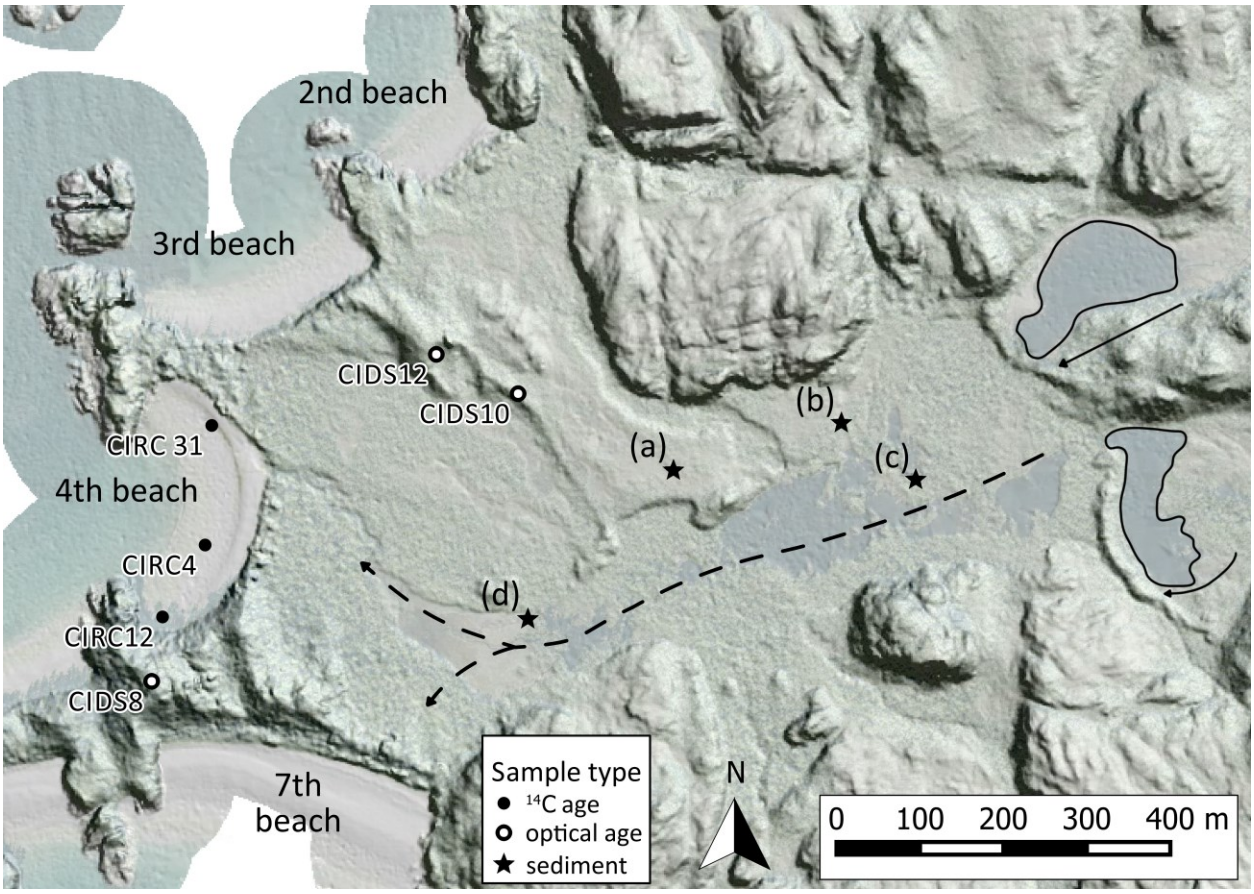

Figure 15. The numbered beaches including geochronology (Appendix 1) and sediment sample (a–d) locations (Appendix 2). Solid arrows highlight two distinct moraines, solid lines outline the moraine-dammed lakes, and the dashed line shows possible glacial meltwater flow routes.

In the intertidal zone on 4th beach, a log (with minor gravel embedded in the wood) was excavated from a consolidated very fine grey sand that contained rare (<5%) clasts of gravel. Sample CIRC4 was collected from the log and was AMS ^{14}C dated to 15.0 – 14.2 ka cal BP (CIRC4, Appendix 1). A small (0.40 m deep) pit was dug into 4th beach and exposed a poorly sorted, grey very fine sand (4th lower, Appendix 2) with minor gravel that was overlain by 0.05 m of brown, moderately sorted fine sand (4th upper, Appendix 2). Capping this deposit was a 0.02 m thick organic mat that crops out in the modern beach. Fossils identified in this bed include *Tsuga heterophylla, Picea sitchensis,* and *Thuja plicata*, species that can currently be found in the study area. Fossil plant material was dated by ^{14}C

between 10.8 – 9.1 ka cal BP (CIRC 12, 16a, 16b, Appendix 1), and an optical date from the underlying fine grey sand yielded an age of 8.72 ± 0.65 ka cal BP (CIBS9a, Appendix 1).

ii) Foggy Cove - An eroded bluff exposure of sediments was found at Foggy Cove behind a cobble/boulder intertidal beach. The stratigraphy, palaeoecology and geochronology was documented in Section 2. Sediments north and west of the bluff consist of large clast sizes (some several m in diameter) similar to those found in Units 3-5 (section 2) of the bluff. To estimate the possible original extent of Foggy Cove sediments before bluff erosion, kelp extent maps can be used: a bouldery substrate provides an important surface required for the establishment of dense kelp bed forests (Stephens et al. 2006). Thus, low tide observations and existing maps of kelp extent (Holmes et al. 2016) can, together, give an indication of potential Late Pleistocene sedimentation (Figure 16) that might have extended nearly, if not entirely, across the mouth of the embayment from the numbered beaches in the south to Cobble Beach in the north.

iii) West Beach to Pruth Bay - Pruth Bay is a cobble beach that hosts Late Holocene (< 1 ka cal BP) aged cultural materials, such as points and flakes (Stafford and Christensen 2014). West Beach is a deep (~200 m at low tide), gently sloping (~1^{o}), fine sand (CIBS2, Appendix 2) dissipative beach. A series of four tall (2-3 m high) relict, forested foredunes exist behind a modern, low (<1 m), stabilized foredune at the southern end of West Beach (found at CIDS3, CIDS4).

In the intertidal zone of Pruth Bay, an excavator pit exposed a ~1 m-thick clast-supported well-rounded, sub-spherical cobble bed with a matrix of bivalve shell fragments, one of which was dated to 0.8 - 0.5 ka cal BP (CIRC 21, Appendix 1, Figure 17). Approximately 100 m and 160 m landward (west) from Pruth Bay, sediments exposed in a drainage cut bank and a shovel pit (CIBS1, Figure 17), respectively, were examined. The former yielded a 1.5 m-deep clast-supported cobble bed that extended horizontally over 10 m and was bounded by soil cover to the east and medium, well-sorted

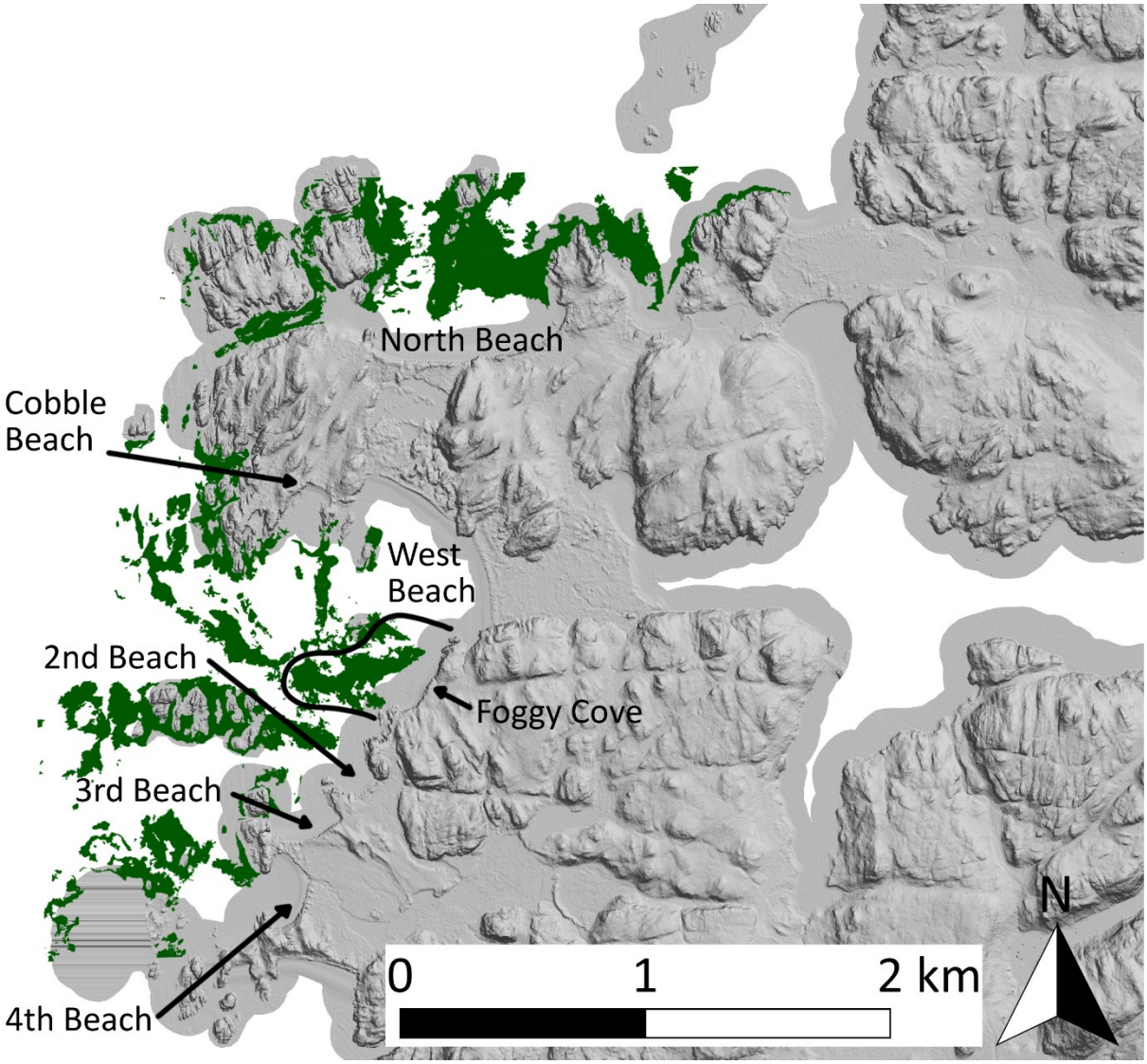

Figure 16. Kelp extent shown in green (modified from Holmes et al. 2016). Solid black line shows the extent of boulders directly observed at low tide at Foggy Cove. The bouldery substrate, approximated by the kelp extent, extends west of 4th beach and Foggy Cove and north of North Beach.

sand to the west. Two clast fabrics were measured from the cobble bed. Fifty-one elongate tabular clasts (*a, b* axes $\geq$1.5x length of *c* axis) were measured in each, and both yielded high (S_1 = 0.76 and 0.72) eigenvalues with average dip direction toward the east (Figure 17). The second exposure was a 2 m deep pit dug with an excavator into unconsolidated sand. Two distinct beds were identified: a lower bed consisting of horizontally laminated medium, well-sorted sand with littoral grain shape (sample CIBS1-4, Appendix 2) with alternating dark and light grey laminae buried at 0.51 ± 0.05 ka cal BP (CIBS1, Appendix 1), and an upper bed, 1 m deep, consists of well-sorted medium sand with aeolian grain shape (samples

CIBS1-1, 1-2, Appendix 2) with planar cross-bedding. Sediments backing West Beach are generally well-sorted fine sand, most of which had aeolian grain shapes (samples CIDS1, 2, 3, 4, Appendix 2) and had burial ages no older than 0.11 ± 0.02 ka cal BP (Appendix 1).

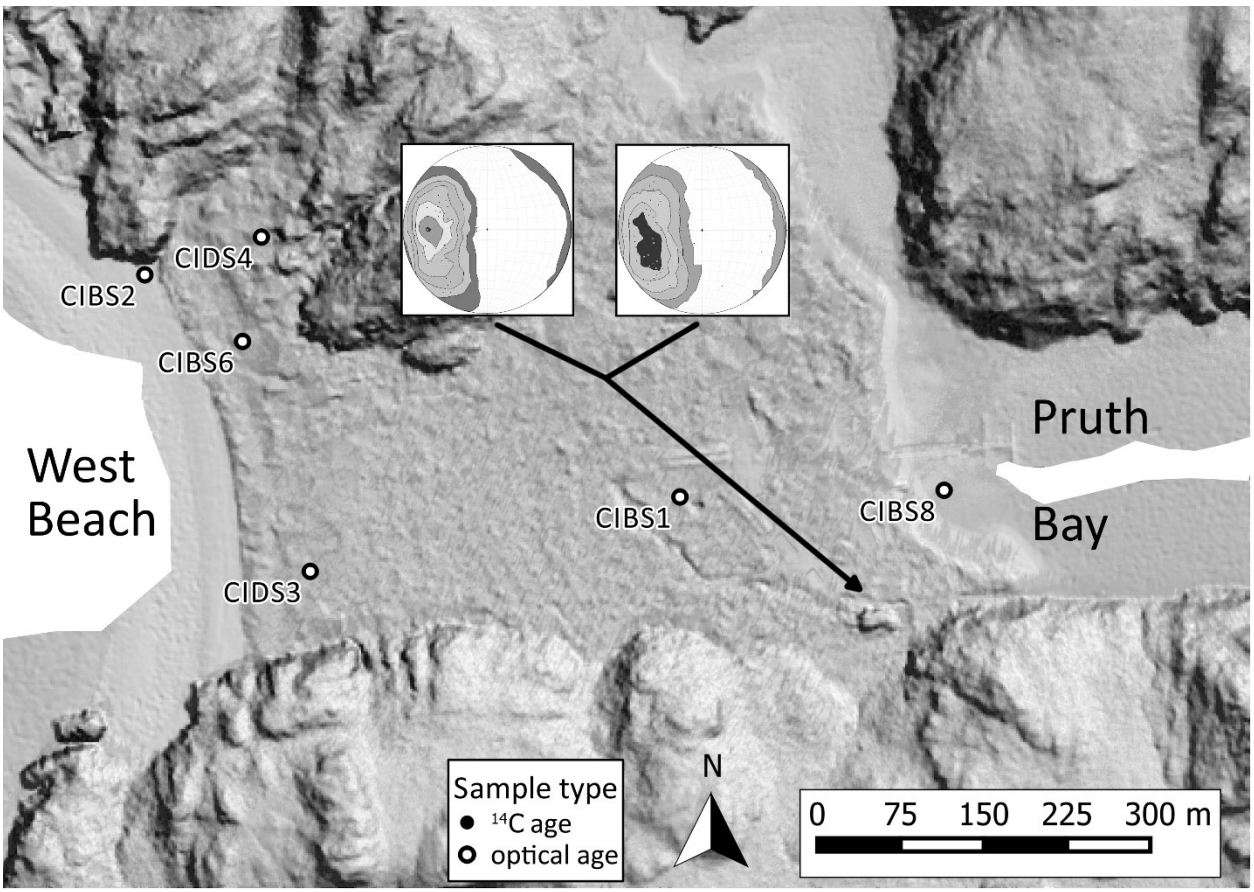

Figure 17. West Beach - Pruth Bay subregion, showing the southern portion of West Beach through to Pruth Bay, including the Hakai Institute (between samples CIBS1 and CIBS8). Geochronology samples and clast fabric stereograms are shown, with contours showing concentration of poles-to-planes.

iv) Cobble Beach - Cobble Beach is a bedrock headland-bound embayment, and its steep (10^{o}) modern beach consists of well-rounded pebbles, cobbles, and boulders of mixed lithologies with a sandy nearshore region. Large, steeply sided ridges (>10m tall) occur north and west of Cobble Beach and are generally aligned northeast-southwest (Figure 14). Auger tests showed that the ridges to the west and north consist of a medium to fine well-sorted sand, while ridges to the north-northeast are bedrock

(Figure 14). The western end of Cobble Beach consists of a 6.6 m tall exposure of unconsolidated sand, likely a wave-cut exposure of one of the large sand ridges immediately west and north of the exposure.

Figure 18. (a) Cobble Beach exposure. Unit descriptions (1, 2, 3) in text. (b) Cross bedding observed in unit 3. (c) Organic material similar to unit 1 outcropping further down the beach, with pocket knife for scale. The Cobble Beach exposure is visible in the background.

Three lithostratigraphic units were identified at Cobble Beach (Figure 18a). Unit 1 is an organic mat of varying thickness (0.04 – 0.30 m), immediately overlying the modern beach, that consists of consolidated fibrous woody peat interbedded with lenses of sand that are rich in disseminated organics. Woody fragments are highly weathered and fossil identification was not attempted. This unit also crops out at other locations in the modern beach face (Figure 18c). AMS ^{14}C ages of woody fragments at a number of locations within the unit indicate that the organic unit was deposited between 7.6 and 5.3 ka cal BP (samples CIRC1, 6, 19a, 19b, Appendix 1, note overlapping sample locations in Figure 14 highlighted by the Cobble Beach label). Unit 2 is 3.3 m of inversely graded very well-sorted fine to medium sands with an aeolian grain shape (sample CICB2—upper (U) through –lower (L), Appendix 2), with cross-beds and undulating beds at the base. Optical dating sample CIDS5 (Appendix 1) was collected from 0.35 m above unit 1 and yielded a burial age of 2.18 ± 0.30 ka cal BP. Unit 3 consists of 2.7 m of very well-sorted, cross-laminated fine sands with minor folding (Figure 18b) and a gradational

lower contact (sample CICB1, Appendix 2). One optical dating sample was collected from 1.17 m below the modern soil (sample CIDS6, Appendix 1) that yielded a burial age of 3.14 ± 0.41 ka cal BP.

v) West Beach to North Beach - The landscape between West Beach and North Beach is a complex arrangement of bedrock outcrops, sandy terraces and ridges, shallow lakes, and prominent sand dunes (Figures 2, 7). The north end of West Beach is backed by a 2-5 m high established foredune, one of the last active dune systems on Calvert Island. Landward of the foredune is a large (~5×10^5 m^2) stabilized dune complex containing large trough blowouts with high sidewalls and depositional lobes approaching 12 m in height (Figures 2, 7). A series of three curvilinear sandy ridges exist on the south, middle, and north shores of Hood Lake, sub-parallel to the modern foredune backing West Beach. Between Hood Lake and North Beach, a tall (15 m), stabilized forested foredune is flanked by a flat, elevated forested sandy platform (sample CIDS15, Figure 19). The foredune varies in height along North Beach, and has a tall wave-eroded scarp (as high as 1.5 m) along its length. The modern North Beach is composed predominantly of medium sand, but is also characterized by a combination of cobble/gravel lags and boulders found on the eastern end. It is steeper (5^o) and less deep (60 m) than West Beach.

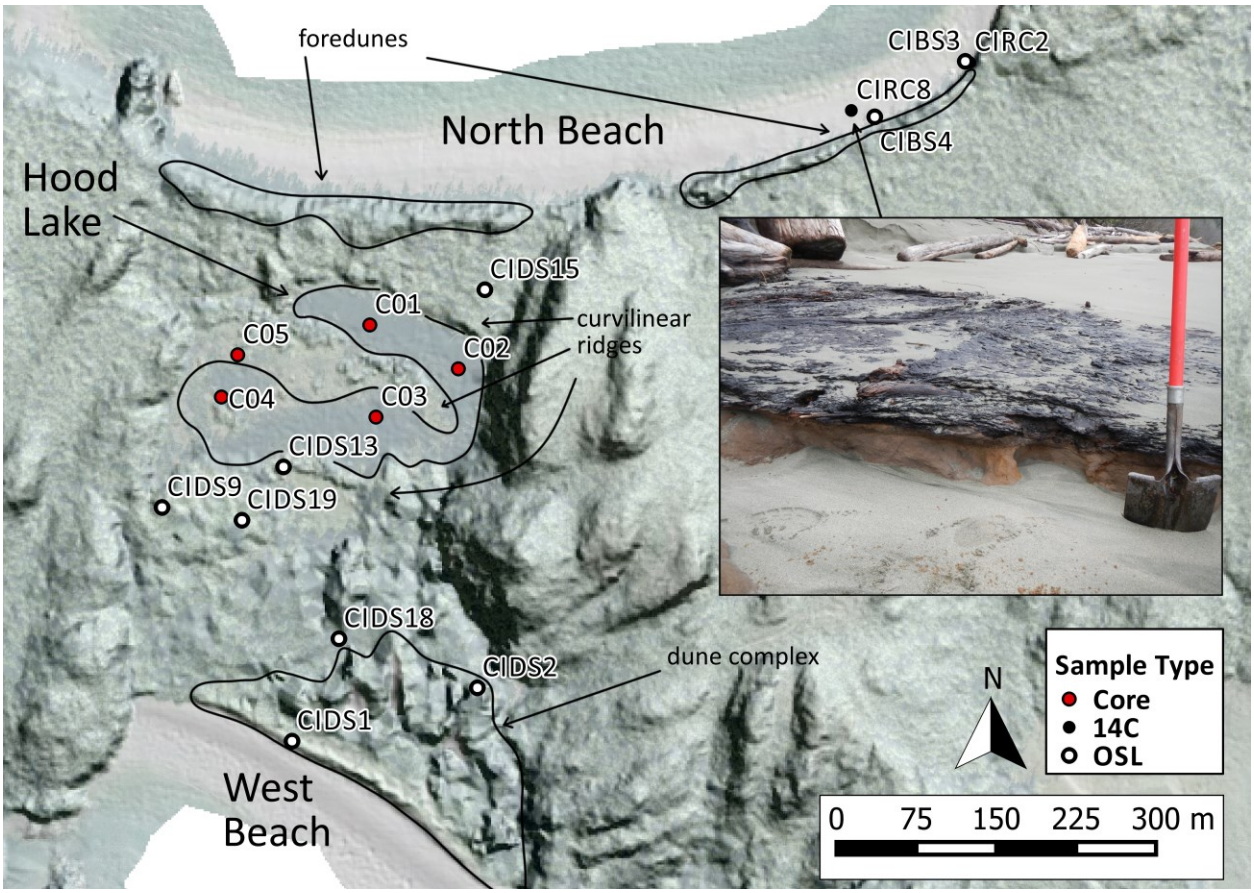

Figure 19. West Beach - North Beach sub-region, including the northern end of West Beach, dune complex backing West Beach, Hood Lake, three curvilinear ridges forming shorelines for Hood Lake, North Beach, and the sizable North Beach foredunes. Geochronological samples and core locations are shown. Inset shows the organic mat cropping out in North Beach, from which CIRC 8 was collected. The orange sands below the mat comprises the unit that optical dating sample CIBS4 was collected from (note that CIBS4 was collected from lower, less oxidized sands in another exposure).

Between West Beach and Hood Lake, sediment and geochronology samples were collected from five shovel pits (CIDS1, 2, 9, 18, 19). The sands were found to have an aeolian grain shape (Appendix 2) and optical ages increased from modern (sample CIDS1) to 0.42 ± 0.07 ka cal BP (CIDS9) (Appendix 1). A shovel pit was dug on the southernmost curvilinear ridge (sample CIDS13, Figure 19), and consisted of sands with an aeolian grain shape (CIDS13, Appendix 2). A subaerial curvilinear ridge parallel to the north and south shores of Hood Lake was cored using a vibracoring unit (core C05, Figures 7, 8) and a moderately well-sorted fine sand (CIDS9, Appendix 2) unit was found to 1.47 m depth. An optical dating sample collected from 0.7 m core depth yielded a burial age of 0.35 ± 0.06 ka cal BP (CIDS17, Appendix 1) and a basal wood sample was dated using ^{14}C to 7.63 – 7.57 ka cal BP (samples CIDS17 and CIRC26a

respectively, Appendix 1, Figure 20). Percussion cores C03 and C04 were collected from the southern portion of Hood Lake. Both show similar, simple stratigraphy, with the upper part of the cores consisting mostly of gyttja overlying brown, well-sorted medium sands. Chronological control is provided by five ^{14}C ages (samples CIRC 27a, 36, 37, 38, 39, Appendix 1), and indicate that at 0.40 m core depth, the sediments had a littoral grain shape (C03-40, Appendix 2) and were deposited between 0.41 – 0.35 ka cal BP. Percussion cores C01 and C02 were collected from the northern portion of Hood Lake and both contained similar stratigraphy. They contained gyttja in the upper portion of the core, alternating organic- and macrofossil-rich (>80%) sediments and well sorted medium sand with an aeolian grain shape (C01-49, Appendix 2) in the middle of the core, and well sorted medium/fine grey littoral sand (samples C01-62 and -95, Appendix 2) at depth. Chronological control is provided by six ^{14}C ages (samples CIRC 29c, 29f, 29g, 29j, 33, and 34, Appendix 1, Figure 20) that suggest sands for the core were deposited between 1.8 and 0.65 ka cal BP.

Along the northern shore of Hood Lake is a ~1 m vertical consolidated sand exposure with subangular cobbles and pebbles at the water level. This exposure formed the base of a large flat-topped landform between Hood Lake and North Beach, that dated to 4.20 ± 0.33 ka cal BP (CIDS15, Figure 19, Appendix 1) and consisted of well sorted fine sand with an aeolian grain shape (CIDS15, Appendix 2). Near the eastern end of North Beach, a distinct, aerially expansive (several m^2) bed of organic materials hosting many well-preserved plant needle and seed macrofossils (*Tsuga heterophylla, Picea sitchensis,* and *Thuja plicata)* crops out in the modern beach (Figure 19, inset). No root fossils were found in this bed and macrofossils were fragmented and weathered. This organic bed, 0.05 – 0.08 m thick, was dated by ^{14}C to 6.70 - 6.66 ka cal BP (CIRC8) and the fine sands below yielded an age of burial of 5.58 ± 0.52 ka cal BP and were of a littoral grain shape (CIBS4, Appendices 1, 2). The slightly inverted ages, a high diversity of fossil species, lack of root fossils, and weathering suggest the organic bed was a reworked deposit. In the dune scarp backing this location is a 3.05 m exposure of sediments that was optical dated

from 2.89 ± 0.29 ka cal BP in sands near the base and ^{14}C dated to 1.9 – 1.5 ka cal BP in a shell midden at the top of the exposure (CIBS3 and CIRC5, respectively, Appendix 1). Another organic layer below this, likely correlative to the organic bed in the lower beach and consistent with optical age CIBS4, was ^{14}C dated to 5.9 – 5.8 ka cal BP (CIRC2, Appendix 1).

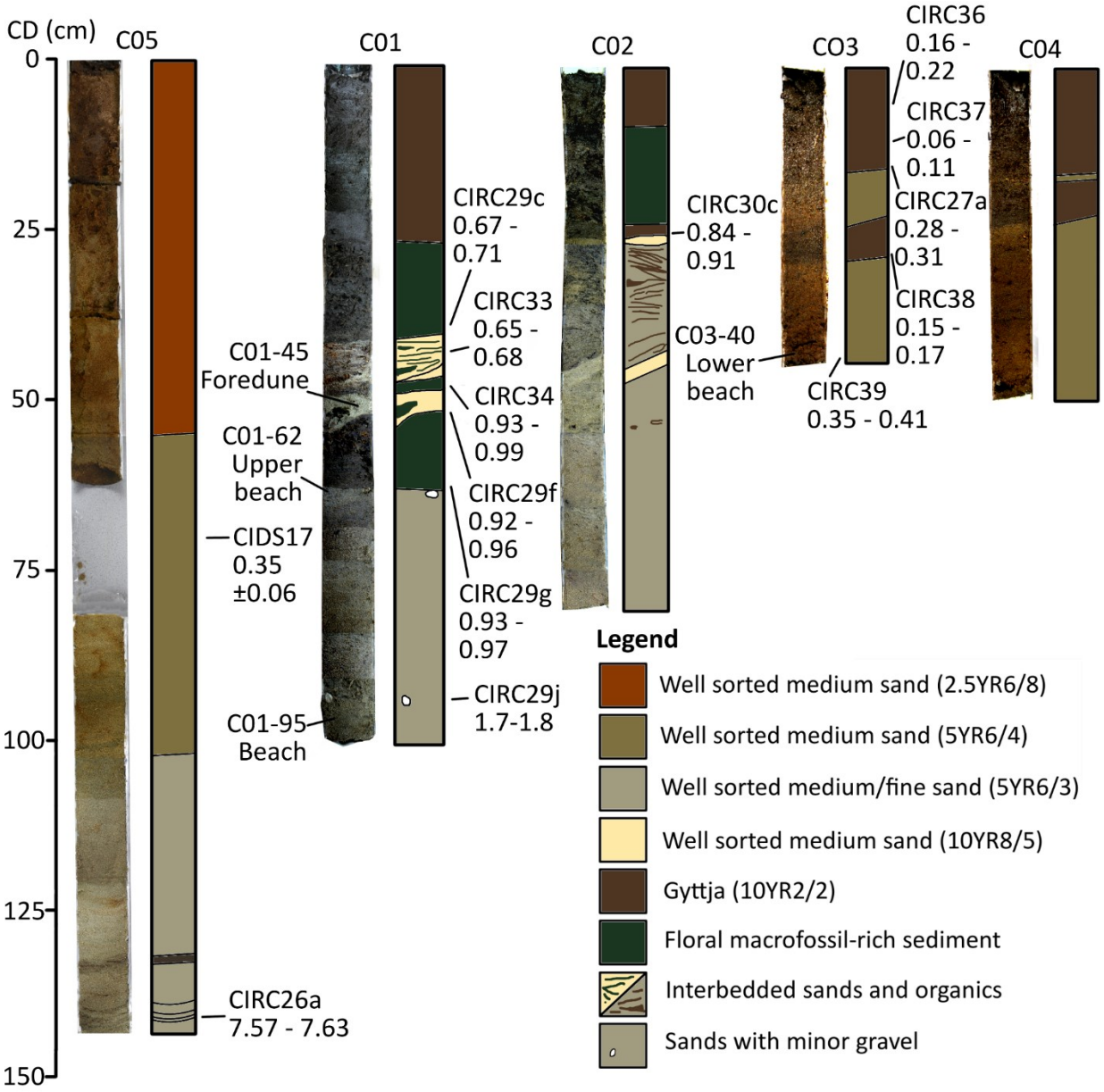

Figure 20. Stitched images (left) and stratigraphic interpretation (right) of cores collected from the Hood Lake area. CD = Core depth, or depth from the lake bottom. Optical age (CIDS17) and 14C ages (CIRC) shown (Appendix 1), and sand depositional setting determined from grain shape provided (see section 3, Appendix 2).

4.5.2. Palaeoecology

Discussion of the palaeoecology of Foggy Cove is provided in section 2. At Hood Lake, Cores C01 and C03 were selected for representative diatom and macrofossil analyses of Hood Lake. In core C01, between 0.98-0.62 m core depth, intertidal diatom species *Coscinodiscus nitidus* and *Amphora lineolata* were found. High numbers of saltwater/lagoon diatoms *Paralia sulcata* and *Diploneis stroemii* and freshwater coastal peat bog diatoms *Diploneis interrupta* and *Eunotia praerupta* were also found. Coastal seaside arrowgrass (*Triglochin maritima*) and amabalis fir (*Abies amabilis*) macrofossils were found near the basal sediments of this core. Radiocarbon ages constrain this portion of the core to between 1.8 – 0.95 ka cal BP (Figure 20).

Between 0.62 – 0.47 m core depth, a high abundance of freshwater peat bog diatoms, notably *Psuedostaurosira brevistrata*, *Frustulia* cf. *rhomboides*, and *Diatoma vulgaris*, were found. There was a continued presence of estuarine intertidal and inner bay species (*Paralia sulcata*, *Diploneis stroemii*, *Cocconeis scutellum*, *Navicula perminuta*). Brackish to slightly brackish species *Diploneis interrupta* and *Navicula phyllepta* were found in this portion of the core. Small amounts of grass (family *Poaceae*) pollen were also found in samples throughout this zone. Radiocarbon ages constrain this portion of the core to between 0.95 – 0.84 ka cal BP (Figure 20).

Between 0.47 – 0 m core depth, there was only one marine, backbarrier species (*Navicula perminuta*), seen in very low abundance near 0.47 m core depth. Dominant species throughout this zone include freshwater *Pinnularia* cf. *marchica* and *Psuedostaurosira brevistrata*. High occurrence of acidophilous (peat bog/marsh associative) species (*Tabellaria fenestrata*, *Eunotia pectinalis*, *Eunotia praerupta*) occur throughout this range of core depths. Presence of *Navicula tripunata* and *Pinnularia brebissonii* in these assemblages shows an increase in nutrient content in the pond. A wide variety of pollen was found in samples from this zone including cedar (family *Cupressaceae*), ericale tetrads (family *Ericaceae*), red alder (*Alnus rubra*), grass (family *Poaceae*), green alder (*Alnus viridis*), sitka spruce (*Picea*

sitchensis), and shore pine (*Pinus contorta* var. *contorta*). Radiocarbon ages constrain this portion of the core to between 0.84 ka cal BP to present (Figure 20).

In Core C03, from 0.44 – 0.20 m core depth, diatom flora consistent with open exposure and marine water influence were most common. The most frequently found species in this zone was delta-front/lagoon associative diatoms *Nitzchia sigma*. High numbers of *Navicula cancellata* (common in surf zone diatom assemblages) and *Diploneis interrupta* (brackish), were found in this depth range. Only one true freshwater, bog associative diatom species, *Stauroneis anceps*, was found. Radiocarbon ages constrain this portion of the core to 0.42 – 0.23 ka cal BP (Figure 20).

From 0.20 – 0 m core depth was an entirely freshwater diatom assemblage. Numerous *Eunotia* species were found in high abundance, as well as *Aulacoseira* spp. and *Amphora* cf. *ovalis*. Most species found were acidophilous and oligotrophic (associated with bog water runoff). Cedar (*Cupressaceae*), green alder (*Alnus viridis*), and grass (*Poaceae*) pollen were found throughout samples in this zone. Radiocarbon ages constrain this portion of the core to 0.23 ka cal BP to present (Figure 20).

4.6. Discussion

4.6.1. Palaeogeography

In Figure 21, the paleogeography of the study area is shown for 8 distinct time steps, tracing the geomorphic evolution from 14 ka cal BP to present. For each map, the symbols represented by the legend include sampling locations and surficial cover, ice is represented by the colour white (ice margins shown as a black dashed line), water by dark blue, and bedrock (which remains essentially constant over 15,000 years) is represented by the hillshade (akin to the map shown in Figure 16).

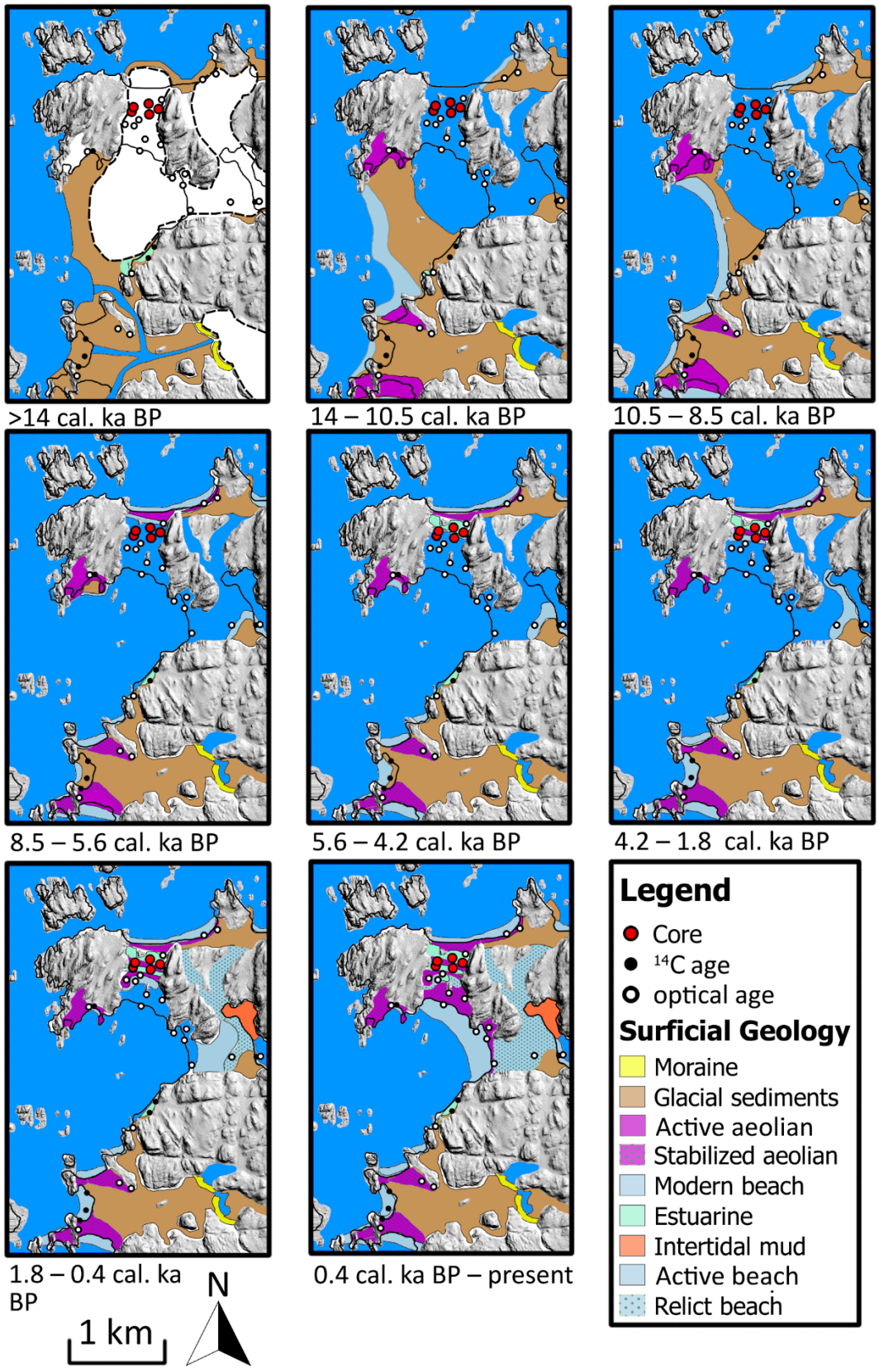

Figure 21. Palaeogeography reconstructed for the study area.

> 14 ka cal BP – The presence of a tidal marsh as found in the stratigraphic section at Foggy Cove area (see section 2), and proximal tree cover as evidenced by logs and branches found in the numbered beaches area (CIRC4, Appendix 1), shows that sometime prior to 14.2 ka cal BP ice had disappeared from the study area. By 14.2 ka cal BP, however, ice was re-advancing into the study area, as evidenced by AMS ^{14}C ages from the Foggy Cove stratigraphic sequence (section 2). This advance was accompanied by slightly higher, but falling RSL (McLaren et al. 2014).

The complete extent of this re-advance is difficult to ascertain as much of the evidence has been removed by erosion over time. The presence of small moraines (Figure 14) suggests a terminal extent for the glacial re-advance instead of at the LGM, as the small moraine size means a CIS origin for these moraines is unlikely. Large boulders of mixed lithology found at 3rd Beach, Foggy Cove, and the east end of North Beach suggest ice may have been proximal to these locations. Whether these boulders were deposited by the CIS or a re-advance is difficult to ascertain without further age determination.

Outwash sediments found west of the moraines in the numbered beaches region, with terracing and relict river incision, suggest that appreciable time passed with the ice margin at the location of the moraines. It's likely that sediment deposition there began with the re-advancing ice front, with woody debris found in 4th beach (14.9 – 14.3 ka cal BP, CIRC4, Appendix 1) corresponding with tree death just prior to ice advance and charcoal, needle fragments, sclerotia, and conifer seeds dated to 14.6 – 14.2 ka cal BP (HW6-b, Appendix 1) found in the lake prior to ice advance.

14 – 10.5 ka cal BP – RSL dropped to slightly lower than present for the majority of this time period (McLaren et al. 2014) and ice retreated from the area, leaving large volumes of outwash sediments. Ice retreated from Foggy Cove between 14.0 – 13.8 ka cal BP and the ice front had backed away from the moraines in the numbered beaches region by as late as 13.4 – 13.3 ka cal BP (section 2). It is likely that large dune systems began forming in coastal areas where sandy sediments were available,

possibly from regionally cold and dry conditions (Galloway et al. 2009), as evidenced by early Holocene dune stabilization ages (e.g., 8.55 ± 1.37 ka cal BP, CIDS10, Appendix 1). Dunes that formed west and south of the modern location of Cobble Beach (remaining relict dune sand now perched on bedrock several m above sea-level) provide good evidence that there were large stores of sediment to the west of this region. In addition, boulders presently found in the nearshore throughout the larger embayment are believed to be eroded from a broader expanse of Foggy Cove sediments (section 4.5.1 (ii), Figure 16). Together, the evidence suggests that subaerial sediments existed much farther west at this time. A small volume of sediment remaining in Pruth Bay, evidenced by the cobbles found only in the bay and in an exposure 100 m west of the bay, was likely deposited proglacially, as fabric measurements of clast imbrication suggest glacio-fluvial deposition toward the west. A colluvial sediment source (e.g., from the bedrock uplands immediately to the south) is unlikely as cobbles would have a different orientation and be less rounded. However, coastal processes can produce rounded, imbricated tabular cobbles (Miall 2013), so it may be that the cobbles were re-worked post-depositionally. Young ages west of this suggest the small volume of sediments didn't extend across Kwakshua Channel, or sediments in this area would be older and there would likely have been archaeological evidence that extended beyond the Late Holocene. There is no evidence that there were any subaerial sediments around the modern location of West Beach through to North Beach.

10.5 – 8.5 ka cal BP - Erosion of the glacial sands and gravels was the main geomorphic driver in the western portion of the study area, with stabilization of the large dune (CIDS 10, Figure 15) in the numbered beaches area resulting from reduced sediment supply. In addition, warmer, wetter climate conditions prevailed on the central coast of British Columbia during this time period (Galloway et al. 2009; Eamer et al. in review), perhaps contributing to a reduction in the transport capacity for aeolian sediments and/or increased stabilization of aeolian dunes by vegetation. A small amount of detrital

organic material found outcropping in the intertidal in the numbered beaches region were also deposited in this timeframe, with a likely source being wave erosion of forested soils as the location of the beach reached the headland.

8.5 – 5.6 ka cal BP - RSL rose to as much as 2 m above present (McLaren et al. 2014), accelerating coastal erosion and redistribution of sediments east, away from the dominant source of wave energy, as well as reducing sediment supply to several large dune complexes. Terrestrial sediments located between West Beach and Cobble Beach eroded during this time period, and it is likely that the large dune complex west of Cobble Beach began to stabilize. Beaches began developing at eastern North Beach as glacial sediments were eroded and redistributed at higher sea-levels, evidenced by burial ages of beach sediments in this region. North Beach expanded west and a large foredune formed behind North Beach with this new source of subaerial sediment.

5.6 – 4.2 ka cal BP - In the numbered beaches region, the remaining active dune complex between 4th and 7th beach (Figure 15) had mostly stabilized and become vegetated. This corresponded with a wet and warm climate regime and a slight rise in RSL around 5 ka cal BP (McLaren et al. 2014), which caused regression of shorelines in the region. Further north, stabilization of the Cobble Beach dune system continued. The complex migrated east over organic materials now buried under aeolian sands at Cobble Beach. Aeolian sediments in behind North Beach became vegetated as RSL dropped and the sediment source moved lower and further from the tall sandy landform.

4.2 – 1.8 ka cal BP – A coastal forest growing behind 4th beach was slowly inundated by the retreating beach, following the general pattern of beach retreat in the numbered beaches area and evidenced by stumps in growth position buried in the modern beach (CIRC31, 32, Appendix 1) dated to

this time period. Further north, a baymouth bar system developed in the newly mobilized sediments in Pruth Bay to close off Kwakshua Channel to energy inputs from the Pacific Ocean. West of this, circulation changes likely fueled subsequent sediment accumulation toward the modern position of West Beach from both Pruth Bay and North Beach. In the modern location for Hood Lake, the presence of marine diatom species associated with salt marshes and salt marsh plants (e.g., seaside arrowgrass) near the end of this time period suggest that a salt marsh began developing.

1.8 – 0.4 ka cal BP - Rapid progradation (estimated at 1.2 m a^{-1} measured between CIBS1 and CIDS3) of the beach-dune complex west of Pruth Bay occurred towards the modern location of West Beach during this time period, as evidenced by optical ages of beach sediments in this region. The salt marsh that had developed at the location of Hood Lake expanded further south, as evidenced by the diatom assemblage in core C03, and became aligned with a series of prograding beaches and foredunes. Larger dune systems began developing near the end of this time period near West Beach, as the position of the beach approached a more open embayment further south, with Hood Lake gradually being cut off from oceanic influence.

0.4 ka cal BP – present - The modern position for West Beach was established in this time period and, with a combined sediment source across a broader embayment, the resultant increase in fetch assisted in the development of a large dune system consisting of extensive trough blowouts with 20 m high depositional lobes built at the northern portion of the beach. Further south, smaller foredunes developed and quickly stabilized as progradation slowed to approximately 0.69 m a^{-1} based on distances between CIDS4 and the modern foredune. Eventually, the present coastal configuration was achieved, with rapid stabilization of both the larger dune complex at the north end and prograding foredunes in

the central portion of West Beach. Presently, appreciable erosion of scarps backing all sandy beaches in the study area are common.

4.6.2. Long-term influences of RSL and climatic changes on aeolian activity and stabilization

Coastal aeolian activity is controlled by three dominant variables: sediment availability, moisture, and competence of the wind regime. Sediment availability varies with the abundance of sand-sized particles on the beach and overall beach width, which controls the effective fetch distance and supply of sand to foredunes (Bauer and Davidson-Arnott 2002; Bauer et al. 2009; Houser 2009). Moisture acts as a key control by: i) limiting supply of sand via cohesion effects, ii) altering effective fetch distances for sand transport development on beaches, and iii) regulating the growth of vegetation, which both limits sand supply and inhibits wind action on vegetated surfaces (Houser and Ellis 2013). Wind competence and directionality may also change with climatic changes (Lancaster 2013). Environmental mechanisms that may have driven changes in these variables in the study area include changing RSL and climate.

RSL change generally modifies sediment availability through a change in the availability (area) of intertidal sands and, thus, a change in fetch conditions. Generally, it is thought that a fall in RSL exposes more source sand and coastal dunes aggrade (e.g., Clague et al. 1982a; Lees 2006), while a rise in RSL may result in a reduction in available sediment, halting dune growth (e.g., Wilson et al. 2004) and potentially eroding dunes. However, a growing body of research suggests that, with ample sand supply, a rise in RSL can also result in dune maintenance and landward transgression, given sufficient accommodation space landward (e.g., Davidson-Arnott 2005; Aargard et al. 2007; Szkornik et al. 2008). On northwestern Calvert Island, a well-established local RSL history (McLaren et al. 2014) helps constrain this relationship. Large dune fields developed during a period of slightly lower RSL in the Late Pleistocene and Early Holocene (14 – 8.5 ka cal BP), and dune building occurred in areas where there

was appreciable sediment supply (Figure 21). Stabilization of the Cobble Beach and southern numbered beach dune fields occurred during the Early to Mid Holocene highstand (8.5 - 5.2 ka cal BP), suggesting that a potential reduction in available sediment supply and reduced beach fetch conditions might have contributed to stabilization.

Detailed palaeoecological and palaeoclimatological data from ~1 km east of the study area (Eamer et al. in review) showed a transition from cool and dry to cold and moist conditions occurred during the Younger Dryas (approximately 13 ka cal BP) unlike other regions in coastal BC that experienced predominantly cold and dry conditions (Lacourse 2005; Stolze et al. 2007; Galloway et al. 2009; Lacourse et al. 2012). Early Holocene (11.7 – 8.2 ka cal BP) forest composition indicates a warming trend, with vegetation assemblages that suggest effective moisture was higher in the study region than in other regions of British Columbia. By the Mid to Late Holocene (8.2 ka cal BP – present), the modern forest assemblage was achieved due to the onset of temperate and wet conditions. Thus, climatological conditions at the study site were perhaps only conducive to dune growth in the early Holocene, when conditions were drier relative to the rest of the record, a link that has been shown elsewhere in the northern hemisphere (e.g., Bateman and Godby 2004; Wilson et al. 2004). This suggests that climate played a role, as one of the numbered beach dunefields stabilized near the end of this dry period (Figure 21), perhaps with the onset of moister conditions. There is also a general trend of stabilization seen at Cobble Beach and again at the numbered beaches through the remainder of the Holocene.

4.6.3. Fire and aeolian activity

The relationship between fire and aeolian activity is well-documented for inland study sites (e.g., Filion 1984; Filion et al. 1991; Arbogast 2004; Barchyn and Hugenholtz 2013). Generally, fires have been observed as a destabilizing force in dune systems by reducing vegetation, delaying re-colonization, and increasing exposed sand for aeolian activity. A recent fire history developed for Calvert Island (Hoffman

et al. 2016) shows that fires occurred regularly through the Holocene with the exception of a distinct fire-free interval from 7.5 – 5.5 ka cal BP. An increase in Late Holocene fire activity was also observed and attributed to anthropogenic activities. In the southern numbered beaches and the Cobble Beach study regions (Figure 21), fire activity corresponded roughly with dune activity, with a reduction in fire generally occurring during a period of stabilization. Generally, there is a lag between reduced fire activity and the stabilization of these dune systems, as expected given ecesis time (~ 5 – 60 years for similar climates (e.g., Desloges and Ryder 1990; McCarthy and Luckman 1993; Larocque and Smith 2003)) and the time taken to fully stabilize a surface after vegetation establishment. Additionally, increased anthropogenic fire activity in the Late Holocene may have destabilized the dunes behind West Beach (Figure 21). Human presence in the West Beach – Pruth Bay region began in the past 1,000 years (Stafford and Christensen 2014) and an increase in fire activity associated with human presence in this specific area may have contributed to dune activity observed during this time period.

4.7. Conclusions

This section provides an account of the evolution of a coastline influenced by sedimentation from the CIS but without the large-magnitude changes (hundreds of m on the inner shore, tens of m on the outer shore) in RSL seen elsewhere along the CIS margin. We utilize geochronology information, geomorphological mapping, sedimentology, stratigraphy, and palaeoecology to reconstruct the past 15,000 years of landscape evolution for northwest Calvert Island. We show that:

- Glaciers re-advanced in the Late Pleistocene between 14.2 – 13.8 ka cal BP, shown in a coarsening upward glacial advance stratigraphic sequence containing a bed with evidence of a salt marsh ^{14}C dated to 15.1 – 14.3 ka cal BP and a cooling climate inferred from the presence of orbitid mites. The advance is reflected in the landscape in a suite of small moraines, extensive outwash

sedimentation, palaeochannels, and boulder deposition, and provides a record of Late Pleistocene glacial re-advance not seen elsewhere on the central coast of BC.

- Coastal evolution involved the redistribution of huge volumes of sandy sediments with 1-2 m (very minimal) RSL change since the Late Pleistocene. Extensive coastal change occurred in spite of the absence of high-magnitude RSL change, with Late Holocene progradation rates of 1.17 m a^{-1} observed and beach reorganization, extensive dune development and stabilization, and marsh growth and marine abandonment characterizing the development of the modern day coastal configuration.
- Aeolian activity was intermittent through the Holocene, and possible causes include gradual changes in climate or sea-level, or event-based changes such as fire. It is likely that all causes have contributed to changes in aeolian activity, with precipitation patterns a dominant driver of sediment availability through the Holocene.

5. Conclusions

5.1. Summary and conclusions

At the outset of this research, a better understanding of the Late Quaternary landscape development following CIS retreat on the RSL hinge line was desired. This dissertation presents results from over five years of research done on the subject by the Geologic History research program at the Hakai Institute. The study documents a new, unique glacial re-advance following CIS deglaciation, presents a new methodology for determining sand mechanism of transport for relict coastal landforms, and integrates these methods and results with further detailed observations of stratigraphy, sedimentology, geomorphology, and palaeoecology to reconstruct landscape development on the hinge line located on the northwest coast of Calvert Island, British Columbia, Canada.

In section 2, a suite of stratigraphic, sedimentary, and palaeoecological data is presented that indicates there was a late-glacial re-advance of ice in the study area occurring between 14.2 and 13.8 ka cal BP. Evidence of Late Pleistocene re-advances of Cordilleran ice is rare, and was, before this study, completely absent on the central coast of BC. The presence of orbitid mites, associated with today's Arctic environments, suggests that the cause of glacial re-advance was climatic cooling. While this is broadly consistent with other palaeoclimatic reconstructions in coastal BC, the evidence provided in section 2 occurs earlier than other documented re-advances.

Section 3 provides a summary of a method that was developed to differentiate the mechanism of transport for sand-sized sediments found in relict coastal landforms. The method required inexpensive and easily obtainable equipment as well as open-sourced software. Based on the principle of shape sorting due to aeolian transport, the shape descriptor "solidity" (akin to sedimentological roundness) was found to describe the difference between sand grains transported via aeolian or littoral processes 76% of the time.

In section 4, the findings from section 2 and the methods from section 3 contribute to a landscape reconstruction of northwest Calvert Island. Additional data comes from a robust geochronology (38 ^{14}C ages and 18 optical dates), sedimentological and stratigraphic observations, diatom and macrofossil identification and interpretation, and further interpretation of a detailed lidar bare earth DEM. Results document a coastline that experienced the redistribution of large volumes of sandy sediments with minimal (1-2 m) of RSL change through the Holocene. Progradation rates were at times higher than 1 m a^{-1} and extensive dune development and stabilization as well as marsh, beach, spit, tombolo, and baymouth bar growth and reorganization characterized the development of the modern day coastal configuration. Aeolian activity was periodic in the Holocene, and factors contributing to changes (i.e., initiation and stabilization) in the development of large dune systems may include a changing climate, minor adjustments in RSL, or fire activity.

5.2. Future directions

Further research on Late Pleistocene ice cover in the central coast region of BC is warranted. There are a number of sedimentary landforms on Calvert Island that suggest a landscape rich in data on ice character and extent, and the region surrounding Calvert remains largely unexplored. Investigations into the CIS LGM extent, post-LGM re-advances of ice, and the dynamics of ice retreat may yield new data important for crustal load modelling and refinement of RSL curves, patterns of human occupation in this increasingly important portion of the coastal migration route, and advances in our understanding of how ice sheets modify climate, ecology, and sedimentary processes in this unique biogeographic zone.

Differentiating the mechanism of transport for sand grains has posed a methodological quandary for decades. Initial successes found through development of the method described in section 3 should be further explored, including testing in different geomorphic, mineralogic, and climatic

environments, extension to different mechanisms of transport (e.g., fluvial, mass wasting), and establishing if mineralogical separation beforehand increases the success of the method. Opportunities also exist for further expansion of the method via integration of these data with other diagnostic sand-grain data (such as petrology, electron microscopy, or GSD).

A simple yet effective expansion of the findings in section 4 would include a broadening of the area of investigation to include more of the study region. Areas of immense archaeological significance, cultural importance, intriguing glacial and coastal landforms, and a rich and unique ecology are all within kms of the study area. It is my hope that the work described above serves to inspire further research in this incredible corner of the world.

6. References

Alley, R.B., Blankenship, D.D., Bentley, C.R., Rooney, S.T. 1986. Deformation of till beneath ice stream B, West Antarctica. Nature 322, 57-59.

Allmendinger, R.W., Cardozo, N.C., Fisher, D. 2012. Structural Geology Algorithms: Vectors and Tensors. Cambridge, England, Cambridge University Press, 289p.

Anderson, R.S., Sørensen, M., Willets, B.B. 1991. A review of recent progress in our understanding of aeolian sediment transport. Aeolian Grain Transport 1, p. 1-19, Springer Vienna.

Andrews, J.T. and Retherford, R.M. 1978. A reconnaissance survey of Late Quaternary sea-levels, Bella Bella/Bella Coola region, central British Columbia coast. Canadian Journal of Earth Sciences 15, 341-350.

Arbogast, A.F. 2004. Middle-Holocene mobilization of aeolian sand in western upper Michigan and the potential relationship with climate and fire. The Holocene 14(3), 464-471.

Armstrong, J.E. and Clague, J.J. 1977. Two major Wisconsin lithostratigraphic units in southwest British Columbia. Canadian Journal of Earth Sciences 14(7), 1471-1480.

Barchyn, T.E. and Hugenholtz, C.H. 2013. Reactivation of supply-limited dune fields from blowouts: A conceptual framework for state characterization. Geomorphology 201, 172-182.

Barclay, D.J., Wiles, G.C., Calkin, P.E. 2003. An 850 year record of climate and fluctuations of the iceberg-calving Nellie Juan Glacier, south central Alaska, USA. Annals of Glaciology 36(1), 51-56.

Barrie, J.V. and Bornhold, B.D. 1989. Surficial geology of Hecate Strait, British Columbia continental shelf. Canadian Journal of Earth Sciences 26, 1241-1254.

Barrie, J.V. and Conway, K.W. 1991. Late Quaternary glaciation and postglacial stratigraphy of the northern Pacific Margin of Canada. Quaternary Research 51, 113-123.

Barrie, J.V. and Conway, K.W. 1999. Late Quaternary glaciation and postglacial stratigraphy of the northern Pacific margin of Canada. Quaternary Research 51, 113-123.

Barrie, J.V., Bornhold, B.D., Conway, K.W., Luternauer, J.L. 1991. Surficial geology of the northwestern Canadian continental shelf. Continental Shelf Research 11(8-10), 701-715.

Barrie, J.V., Hetherington, R., Macleod, R. 2014. Chapter 22: Pacific margin, Canada shelf physiography: a complex history of glaciation, tectonism, oceanography and sea-level change. Geological Society, London, Memoirs 41, 305-313.

Barrows, T.T., Stone, J.O., Fifield, L.K., Cresswell, R.G. 2001. Late Pleistocene glaciation of the Kosciuszko Massif, Snowy Mountains, Australia. Quaternary Research 55**,** 179-189.

Bateman, M.D. and Godby, S.P. 2004. Late-Holocene inland dune activity in the UK: a case study from Breckland, East Anglia. The Holocene 14(4), 579-588.

Bauer, B.O. 1991. Aeolian decoupling of beach sediments: Association of American Geographers Annal 81(2), 290-303.

Bauer, B.O. and Davidson-Arnott, R.G.D. 2002. A general framework for modeling sediment supply to coastal dunes including wind angle, beach geometry, and fetch effects. Geomorphology 49, 89-108.

Bauer, B.O., Davidson-Arnott, R.G.D., Hesp, P.A., Namikas, S.L., Ollerhead, J., Walker, I.J. 2009. Aeolian sediment transport on a beach: Surface moisture, wind fetch, and mean transport. Geomorphology 105(1-2), 106-116.

Bendle, J.M., Palmer, A.P., Carr, S.J. 2015. A comparison of micro-CT and thin section analysis of Lateglacial glaciolacustrine varves from Glen Roy, Scotland. Quaternary Science Reviews 114, 61-77.

Benson, L., Burdett, J., Lund, S., Kashgarian, M., Mensing, S. 1997. Nearly synchronous climate change in the Northern Hemisphere during the last glacial termination. Letters to Nature 388, 263-265.

Bindschadler, R.A. and Scambos, T.A. 1991. Satellite-image-derived velocity field of an Antarctic ice stream. Science 252(5003), 242-246.

Birks, H.H. 2001. Plant macrofossils. In: Smol, J.P., Birks, H.J.B., Last, W.M. (Eds.), Tracking environmental change using lake sediments. 3rd Volume, Kluwer Academic Publishers, Dordrecht, The Netherlands, pp. 49-74.

Blaise, B., Clague, J.J., Mathewes, R.W. 1990. Time of maximum late Wisconsin glaciation, west coast of Canada. Quaternary Research 34, 282-295.

Blott, S.J., and Pye, K., 2001. GRADISTAT: a grain size distribution and statistics package for the analysis of unconsolidated sediments: Earth Surface Processes and Landforms 26, 1237-1248.

Bobrowsky, P.T. and Clague, J.J. 1992. Neotectonic investigations on Vancouver Island (92B, F). In *Geological fieldwork 1991*. British Columbia Misistry of Energy, Mines and Petroleum Resources, Paper 1992-1, pp 325-329.

Booth, D.B. 1986. Mass balance and sliding velocity of the Puget lobe of the Cordilleran ice sheet during the last glaciation. Quaternary Research 29, 269-280.

Booth, D.B. 1991. Glacier physics of the Puget lobe, southwest Cordilleran ice sheet. Géographie Physique et Quaternaire 45, 301-315.

Booth, D.B., Troost, K.G., Clague, J.J., Waitt, R.B. 2003. The Cordilleran Ice Sheet. Development in Quaternary Science 1, 17-43.

Bristowe, W.S. 1958. The world of spiders. HarperCollins, London, UK, pp. 304.

Brown, K.J. and Hebda, R.J. 2002. Origin, development, and dynamics of coastal temperate conifer rainforests of southern Vancouver Island, Canada. Canadian Journal of Forest Research 32(2), 353-372.

Campeau, S., Pienitz, R., Héquette, A. 1998. Diatoms from the Beaufort Sea coast, southern Arctic Ocean (Canada). Modern analogues for reconstructing Late Quaternary environments and relative sea-levels. Vol. 42. Gebrüder Borntraeger Science Publishers. Stuttgart, Germany. 244p.

Cardozo, N. and Allmendinger, R.W. 2013. Spherical projections with OSXStereonet. Computers and Geosciences 51, 193-205.

Clague, J.J. 1976. Quadra Sand and its relation to the late Wisconsin glaciation of southwest British Columbia. Canadian Journal of Earth Sciences 13, 803-815.

Clague, J.J. 1981. Late Quaternary geology and geochronology of British Columbia, Part 2: Summary and discussion of radiocarbon dated Quaternary history. Geological Survey of Canada Paper No. 80-35. 41p.

Clague, J.J. 1984. Deglaciation of the Prince Rupert – Kitimat area, British Columbia. Canadian Journal of Earth Sciences 22, 256-265.

Clague, J.J. 1985. Deglaciation of the Prince Rupert – Kitimat area, British Columbia. Canadian Journal of Earth Sciences 22, 256 – 265.

Clague, J.J. 1986. The Quaternary stratigraphic record of British Columbia-evidence for episodic sedimentation and erosion controlled by glaciation. Canadian Journal of Earth Sciences 23, 885-894.

Clague, J.J. 1989. Quaternary geology of the Canadian Cordillera (Chapter 1). In: Fulton, R.J. (ed), Quaternary Geology of Canada and Greenland. Geological Survey of Canada, Ottawa, pp. 15-96.

Clague, J.J. 2009. Cordilleran ice sheet. In Encyclopedia of Palaeoclimatology and Ancient Environments, pp 206-211. Springer Netherlands.

Clague, J.J. and James, T.S. 2002. History and isostatic effects of the last ice sheet in southern British Columbia. Quaternary Science Reviews 21, 71-87.

Clague, J.J., Armstrong, J.E., Mathews, W.H. 1980. Advance of the late Wisconsin Cordilleran ice sheet in southern British Columbia since 22,000 yr B.P. Quaternary Research 13, 322-326.

Clague, J.J., Harper, J.R., Hebda, R.J., Howes, D.E. 1982a. Late Quaternary sea-levels and crustal movements, coastal British Columbia. Canadian Journal of Earth Science 19, 597-618.

Clague, J.J., Mathewes, R.W., Warner, B.G. 1982b. Late Quaternary geology of eastern Graham Island, Queen Charlotte Islands, British Columbia. Canadian Journal of Earth Science 19, 1786-1795.

Clague, J.J., Mathewes, R.W., Guilbault, J-P., Hutchinson, I., Ricketts, B.D. 1997. Pre-Younger Dryas resurgence of the southwestern margin of the Cordilleran ice sheet, British Columbia, Canada. Boreas 26, 261-278.

Clague, J.J., Mathewes, R.W., Guilbault, J-P., Hutchinson, I., Ricketts, B.D. 1998. Pre-Younger Dryas resurgence of the southwestern margin of the Cordilleran ice sheet, British Columbia, Canada: Reply to comments. Boreas Comments 27, 229-230.

Clague, J.J., Bobrowsky, P.T., Hutchinson, I. 2000. A review of geological records of large tsunamis at Vancouver Island, British Columbia, and implications for hazard. Quaternary Science Reviews 19, 849-863.

Clague, J.J., Froese, D., Hutchinson, I., James, T.S., Simon, K.M. 2005. Early growth of the last Cordilleran ice sheet deduced from glacio-isostatic depression in southwest British Columbia, Canada. Quaternary Research 63(1), 53-59.

Clark, P.U. and Mix, A.C. 2002. Ice sheets and sea-level of the Last Glacial Maximum. Quaternary Science Reviews 21(1-3), 1-7.

Clark, P.U., Clague, J.J., Curry, B.B., Dreimanis, A., Hicock, S.R., Miller, G.H., Berger, G.W., Eyles, N., Lamothe, M., Miller, B.B., Mott, R.J., Oldale, R.N., Stea, R.R., Szabo, J.P., Thorleifson, L.H., Vincent, J-S. 1993. Initiation and development of the Laurentide and Cordilleran Ice Sheets following the last interglaciation. Quaternary Science Reviews 12, 79-114.

Coulson, S.J. and Birkemoe, T. 2000. Long-term cold tolerance in Arctic invertibrates: recovery after 4 years at below -20°C. Canadian Journal of Zoology 78, 2055-2058.

Culver, S.J., Bull, P.A., Campbell, S., Shakesby, R.A. 1983. Environmental discrimination based on quartz grain surface textures: a statistical investigation. Sedimentology 30, 129-136.

Dallimore, A., Enkin, R.J., Pienitz, R., Southon, J.R., Baker, J., Wright, C.A., Pedersen, T.F., Calvert, S.E., Ivanochko, T., Thomson, R.E. 2008. Postglacial evolution of a Pacific coastal fjord in British Columbia, Canada: interactions of sea-level change, crustal response, and environmental fluctuations – results from MONA core MD02-2494. Canadian Journal of Earth Sciences 45, 1345-1362.

Davidson-Arnott, R.G.D. 2005. Conceptual model of the effects of sea-level rise on sandy coasts. Journal of Coastal Research 21(6), 1166-1172.

Davis, E.E. and Riddihough, R.P. 1982. The Winona Basin: structure and tectonics. Canadian Journal of Earth Sciences 19(4), 767-788.

Day, J.W., Pont, D., Hensel, P.F. and Ibañez, C., 1995. Impacts of sea-level rise on deltas in the Gulf of Mexico and the Mediterranean: the importance of pulsing events to sustainability. Estuaries 18(4), 636-647.

Desloges, J.R. and Ryder, J.M. 1990. Neoglacial history of the Coast Mountains near Bella Coola, British Columbia. Canadian Journal of Earth Sciences, 27(2), 281-290.

Eamer, J.L., McLaren, D., Trant, T. In review. Late Quaternary vegetation dynamics on Calvert Island, British Columbia. Botany #cjb-2017-0045.

Easterbrook, D.J. 1992. Advance and retreat of Cordilleran Ice Sheets in Washington, U.S.A. Géographie physique et Quaternaire 46(1), 51-68.

Easterbrook, D.J. and Kovanen, D.J. 1998. Pre-Younger Dryas resurgence of the southwestern margin of the Cordilleran ice sheet, British Columbia, Canada: Comments. Boreas Comments 27, 225-228.

Fairbanks, R.G. 1989. A 17,000-year glacio-eustatic sea-level record: influence of glacial melting rates on the Younger Dryas event and deep-ocean circulation. Nature 342, 637-642.

Filion, L. 1984. A relationship between dunes, fire and climate recorded in the Holocene deposits of Quebec. Nature 309, 543-546.

Filion, L., Saint-Laurent, D., Desponts, M. Payette, S. 1991. The late Holocene record of aeolian and fire activity in northern Québec, Canada. The Holocene 1(3), 201-208.

Fletcher, C.H., Romine, B.M., Genz, A.S., Barbee, M.M., Dyer, M., Anderson, T.R., Lim, S.C., Vitousek, S., Bochicchio, C., Richmond, B.M. 2011. National assessment of shoreline change: Historical shoreline change in the Hawaiian Islands. U.S. Geological Survey, Open-File Report 2011-1051, 55p.

Folk, R.L. 1966. A review of grain size parameters: Sedimentology 6, 73-93.

Folk, R.L. and Ward, W.C. 1957. Brazos River Bar: A study in the significance of grain size parameters. Journal of Sedimentary Petrology 27(1), 3-26.

Fournier, G.R. 1964. Partial immersion technique for the photography of sand grain surfaces: Journal of Sedimentary Petrology 34(3), 473-482.

Friedman, G.M. 1961. Distinction between dune, beach, and river sands from their textural characteristics: Journal of Sedimentary Petrology 31(4), 514-529.

Friele, P.A. and Hutchinson, I. 1993. Holocene sea-level change on the central west coast of Vancouver Island, British Columbia. Canadian Journal of Earth Sciences 30, 832-840.

Friele, P.A. and Clague, J.J. 2002. Re-advance of glaciers in the British Columbia Coast Mountains at the end of the last glaciation. Quaternary International 87, 45-58.

Friele, P.A., Ekes, C., Hicken, E.J. 1999. Evolution of Cheekye fan, Squamish, British Columbia: Holocene sedimentation and implications for hazard assessment. Canadian Journal of Earth Sciences 36, 2023-2031.

Galloway, J.M., Doherty, C.T., Patterson, R.T., Roe, H.M. 2009. Postglacial vegetation and climate dynamics in the Seymour-Belize Inlet Complex, central coastal British Columbia, Canada: palynological evidence from Tiny Lake. Journal of Quaternary Science 24(4), 322-335.

Guilbault, J.P., Clague, J.J., LaPoint, M. 1996. Foraminiferal evidence for the amount of coseismic subsidence during a late Holocene earthquake on Vancouver Island, west coast of Canada. Quaternary Science Reviews 15, 913-937.

Gomez, B., Dowdeswell, J.A., Sharp, M. 1988. Microstructural control of quartz sand grain shape and texture: Implications for the discrimination of debris transport pathways through glaciers: Sedimentary Geology 57, 119-129.

Gosse, J.C., Evenson, E.B., Klein, J., Lawn, B., Middleton, R. 1995. Precise cosmogenic ^{10}Be measurements in western North America: Support for a global Younger Dryas cooling event. Geology 23(10), 877-880.

Hammer, M. 1950. Investigations on the Microfauna of Northern Canada, part 1. Oribatidae. Acta Arctica 4, 1-108.

Hebda, R.J., Howes, D., Maxwell, B. 1997. Brooks Peninsula as an ice age refugium. In: Hebda, R.J., Haggarty, J.C. (Eds.), Brooks Peninsula: an ice age refugium on Vancouver Island. Royal BC Museum, Victoria BC, pp. 15.1-15.7.

Hendy, I.L., Kennett, J.P., Roark, E.B., Ingram, B.L. 2002. Apparent synchroneity of submillennial scale climate events between Greenland and Santa Barbara Basin, California from 30-10 ka. Quaternary Science Reviews 21, 1167-1184.

Hetherington, R., Barrie, J.V., Reid, R.G.B., MacLeod, R., Smith, D.J. 2004. Palaeogeography, glacially induced crustal displacement, and Late Quaternary coastlines on the continental shelf of British Columbia, Canada. Quaternary Science Reviews 23, 295-318.

Hicock, S.R. and Armstrong, J.E. 1981. Coquitlam Drift: a pre-Vashon Fraser glacial formation in the Fraser Lowland, British Columbia. Canadian Journal of Earth Sciences 18, 1443-1451.

Hicock, S.R. and Fuller, E.A. 1995. Lobal interactions, rheologic superposition, and implications for a Pleistocene ice stream on the continental shelf of British Columbia. Geomorphology 14, 167-184.

Hicock, S.R. and Lian, O.B. 1995. The Sisters Creek Formation: Pleistocene sediments representing a nonglacial interval in southwewstern British Columbia at about 18 ka. Canadian Journal of Earth Sciences 32(6), 758-767.

Hicock, S.R., and Lian, O.B. 1999. Cordilleran Ice Sheet interactions and glaciotectonic superposition through stadial maxima along a mountain front in southwestern British Columbia. Boreas 28, 531–542.

Hicock, S.R. and Dreimanis, A. 1985. Glaciotectonic structures as useful ice-movement indicators in glacial deposits: four Canadian case studies. Canadian Journal of Earth Sciences 22, 339-346.

Hicock, S.R. and Lian, O.B. 1995. The Sisters Creek Formation: Pleistocene sediments representing a nonglacial interval in southwestern British Columbia at about 18 ka. Canadian Journal of Earth Sciences 32, 758-767.

Hicock, S.R., Hebda, R.J., Armstrong, J.E. 1982. Lag of the Fraser glacial maximum in the Pacific Northwest: pollen and macrofossil evidence from western Fraser Lowland, British Columbia. Canadian Journal of Earth Sciences 19, 2288-2296.

Hicock, S.R., Goff, J.R, Lian, O.B., Little, E.C. 1996. On the interpretation of subglacial till fabric. Journal of Sedimentary Research 66, 928-934.

Hicock, S.R., Lian, O.B., Mathewes, R.W. 1999. 'Bond cycles' recorded in terrestrial Pleistocene sediments of southwestern British Columbia, Canada. Journal of Quaternary Science 14(5), 443-449.

Hoffman, K., Gavin, D., Lertzman, K., Smith, D., Starzomski, B. 2016. 13,000 years of fire history derived from soil charcoal in a British Columbia coastal temperate rain forest. Ecosphere 7(7), 1-13.

Holmes, K., Rechsteiner, E., Burt, J. 2016. Northwest Calvert Island kelp canopy study area. Obtained from https://www.hakai.org/blog/geospatial-technology/kelp-it-changin' on June 30, 2016.

Houser, C. 2009. Synchronization of transport and supply in beach-dune interaction: Progress in Physical Geography 33, 733-746.

Houser, C. and Ellis, J. 2013. Beach and dune interaction. Treatise on Geomorphology 10, 267-288.

Jackson, L.E., Ward, B., Duk-Rodkin, A., Hughes, O.L. 1991. The last Cordilleran Ice Sheet in southern Yukon Territory. Géographie physique et Quaternaire 45(3), 341-354.

James, T., Rogers, G., Cassidy, J., Dragert, H., Hyndman, R., Leonard, L., Nykolaishen, L., Riedel, M., Schmidt, M., Wang, K. 2013. Field studies target 2012 Haida Gwaii Earthquake. Eos, Transactions American Geophysical Union 94(22), 197-198.

James, T.S., Cassidy, J.F., Rogers, G.C., Haeussler, P.J. 2015. Introduction to the special issue on the 2012 Haida Gwaii and 2013 Craig earthquakes at the Pacific-North America Plate boundary (British Columbia, Alaska). Bulletin of the Seismological Society of America 105(2B), 1053-1057.

Jermy, A.C., Simpson, D.C., Foley, M.J.Y., Porter, M.S. 2007. General structure of Cyperaceae. Sedges of the British Isles. BSBI Handbook No. 1 (3rd edition). Botanical Society of the British Isles, 2-26.

Josenhans, H.W., Fedje, D.W., Conway, K.W., Barrie, J.V. 1995. Post glacial sea-levels on the Western Canadian continental shelf: evidence for rapid change, extensive subaerial exposure, and early human habitation. Marine Geology 125**,** 73-94.

Kasper-Zubillaga, J.J. 2009. Roundness in quartz grains from inland and coastal dune sands, Altar Desert, Sonora, Mexico, Sociedad Geológica Mexicana Boletín, 61(1), 1-12.

Kasper-Zubillaga, J.J., and Dickenson, W.W. 2001. Discriminating depositional environments of sands from modern source terranes using modal analysis. Sedimentary Geology 143, 149-167.

Kasper-Zubillaga, J.J., Dickenson, W.W., Carranza-Edwards, A., Hornelas-Orozco, Y. 2005. Petrography of quartz grains in beach and dune sands of Northland, North Island, New Zealand. New Zealand Journal of Geology and Geophysics 48(4), 649-660.

Kelly, R.L. 2003. Maybe we do know when people first came to North America; and what does it mean if we do? Quaternary International 109-110, 133-145.

Kiefer, T. and Kienast, M. 2005. Patterns of deglacial warming in the Pacific Ocean: a review with emphasis on the time interval of Heinrich event 1. Quaternary Science Reviews 24, 1063-1081.

Kienast, S.S. and McKay, J.L. 2001. Sea Surface Temperatures in the subarctic Northeast Pacific reflect millennial-scale climate oscillations during the last 16kyrs. Geophysical Research Letters 28(8), 1563-1566.

Kimura, G., Hina, S., Hamada, Y., Kameda, J., Tsuji, T., Kinoshita, M., Yamaguchi, A. 2012. Runaway slip to the trench due to rupture of highly pressurized megathrust beneath the middle trench slope: the tsunamigenesis of the 2011 Tōhoku earthquake off the east coast of northern Japan. Earth and Planetary Science Letters 339-340, 32-45.

Kovanen, D.J. and Easterbrook, D.J. 2002. Timing and extent of Allerød and Younger Dryas age (ca. 12500 – 10000 ^{14}C yr B.P.) oscillations of the Cordilleran Ice Sheet in the Fraser Lowland, Western North America. Quaternary Research 57, 208-224.

Kovanen, D.J. and Slaymaker, O. 2003. Lake Terrell upland glacial resurgences and implications for late-glacial history, northwestern Washington State, U.S.A. Canadian Journal of Earth Science 40(12), 1767-1772.

Kovanen, D.J. and Slaymaker, O. 2004a. Glacial imprints of the Okanogan Lobe, southern margin of the Cordilleran Ice Sheet. Journal of Quaternary Science 19, 547-565.

Kovanen, D.J. and Slaymaker, O. 2004b. Relict shorelines and ice flow patterns of the northern Puget Lowlands from lidar data and digital terrain modelling. Geografiska Annaler 86(4), 385-400.

Krinsley, D.H. and Donahue, J. 1968. Environmental interpretation of sand grain surface textures by electron microscopy. Geological Society of America Bulletin 79, 743-748.

Kröner, S. and Carbó, M.T.D. 2013. Determination of minimum pixel resolution for shape analysis: Proposal of a new data validation method for computerized images. Powder Technology 245, 297-313.

Krumbein, W.C. 1941. Measurement and geological significance of shape and roundness of sedimentary particles. Journal of Sedimentary Petrology 11(2), 64-72.

Lacourse, T. 2005. Late Quaternary dynamics of forest vegetation on northern Vancouver Island, British Columbia, Canada. Quaternary Science Reviews 24, 105-121.

Lacourse, T., Delepine J.M., Hoffman, E.H., Mathewes, R.W. 2012. A 14,000 year vegetation history of a hypermaritime island on the outer Pacific coast of Canada based on fossil pollen, spores and conifer stomata. Quaternary Research 78, 572-582.

Lakeman, T.R., Clague, J.J., Menounos, B. 2008. Advance of alpine glaciers during final retreat of the Cordilleran ice sheet in the Finlay River area, northern British Columbia, Canada. Quaternary Research 69, 188-200.

Lancaster, N. 2013. Climate Change and Aeolian Processes. Treatise on Geomorphology 13, 132-151.

Larocque, S.J. and Smith, D.J. 2003. Little Ice Age glacial activity in the Mt. Waddington area, British Columbia Coast Mountains, Canada. Canadian Journal of Earth Sciences 40(10), 1413-1436.

Lay, T., Ye, L., Kanamori, H., Yamazaki, Y., Cheung, K.F., Kwong, K., Koper, K.D. 2013. The October 28, 2012 M_W 7.8 Haida Gwaii underthrusting earthquake and tsunami: slip partitioning along the Queen Charlotte Fault transpressional plate boundary. Earth and Planetary Science Letters 375, 57-70.

Lees, B. 2006. Timing and formation of coastal dunes in Northern and Eastern Australia. Journal of Coastal Research 22, 251-268.

Letham, B., Martindale, A., Macdonald, R., Guiry, E., Jones, J., Ames, K.M. 2016. Postglacial relative sea-level history of the Prince Rupert area, British Columbia, Canada. Quaternary Science Reviews 153, 156-191.

Lewis, T., Francus, P., Bradley, R.S., and Kanumaru, K. 2010. An automated system for the statistical analysis of sediment texture and structure at the micro scale. Computers and Geosciences 36, 1374-1383.

Lian, O.B. and Hickin, E.J. 1996. Early postglacial sedimentation of lower Seymour Valley, southwestern British Columbia. Géographie physique et Quaternaire 50, 95–102.

Lian, O.B. and Hicock, S.R. 2000. Thermal conditions beneath parts of the last Cordilleran Ice Sheet near its centre as inferred from subglacial till, associated sediments, and bedrock. Quaternary International 68-71, 147-162.

Lian, O.B. and Roberts, R.G. 2006. Dating the Quaternary: progress in luminescence dating of sediments. Quaternary Science Reviews 25, 2449-2468.

Lowe, J.J., Hoek, W.Z., INTIMATE group. 2001. Inter-regional correlation of palaeoclimatic recores for the Last Glacial-Interglacial Transition: a protocol for improved precision recommended by the INTIMATE project group. Quaternary Science Reviews 20, 1175-1187.

Lowell, T.V., Heusser, C.J., Andersen, B.G., Moreno, P.I., Hauser, A., Heusser, L.E., Schlüchter, C., Marchant, D.R., Denton, G.H. 1995. Interhemispheric correlation of late Pleistocene glacial events. Science 269, 1541-1549.

Luternauer, J.L., Conway, K.W., Clague, J.J., Blaise, B. 1989. Late Quaternary geology and geochronology of the central continental shelf of western Canada. Marine Geology 89, 57-68.

Margold, M., Jansson, K.N., Kleman, J., Stroeven, A.P., Clague, J.J. 2013. Retreat pattern of the Cordilleran Ice Sheet in central British Columbia at the end of the last glaciation reconstructed from glacial meltwater landforms. Boreas 42, 830-847.

Mark, D.M. 1973. Analysis of axial orientation data, including till fabrics. Geological Society of America Bulletin 84, 1369-1374.

Mason, C.C. and Folk, R.L. 1958. Differentiation of beach, dune, and aeolian flat environments by size analysis, Mustang Island, Texas. Journal of Sedimentary Petrology 28(2), 211-226.

Mathewes, R.W. and Heusser, L.E. 1981. A 12 000 year palynological record of temperature and precipitation trends in southwestern British Columbia. Canadian Journal of Botany 59(5), 707-710.

Mathewes, R.W., Heusser, L.E., Patterson, R.T. 1993. Evidence for a Younger Dryas-like cooling event on the British Columbia coast. Geology 21, 101-104.

Mathewes, R.W., Lian, O.B., Clague, J.J., Huntley, M.J.W. 2015. Early Wisconsinan (MIS 4) glaciation on Haida Gwaii, British Columbia, and implications for biological refugia. Canadian Journal of Earth Sciences 52(11), 939 – 951.

Mathews, W.H. 1991. Ice sheets and ice streams: thoughts on the Cordilleran Ice Sheets symposium. Géographie physique et Quaternaire 45(3), 263-267.

Mazzotti, S., Dragert, H., Henton, J., Schmidt, M., Hyndman, R., James, T., Lu, Y., Craymer, M. 2003. Current tectonics of northern Cascadia from a decade of GPS measurements. Journal of Geophysical Research 108(B12), 1-1 – 1-18.

Mazzotti, S., Lambert, A., Van der Kooij, M., Mainville, A. 2009. Impact of anthropogenic subsidence on relative sea-level rise in the Fraser River delta. Geology 37(9), 771-774.

Mazzullo, J., Sims, D., Cunningham, D. 1986. The effects of aeolian sorting and abrasion upon the shapes of fine quartz sand grains. Journal of Sedimentary Petrology 56(1), 45-56.

McCarthy, D.P. and Luckman, B.H. 1993. Estimating ecesis for tree-ring dating of moraines: a comparative study from the Canadian Cordillera. Arctic and Alpine Research 25(1), 63-68.

McCrumb, D.R. and Swanson, T.W. 1998. Cosmogenic CI-36 age constraints on the deglaciation history of the Cordilleran Ice Sheet from Howe Sound, British Columbia. Geological Society of America Abstracts with Program 30**,** A-125.

McLaren, D., Martindale, A., Fedje, D., Mackie, Q. 2011. Relict shorelines and shell middens of the Dundas Island Archipelago. Canadian Journal of Archaeology 35, 86-116.

McLaren, D., Fedje, D., Hay, M., Mackie, Q., Walker, I.J., Shugar, D.H., Eamer, J.B.R., Lian, O.B., Neudorf C. 2014. A post-glacial sea-level hinge on the central Pacific coast of Canada. Quaternary Science Reviews 97, 148-169.

McLaren, D., Rahemtulla, F., Gitla, Fedje, D. 2015. Prerogatives, sea-level, and the strength of persistent places: Archaeological evidence for long-term occupation of the central coast of British Columbia. BC Studies 187, 155-191.

Menounos, B., Osborn, G., Clague, J.J., Luckman, B.H. 2009. Latest Pleistocene and Holocene glacier fluctuations in western Canada. Quaternary Science Reviews 28, 2049-2074.

Miall, A. 2013. Principles of sedimentary basin analysis. Springer Science and Business Media, 490p.

Milliman, J.D., Broadus, J.M., Gable, F. 1989. Environmental and economic implications of rising sea-level and subsiding deltas: the Nile and Bengal examples. Ambio 18(6), 340-345.

Mood, B. and Smith, D. 2015. Latest Pleistocene and Holocene behaviour of Franklin Glacier, Mt. Waddington area, British Columbia Coast Mountains, Canada. The Holocene 25(5), 784-794.

Moss, A.J. and Green, P. 1975. Sand and silt grains: Predetermination of their formation and properties by microfractures in quartz. Geological Society of Australia Journal 22(4), 485-495.

Nelson, A.R., Shennan, I., Long, A.J. 1996. Identifying coseismic subsidence in tidal-wetland stratigraphic sequences at the Cascadia subduction zone of western North America. Journal of Geophysical Research 101(B3): 6115-6135.

Neudorf, C.M., Brennand, T.A., Lian, O.B. 2015a. Comparisons between macro- and microfabrics in a pebble-rich, sandy till deposited by the Cordilleran Ice Sheet: Boreas 44(3), 483-501.

Neudorf, C.M., Lian, O.B., Walker, I.J., Shugar, D.H., Eamer, J.B.R., Griffin, L.C.M. 2015b. Toward a luminescence chronology for coastal dune and beach deposits on Calvert Island, British Columbia central coast, Canada. Quaternary Geochronology 30, 275-281.

Osborn, G. and Gerloff, L. 1997. Latest Pleistocene and early Holocene fluctuations of glaciers in the Canadian and northern American Rockies. Quaternary International 38/39, 7-19.

Parkin, G.W. and Hicock, S.R. 1989. Sedimentology of a Pleistocene glaciogenic diamicton sequence near Campbell River, British Columbia. In *Genetic Classification of Glacigenic Deposits.* Edited by Goldthwait RP and Matsch CL. Balkema, Rotterdam: 97-117.

Peel, M.C., Finlayson, B.L., McMahon, T.A. 2007. Updated world map of the Köppen-Geiger climate classification. Hydrology and Earth System Sciences 11, 1633-1644.

Pellatt, M.G., Mathewes, R.W., Clague, J.J. 2002. Implications of a late-glacial pollen record for the glacial and climatic history of the Fraser Lowland, British Columbia. Palaeogeography, Palaeoclimatology, Palaeoecology 180(1-3), 147-157.

Peterson, C.D., Clague, J.J., Carver, G.A., Cruikshank, K.M. 2013. Recurrence intervals of major palaeotsunamis as calibrated by historic tsunami deposits in three localities: Port Alberni, Cannon Beach, and Crescent City, along the Cascadia margin, Canada and USA. Natural Hazards 68, 321-336.

Plafker, G. 1972. Alaskan earthquake of 1964 and Chilean earthquake of 1960: implications for arc tectonics. Journal of Geophysical Research 77(5), 901-925.

Potter, P.E. 1986. South America and a few grains of sand: part 1 - beach sands. Journal of Geology 94, 301-319.

Purkait, B. 2010. The use of grain-size distribution patterns to elucidate aeolian processes on a transverse dune of Thar Desert, India. Earth Surface Processes and Landforms 35, 525-530.

Purkait, B. and Majumdar, D.D. 2014. Distinguishing different sedimentary facies in a deltaic system: Sedimentary Geology 308, 53-62.

Rasband, W.S. 2010. ImageJ, US National Institutes of Health, Bethesda, MD, USA. http://rsb.info.nih.gov/ij/docs/index.html.

Reasoner, M.A. 1986. An inexpensive, lightweight percussion core sampling system. Géographie Physique et Quaternaire 40, 217-219.

Retherford, R.M. 1972. Late Quaternary geologic environments and their relation to Archaeological studies in the Bella Bella-Bella Coola region of the British Columbia coast. Unpublished MS thesis, University of Colorado, 128p.

Roddick, J.A. 1996. Geology, Rivers Inlet – Queens Sound, British Columbia (92M), (102P); Geological Survey of Canada, Open File 3278.

Rogerson, R.J. and Hudson, H.M. 1983. Quartz surface microtextures and grain-size characteristics of Quaternary sediments in the Porcupine Strand area of coastal Labrador, Newfoundland, Canada. Canadian Journal of Earth Sciences 20, 377-387.

Ruiz, F., Rodriguez-Vidal, J., Abad, M., Caceres, L.M., Carretero, M.I., Pozo, M., Rodriguez-Llanes, J.M., Gomez-Toscano, F., Izquierdo, T., Font, E., Toscano, A. 2013. Sedimentological and geomorphological imprints of Holocene tsunamis in southwestern Spain: An approach to establish the recurrence period. Geomorphology 203, 97-104.

Ryder, J.M. and Clague, J.J. 1989. British Columbia (Quaternary stratigraphy and history, area of Cordilleran Ice Sheet). In *Quaternary Geology of Canada and Greenland*, edited by RJ Fulton. Geological Survey of Canada, Geology of Canada. No. 1, pp. 48-58.

Ryder, J.M., Fulton, R.J., Clague, J.J. 1991. The Cordilleran ice sheet and the glacial geomorphology of southern and central British Columbia. Géographie physique et Quaternaire 45(3), 365-377.

Saunders, I.R., Clague, J.J., Roberts, M.C. 1987. Deglaciation of Chilliwack River valley, British Columbia. Canadian Journal of Earth Sciences 24, 915-923.

Shennan, I. and Hamilton, S. 2006. Coseismic and pre-seismic subsidence associated with great earthquakes in Alaska. Quaternary Science Reviews 25, 1-8.

Shennan, I., Bradley, S., Milne, G., Brooks, A., Bassett, S., and Hamilton, S. 2006. Relative sea-level changes, glacio isostatic modelling and ice-sheet reconstructions from the British Isles since the Last Glacial Maximum. Journal of Quaternary Science 21(6), 585-599.

Shugar, D.H. and Clague, J.J. 2011. The sedimentology and geomorphology of rock avalanche deposits on glaciers. Sedimentology 58, 1762-1783

Shugar, D.H., Walker, I.J., Lian, O.B., Eamer, J.B.R., Neudorf, C., McLaren, D., Fedje, D. 2014. Post-glacial sea-level change along the Pacific coast of North America. Quaternary Science Reviews 97, 170-192.

Slangen, A.B.A., Carson, M., Katsman, C.A., van de Wal, R.S.W., Köhl, A., Vermeersen, L.L.A., Stammer, D. 2014. Projecting twenty-first century regional sea-level changes. Climatic Change 124(1), 317-332.

Smith, D.E., Harrison, S., Firth, C.R., Jordan, J.T. 2011. The early Holocene sea level rise. Quaternary Science Reviews 30, 1846-1860.

Soutendam, C.J.A. 1967. Some methods to study surface textures of sand grains: Sedimentology 8, 281-290.

Stafford, J. and Christensen, T. 2014. Permit 2010-216 Site EjTa-1, Hakai Beach Institute, Calvert Island: Site Alteration Permit Report. Unpublished Archaeology report available through the Hakai Beach Institute.

Stark, N., Hay, A.E., Chee, R., Lake, C.B. 2014. The impact of particle shape on the angle of internal friction and the implications for sediment dynamics at a steep, mixed sand-gravel beach. Earth Surface Dynamics 2(2), 469-480.

Stephens, J.S. Jr., Larson, R.J., Pondella, D.J. II. 2006. Rocky reefs and kelp beds. In: Allen, L.G., Horn, M.H., (eds.), The ecology of marine fishes: California and adjacent waters. University of California Press, pp. 227-252.

Stolze, S., Roe, H.M., Patterson, R.T., Monecke, T. 2007. A record of Lateglacial and Holocene vegetation and climate change from Woods Lake, Seymour Inlet, coastal British Columbia, Canada. Review of Palaeobotany and Palynology 147, 112-127.

Strelin, J., Casassa, G., Rosqvist, G. and Holmlund, P. 2008. Holocene glaciations in the Ema glacier valley, Monte Sarmiento massif, Tierra del Fuego. Palaeogeography, Palaeoclimatology, Palaeoecology 260(3), 299-314.

Stuiver, M., Reimer, P.J., Reimer, R.W. 2013. Calib 7.0. 14CHRONO Centre, Queen's University Belfast, Belfast. http://www.calib.org (accessed 01.09.2014).

Sun, D., Bloemendal, J., Rea, D.K., Vandenberghe, J., Jiang, F., An, Z., Su, R. 2002. Grain-size distribution function of polymodal sediments in hydraulic and aeolian environments, and numerical partitioning of the sedimentary components. Sedimentary Geology 152, 263-277.

Szeliga, W. 2013. 2012 Haida Gwaii quake: insight into Cascadia's subduction extent. Eos, Transactions American Geophysical Union 94, 85-96.

Szkornik, K., Gehrels, W.R., Murray, A.S. 2008. Aeolian sand movement and relative sea level rise in Ho Bugt, western Denmark, during the 'Little Ice Age'. The Holocene 18(6), 951-965.

Taylor, M.A., Hendy, I.L., Pak, D.K. 2014. Deglacial ocean warming and marine margin retreat of the Cordilleran Ice Sheet in the North Pacific Ocean. Earth and Planetary Science Letters 403, 89-98.

Usinger, R.L. 1968. Aquatic Hemiptera. In: Usinger, R.L. (Ed.), Aquatic insects of California. University of California Press, Berkeley and Los Angeles, pp. 182-228.

van Barneveld, J.W., Rafiq, M., Harcombe, G.F., Ogilvie, R.T. 1980. An Illustrated Key to Gymnosperms of British Columbia. Province of British Columbia. 32p.

van Der Meer, J.J.M., Menzies, J. 2011. The micromorphology of unconsolidated sediments. Sedimentary Geology 238(3-4), 213-232.

Vincent, P. 1986. Differentiation of modern beach and coastal dune sands – a logistic regression approach using the parameters of the hyperbolic function. Sedimentary Geology 49, 167-176.

Visher, G.S. 1969. Grain size distributions and depositional processes. Journal of Sedimentary Petrology 39(3), 1074-1106.

Vos, K., Vandenberghe, N., and Elsen, J. 2014. Surface textural analysis of quartz grains by scanning electron microscopy (SEM): From sample preparation to environmental interpretation. Earth-Science Reviews 128, 93-104.

Wadell, H. 1932. Volume, shape, and roundness of rock particles. The Journal of Geology, 443-451.

Warner, B.G. 1984. Late Quaternary palaeoecology of eastern Graham Island, Queen Charlotte Island, British Columbia, Canada. PhD Thesis, Simon Fraser University, Burnaby, Canada, 190p.

Warner, B.G. 1990. Plant macrofossils. In: Warner, B.G. (Ed.), Methods of Quaternary Ecology. Geoscience Canada Reprint Series 5, Geological Association of Canada, St John's Newfoundland, pp. 53-63.

Warnke, D.A. and Gram, R. 1969. The study of mineral-grain surfaces by interference microscopy. Notes: Journal of Sedimentary Petrology 39(4), 1599-1604.

Wassenaar, L.I., Brand, U., Terasmae, J. 1988. Isotopic and elemental geochemistry of marine invertebrates from the late Quaternary Fort Langley Formation and Capilano Sediments, southwestern British Columbia, Canada. Chemical Geology 73, 221-231.

Wilson, P., McGourty, J., Bateman, M.D. 2004. Mid- to late-Holocene coastal dune event stratigraphy for the north coast of Northern Ireland. The Holocene 14(3), 406-416

Wolfe, S.A., Walker, I.J., Huntley, D.J. 2008. Holocene coastal reconstruction, Naikoon peninsula, Queen Charlotte Islands, British Columbia. Geological Survey of Canada, Current research 2008-12, 16p.

Yokoyama, Y., Lambeck, K., De Deckker, P., Johnston, P., Fifield, L.K. 2000. Timing of the Last Glacial Maximum from observed sea-level minima. Nature 406, 713-716.

Zack, G.W., Rogers, W.E., Latt, S.A. 1977. Automatic measurement of sister chromatid exchange frequency. The Journal of Histochemistry and Cytochemistry 25(7), 741-753.

7. Appendices

Appendix 1. Geochronological samples collected for this study. All AMS ^{14}C samples were processed at the UCIAMS lab (preprocessing on CIRC15b, 18c, 20a performed by Alice Telka). Sample elevations (Z) were calculated from a bare earth lidar DEM, incorporate sample depth, and are assumed to be accurate within ± 0.15 m.

Sample Name	UCIAMS #	Region	UTM (mN,mE) (zone 9)	Sample Z (m asl)	AMS ^{14}C age (± 1σ)	Cal. ka cal BP (2σ)	Optical age (ka cal BP ± 1σ)	Notes
CIRC1[*1, 3]	115815	Cobble Beach	5723352, 558826	2.78	5790 ± 20	6.66 - 6.53		Wood collected from 60 cm thick organic-rich unit that in a wave-cut scarp at Cobble Beach, under ~ 6.5m of exposed, well-sorted sands.
CIRC2[*2, 3]	115816	North Beach	5723990, 559851	2.94	5045 ± 20	5.89 – 5.80		Bark and cone collected from 3 m below modern forest floor soil in beach scarp, from base of organic-rich sediment.
CIRC4	115817	Numbered beaches	5721652, 558758	0.29	12455 ± 30	14.92 – 14.27		Wood sample from a ~10 cm diameter log in fine sand and silt matrix with a low concentration of semi-rounded pebbles.
CIRC5[*2, 3]	115764	North Beach	5723990, 559851	5.94	2410 ± 15	1.86 – 1.46		Shell collected from the base of shell midden exposed in beach scarp, 60cm below modern forest floor soil.
CIRC6[*1, 3]	128331	Cobble Beach	5723352, 558826	3.18	4680 ± 20	5.42 – 5.32		Wood collected from the top of organic-rich sediment from which CIRC1 was sampled.
CIRC8[*3, 3]	128332	North Beach	5723945, 559740	2.23	5870 ± 20	6.74 – 6.65		Wood and needles collected from a well preserved organic-rich sediment outcropping from modern beach face, above fine sand/silt bed.
CIRC12[*4]	128335	Numbered beaches	5721566, 558707	0.75	9465 ± 20	11.04 – 10.78		Wood sample collected from wood-rich organic unit that overlies 5 cm of well sorted sands that, in turn, overly silts/fine sands from which CIRC4 was collected.
CIRC14[*5]	128336	Foggy Cove (FC_1)	5722556, 559335	4.0	12575 ± 25	15.12 – 14.73		Woody sediment collected from organic layer (unit 2) full of macro-floral fossils within sands and gravels.
CIRC15b[*5]	141766	Foggy Cove (FC_1)	5722556, 559335	4.0	12590 ± 30	15.13 – 14.74		Woody sediment sampled from the same unit (2) as CIRC14.
CIRC16a[*4]	141767	Numbered beaches	5721566, 558707	0.75	9355 ± 25	10.61 – 10.51		Wood fragment sampled from organic layer from which CIRC12 was collected.
CIRC16b[*4]	141768	Numbered beaches	5721566, 558707	0.75	8590 ± 230	10.21 – 9.08		Bulk organic sediments sampled from organic sandy unit from which samples CIRC12 and 16a were collected.

Sample Name	UCIAMS #	Region	UTM (mN,mE) (zone 9)	Sample Z (m asl)	AMS ^{14}C age (± 1σ)	Cal. ka cal BP (2σ)	Optical age (ka cal BP ± 1σ)	Notes
CIRC18c[*][6]	141769	Foggy Cove (FC_3)	5722338, 559148	6.0	12485 ± 30	15.01 – 14.34		Wood fragment sampled from the same unit (2) from which CIRC14 and 15b were collected.
CIRC19a[*][1], [3]	141770	Cobble Beach	5723352, 558826	3.18	4600 ± 15	5.32 – 5.30		Bulk organic sediments collected from the top the of organic unit from whichCIRC1 and 6 were collected
CIRC19b[*][1], [3]	141771	Cobble Beach	5723352, 558826	2.78	6665 ± 20	7.58 – 7.50		Bulk organic sediments collected from the bottom of organic bed unit from which CIRC1 and 6 were collected.
CIRC20a	141772	Foggy Cove (FC_2)	5722465, 559285	9.0	12050 ± 30	14.02 – 13.77		Wood fragment from palaeosol within Unit 5, overlying sands and gravels overlying Unit 2, from which CIRC 14, 15b, 18c were sampled.
CIRC21[1,*][7]	141773	Pruth Bay	5722930, 560170	-0.4	1405 ± 20	0.78 – 0.51		Shell sampled from below well-rounded cobbles exposed in excavator pit in the intertidal zone.
CIRC23b	141774	Little Wolf	5724023, 560306	0.48	575 ± 15	0.63 – 0.60		Wood fragments sampled from highly consolidated relict sand outcropping from the modern beach.
CIRC25[*][5]	145444	Foggy Cove (FC_1)	5722556, 559335	5.5	12180 ± 60	14.24 – 13.84		Wood sampled from organic–rich sediments interbedded with sands and gravels (Unit 3) 1 m above unit 2 where CIRC14,15b,18c were sampled from.
CIRC26a[*][8]	145445	Hood Lake	5723716, 559164	2.6	6745 ± 20	7.63 – 7.57		Wood fragment sampled from base of vibracore C05
CIRC27a[*][9]	159967	Hood Lake	5723658, 559294	2.94	235 ± 20	0.31 – 0.28		Sedge fragment sampled from just above sand unit in core CO3 at 22 cm depth.
CIRC29c[*][10]	145446	Hood Lake	5723744, 559288	2.24	760 ± 20	0.71 – 0.67		Wood fragment sampled from unit of macro-floral fossil rich sediments at 30 cm depth in core C01.
CIRC29f[*][10]	145447	Hood Lake	5723744, 559288	2.09	1015 ± 15	0.96 – 0.92		Wood fragment sampled from just below a 2 cm thick unit of clean unaltered sand, at 53 cm depth in core C01
CIRC29g[*][10]	145448	Hood Lake	5723744, 559288	2.0	1045 ± 15	0.97 – 0.93		Wood fragment sampled at base of peaty fibrous unit above basal sands, at 62 cm depth in C01.
CIRC29j[*][10]	145449	Hood Lake	5723744, 559288	1.68	1810 ± 20	1.82 – 1.70		Beetle shell sampled from sands from base of core, at 94 cm depth in core C01.
CIRC30c	145450	Hood Lake	5723703, 559371	2.57	925 ± 15	0.91 – 0.84		Rootlets and woody material sampled from peaty unit just above sand bed, at 29 cm depth in core C02.
CIRC31[*][11]	159968	Numbered beaches	5721795, 558166	0.72	3055 ± 15	3.34 – 3.28		Wood fragment sampled from stump rooted(?) in relict sands and silts outcropping from the modernbeach.
CIRC32[*][11]	159969	Numbered beaches	5721795, 558166	0.72	1530 ± 15	1.42 – 1.37		Wood fragment sampled from stump rooted(?) in relict sands and silts outcropping from the modernbeach.

Sample Name	UCIAMS #	Region	UTM (mN,mE) (zone 9)	Sample Z (m asl)	AMS ^{14}C age (± 1σ)	Cal. ka cal BP (2σ)	Optical age (ka cal BP ± 1σ)	Notes
CIRC33[*][10]	159970	Hood Lake	5723744, 559288	2.31	690 ± 15	0.68 – 0.65		Wood fragment collected from interbedded sands and organics at 30.5 cm depth in core C01.
CIRC34[*][10]	159971	Hood Lake	5723744, 559288	2.18	1060 ± 20	0.99 – 0.93		Wood fragment collected from organic rich sediment at 44 cm depth of core C01.
CIRC36[*][9]	159972	Hood Lake	5723658, 559294	3.09	185 ± 15	0.22 – 0.16		Seeds sampled from gyttja at7 cm depth in core C03
CIRC37[*][9]	159973	Hood Lake	5723658, 559294	2.98	135 ± 15	0.11 – 0.06		Grass sampled from peaty unit at 18 cm depth in core C03.
CIRC38[*][9]	159974	Hood Lake	5723658, 559294	2.83	215 ± 15	0.17-0.15		Wood fragment sampled from gyttja at 32.5 cm depth in core C03.
CIRC39[*][9]	159975	Hood Lake	5723658, 559294	2.76	335 ± 15	0.41 – 0.35		Wood fragments sampled from sands at 40 cm core depth at the base of C03.
CIDS1[3]		West Beach	5723354, 559215	5.3			0.04 ± 0.004	Sand from modern foredune sampled at 20 cm depth
CIDS2[3]		Behind West Beach	5723404, 559389	15.7			0.07 ± 0.02	Sand from relict (forested) depositional lobe behind blowout, ~130m east of modern foredune. Sample depth 60cm
CIDS3[3]		Behind West Beach	5722862, 559634	3.6			0.09 ± 0.02	Sand from low-lying relict (forested) foredune, ~72 m inland of the modern West Beach, sample depth 70 cm
CIDS4[3]		Behind West Beach	5723163, 559590	7.8			0.11 ± 0.02	Sand from a large (~2 m tall) relict foredune in a set of relict foredunes, ~100 m inland from the backshore of West Beach, sample depth 65 cm
CIDS5[*][1]		Cobble Beach	5723352, 558826	3.82			2.18 ± 0.30	Sand from 34 cm above organic-rich unit (samples CIRC 1,6,19a) in a ~6 m tall exposure of well sorted medium sand from wave-eroded exposure
CIDS6[*][1]		Cobble Beach	5723352, 558826	5.83			3.14 ± 0.41	Sand from 117 cm below modern soil at top of sandy wave-eroded exposure from CIDS5
CIDS8[3]		Numbered beaches	5721489, 558694	34.6			3.75 ± 0.34	Sand sample collected from C horizon under deep Ortstein (cemented) horizon in a well-developed ~150 cm thick podzol in well-sorted sand. Sample depth 2 m
CIDS9[3]		Behind West Beach	5723573, 559093	8.39			0.42 ± 0.07	Sand sample collected from mottled, well-sorted sands with minor brunisol development with depth. Sample depth 76 cm

Sample Name	UCIAMS #	Region	UTM (mN,mE) (zone 9)	Sample Z (m asl)	AMS ^{14}C age (± 1σ)	Cal. ka cal BP (2σ)	Optical age (ka cal BP ± 1σ)	Notes
CIDS10[3]		Numbered beaches	5721833, 559133	12.95			8.55 ± 1.37	Sand sample collected from the C horizon, under a strong placic horizon, of a well developed podzol formed in a relict dune. Sands were well-sorted and medium. Sample depth 96cm.
CIDS11[3]		Wolf Beach	5724468, 561080	1.54			0.004 ± 0.02	Sand in 140 cm deep trench dug into eroded foredune perched on bedrock in the modern beach setting. Sample depth 112 cm.
CIDS15		Behind North Beach	5723777, 559396	7.55			4.20 ± 0.33	Sample from upper flat terrace between North Beach and Hood Lake. Well sorted sands collected from the C horizon of a well developed podzol with well developed placic horizon. Sample depth 90 cm.
CIDS16		Behind Wolf Beach	5724268, 561006	5.35			7.24 ± 0.55	Sand sample from a flat terrace between Wolf Beach and Kwakshua Channel. Deep (100 cm) podzol development, sampled from BC horizon at 80 cm depth
CIDS17*[8]		Hood Lake	5723716, 559164	3.21			0.35 ± 0.06	Sand sample collected from 111 cm depth in well sorted medium sands in vibracore from relict dune ridge in the middle of Hood Lake.
CIBS1[3]		Between West Beach and Pruth Bay	5722929, 559967	2.7			0.51 ± 0.05	Sand sample collected from finely laminated medium/fine sands from excavator pit near Hakai Institute, sample depth 1.5 m.
CIBS2[3]		West Beach	5723129, 559485	1.9			0.030 ± 0.01	Modern beach sand sample near base of foredune in the backshore, ~50 m inland from low tide level, sample depth 38 cm.
CIBS3*[2], [3]		North Beach	5723991, 559847	3.6			2.89 ± 0.29	Sand sample collected from cemented, well sorted medium sands in beach scarp bracketed by CIRC2 and CIRC5.
CIBS4*[3], [3]		North Beach	5723939, 559762	3.0			5.58 ± 0.52	Sand sample collected below modern beach in relict sand near the upper contact (5 cm below organic-rich sand). (CIRC8)
CIBS6, [3]		Behind West Beach	5723069, 559573	4.83			0.19 ± 0.02	West Beach sand sample collected from massive, well-sorted sands in excavator pit 40 m inland from the modern beach, sample depth 1.5 m
CIBS9a		Numbered beaches	5721566, 558707	0.55			8.72 ± 0.65	Silty sand sample collected in 4th beach 20 cm below organic bed containing CIRC 12, 16a, 16b.

Sample Name	UCIAMS #	Region	UTM (mN,mE) (zone 9)	Sample Z (m asl)	AMS ^{14}C age (± 1σ)	Cal. ka cal BP (2σ)	Optical age (ka cal BP ± 1σ)	Notes
HW6-a[2]	118019	Numbered beaches	5722232, 559819	9.4	11565 ± 25	13.44 – 13.34		*Pinus contorta* seed, *Picea* seed and needle fragments collected at 204-205 cm core depth at the base of gyttja, above silts and clays
HW6-b[2]	118020	Numbered beaches	5722232, 559819	9.4	12400 ± 35	14.59 – 14.18		*Sphagnum* sp., charcoal, needle fragments, sclerotia, conifer seed collected at 182-183 cm core depth at the silts and clays, above basal blue clay

[1] Marine sample corrected for the marine reservoir effect and using the MARINE13 dataset
[2] Ages from McLaren et al. (2014)
[3] Previously published in Neudorf et al. (2015b)
*[x] Samples with matching numbers are horizontally co-located (sampled at different depths) and may overlap in maps

Appendix 2. Sedimentological properties of samples in the study area. Grain size distribution statistics and descriptions are based on Folk and Ward (1957), and depositional environment (i.e., littoral or aeolian) was inferred from grain shape (section 3).

Sample	Mean (μm)	Sorting (σ)	Skew	Description	Depositional Environment	Test statistic
CIDS1	197.0	1.262	Symmetrical	Very well sorted fine sand	Foredune	0.65
CIDS2	213.2	1.263	Symmetrical	Very well sorted fine sand	Undetermined	
CIDS3	221.6	1.227	Symmetrical	Very well sorted fine sand	Undetermined	
CIDS4	234.7	1.251	Symmetrical	Very well sorted fine sand	Foredune	1.29
CIDS8	234.4	1.413	Coarse	Well sorted fine sand	Depositional lobe	1.88
CIDS9	225.5	2.149	Coarse	Moderately well sorted fine sand	Aeolian basin	1.49
CIDS10	278.6	1.554	Symmetrical	Moderately well sorted medium sand	Aeolian basin	1.00
CIDS12	224.4	1.413	Coarse	Well sorted fine sand	Depositional lobe	0.98
CIDS13	197.8	1.269	Symmetrical	Very well sorted fine sand	Foredune	0.54
CIDS14	199.4	1.278	Symmetrical	Well sorted fine sand	Undetermined	
CIDS15	198.7	1.277	Symmetrical	Well sorted fine sand	Aeolian basin	1.61
CIDS16	146.9	1.338	Symmetrical	Well sorted fine sand	Upper beach	1.14
CIDS17	143.9	1.300	Symmetrical	Well sorted fine sand	Foredune	1.88
CIDS18	231.6	1.252	Symmetrical	Very well sorted fine sand	Depositional lobe	0.91
CIDS19	146.9	1.321	Symmetrical	Well sorted fine sand	Undetermined	
CIBS1-1	285.9	1.456	Coarse	Moderately well sorted medium sand	Depositional lobe	1.50
CIBS1-2	265.3	1.304	Symmetrical	Well sorted medium sand	Aeolian basin	1.83
CIBS1-3	364.4	1.483	Symmetrical	Moderately well sorted medium sand	Undetermined	
CIBS1-4	280.7	1.347	Symmetrical	Well sorted medium sand	Upper beach	0.54
CIBS2	219.0	1.218	Fine	Very well sorted fine sand	Lower beach	1.10
CIBS3	347.5	1.385	Coarse	Well sorted medium sand	Undetermined	
CIBS4	217.6	1.246	Fine	Very well sorted fine sand	Lower beach	1.10
FC unit 1-L	971.4	3.348	Very fine	Poorly sorted coarse sand		
FC unit 1-U	161.9	2.509	Coarse	Poorly sorted fine sand		
FC unit 2	114.7	4.832	Symmetrical	Very poorly sorted very fine sand		
FC unit 3-L	14.72	12.67	Coarse	Very poorly sorted medium silt		
FC unit 3-M	263.4	1.517	Coarse	Moderately well sorted medium sand		
FC unit 3-U	958.2	2.923	Symmetrical	Poorly sorted coarse sand		
FC unit 4	348.3	5.957	Symmetrical	Very poorly sorted medium sand		
FC unit 5	220.9	2.785	Coarse	Poorly sorted fine sand		
CICB1	249.7	1.212	Symmetrical	Very well sorted fine sand	Undetermined	
LW1	276.9	1.499	Symmetrical	Moderately well sorted medium sand	Undetermined	
LW2	481.4	1.741	Symmetrical	Moderately sorted medium sand		
CICB2-U	252.7	1.203	Symmetrical	Very well sorted medium sand	Depositional lobe	0.27
CICB2-M	258.8	1.234	Coarse	Very well sorted medium sand	Depositional lobe	1.12
CICB4-L	239.4	0.337	Symmetrical	Very well sorted fine sand	Undetermined	
CIRC23b	276.9	1.499	Symmetrical	Moderately well sorted medium sand	Upper beach	0.33
Fig. 15a	492.1	3.184	Symmetrical	Poorly sorted medium sand	Undetermined	
Fig. 15b	95.21	3.822	Symmetrical	Poorly sorted very fine sand		
Fig. 15c	512.9	3.402	Coarse	Poorly sorted coarse sand	Undetermined	
Fig. 15d	224.1	1.541	Fine	Moderately well sorted fine sand	Undetermined	
4^{th} upper	154.5	1.988	Symmetrical	Moderately sorted fine sand	Undetermined	
4^{th} lower	92.48	4.471	Fine	Very poorly sorted very fine sand		
C01-49					Foredune	0.80
C01-62					Upper beach	0.89
C01-95					Beach	1.83
C03-20					Undetermined	
C03-40					Lower beach	1.06

Appendix 3. Description of sampling, laboratory procedures, and implications for optical dating in this study.

In this study, a robust geochronology based on radiocarbon ages combined with optical ages is presented for providing a temporal framework for landscape development on Calvert Island in the Late Quaternary. There have been a number of paleoenvironmental studies of the British Columbia coast that have utilized optical dating (e.g. Lian et al. 1995; Huntley and Clague 1996; Wolfe et al. 2008), however in those studies determination of an equivalent dose and anomalous fading rates used the multiple aliquot dating technique. Moreover, optical dating is inherently experimental and laboratory protocols have to be developed and tested at each new field site (Lian and Roberts, 2006). For this study, Neudorf et al. (2015b) developed and tested a single aliquot regenerative dose (SAR) protocol applicable to the sediments found on Calvert Island. The benefits of using a single aliquot procedure over using multiple aliquot techniques include a reduction in uncertainty associated with the variability in the luminescence properties of grains that make up each aliquot (in multi aliquot procedures, 20-50 aliquots may be used to arrive at one age value, whereas with single-aliquot techniques each aliquot provides a unique age value). Lian and Roberts (2006) also state that perhaps the greatest benefit of the SAR procedure for Quaternary scientists is that the distribution of equivalent doses from single aliquots of a sample can be analyzed, which sometimes allows for age populations to be distinguished and separated, and limiting ages to be calculated using robust statistics (e.g. Neudorf et al. 2017). This often allows for the issue of sample contamination to be addressed. For other benefits of the SAR procedure, refer to Lian and Roberts (2006).

For this work, sand samples were collected from a range of suitable depositional environments of various hypothesized age, including a modern active foredune (CIDS1), an ancient beach (e.g., CIBS3), and ancient sand dunes (e.g., CIDS5). Samples were collected by hammering a small diameter (between 0.04 and 0.08 m) aluminum tube into a recently excavated and exposed face. Samples CIBS3, CIBS4, CIDS5, and CIDS6 were collected in stratigraphic context with AMS ^{14}C samples (CIRC1, CIRC2, CIRC5,

CIRC6, CIRC8, CIRC19a, and CIRC19b) which allowed optical dating protocols to be tested. See Appendix 1 for sample descriptions.

Findings showed that optical signals from Calvert Island-sourced quartz are too dim for optical dating, and that the thermally-stable 'fast' component desired for dating was either negligible or missing. Feldspar on Calvert Island provides a sufficiently bright signal, and so a SAR protocol was developed for optical dating of the K-feldspar. Typical SAR protocols involve measurement of the 'natural' infrared stimulated luminescence signal (L_n), followed by measurement of the corresponding signal induced by a test dose of ~1 Gy given in the laboratory (T_n). A dose-response curve is then generated from the luminescence signals induced by a series of regenerative doses given in the laboratory (L_x). The equivalent dose for each aliquot is estimated by interpolation by projecting L_n/T_n on to the dose-response curve. Typical quality control components of SAR protocols, as described by Lian and Roberts (2006), include: i) accounting for sensitivity changes by normalizing each L_x signal using a test dose signal (T_x) that is measured after each L_x measurement, ii) checking the efficacy of the sensitivity correction by repeating one L_x measurement in the dose-response curve (the recycling ratio test), iii) checking for recuperation (this includes the build-up of a residual signal from one SAR cycle to the as a result of incomplete beaching of the sample during L_x measurements and the transfer of electrons from light-insensitive trap to light sensitive traps during preheating) by measuring an L_x signal after no laboratory radiation (the "0" dose point), and iv) a "dose recovery" test, where fresh aliquots are bleached at room temperature, given a known laboratory dose, and subsequently measured using the established SAR protocol to confirm the correct (given) dose is recovered. Important components, including additional quality controls, of the SAR method used in this study include:

1. A 'hotwash' treatment (cf. Murray and Wintle 2003): a high-temperature (20°C higher than the preheat temperature) optical stimulation at the end of each SAR cycle. This step is used to reduce recuperation. In this study, the hotwash had little effect on the aliquot measured-

to-given dose ratios (see “dose recovery” test above) but resulted in noticeably lower recuperation values.

2. Low preheat temperatures: high preheat temperatures (e.g. 220°C – 280°C) distorted the dose-response curve, likely reflecting thermal degradation of the luminescence signal. Therefore the lowest preheat temperature on the preheat temperature plateau was used (160°C, for 10 s).
3. Anomalous fading measurements and corrections: anomalous fading, a problem specific to feldspars, refers to the loss of electrons from traps that are thermally stable on geologic timescales, resulting in ages that are too young. Fading rates (g-values) were measured using 12 aliquots from each sample using a method modified from Auclair et al. (2003). Optical ages were corrected for fading using the procedure of Huntley and Lamothe (2001).
4. Phototransfer measurements and corrections: using a sample collected from an intertidal zone where much of the high-energy UV light responsible for charge transfer is blocked by the water column, the difference between the equivalent dose of this sample and a the same sediments after ~3 hours of exposure to direct sunlight was assumed to be the result of phototransfer, which results in the overestimation of the equivalent dose (and older ages). This difference was subtracted from age estimates of dune sand samples that were assumed to be fully bleached before deposition. Testing of this phototransfer correction on modern dune samples yielded optical ages much closer to modern, as expected, and thus the correction was applied to all dune samples optically dated in this study.

Uncertainties in optical ages include those that result during laboratory measurements (analytical uncertainties, Duller 2007) and those that originate in the environment (e.g., those due to insufficient bleaching of the sediment prior to final burial, microdosimtery at the sample site, insufficient knowledge of samples’ water content over time, and radioactive disequilibrium). The uncertainties (±

values) associated with each optical age only take into account analytical uncertainties, and an error value is typically added to the water content used in the dose rate calculation to take into account any reasonable variation since deposition. However, for these samples, error associated with environmental factors are expected to be minor as all samples were collected from well-drained, well-sorted sand that was deposited in environments where sufficient sunlight exposure prior to burial is expected. This is supported by the fact that the SAR protocol applied in this study, and detailed in Neudorf et al. (2015b), yielded optical ages that show consistency with AMS ^{14}C ages from the same sites.

Additional references for Appendix 3:

Auclair, M., Lamothe, M., Huot, S., 2003. Measurement of anomalous fading for feldspar IRSL using SAR. Radiation Measurements 37, 487-492.

Duller, G.A.T., 2007. Assessing the error on equivalent dose estimates derived from single aliquot regenerative dose measurements. Ancient TL 25(1), 15-24.

Huntley, D.J. and Clague, J.J., 1996. Optical dating of tsunami-laid sands. Quaternary Research 46, 127-140.

Huntley, D.J. and Lamothe, M., 2001. Ubiquity of anomalous fading in K-feldspars and the measurement and correction for it in optical dating. Canadian Journal of Earth Sciences 38, 1093-1106.

Lian, O.B., Hu, J., Huntley, D.J., Hicock, S.R., 1995. Optical dating studies of quaternary organic-rich sediments from southwestern British Columbia and northwestern Washington State. Canadian Journal of Earth Sciences 32, 1194-1207.

Murray, A.S. and Wintle, A.G., 2003. A single aliquot regenerative dose protocol: potential for improvements in reliability. Radiation Measurements 37, 377-381.

Neudorf, C.M., Smith, N., Lepofsky, D., Toniello, G., Lian, O.B., 2017. Between a rock and a soft place: Using optical ages to date aancient clam gardens on the Pacific Northwest. PLOS one 12(2), e0171775.